Digitized Theses   Digitized Special Collections

1978

Evolution Of The Al Amar-idsas Region Of The Arabian Shield; Kingdom Of Saudi Arabia

Zohair Abdul Nawab

Follow this and additional works at: https://ir.lib.uwo.ca/digitizedtheses

NOTICE

The quality of this microfiche is heavily dependent upon the quality of the original thesis submitted for microfilming. Every effort has been made to ensure the highest quality of reproduction possible.

If pages are missing, contact the university which granted the degree.

Some pages may have indistinct print especially if the original pages were typed with a poor typewriter ribbon or if the university sent us a poor photocopy

Previously copyrighted materials (journal articles, published tests, etc.) are not filmed.

Reproduction in full or in part of this film is governed by the Canadian Copyright Act, R.S.C. 1970, c. C-30. Please read the authorization forms which accompany this thesis.

AVIS

La qualité de cette microfiche dépend grandement de la qualité de la thèse soumise au microfilmage. Nous avons tout fait pour assurer une qualité supérieure de reproduction.

S'il manque des pages, veuillez communiquer avec l'université qui a conféré le grade.

La qualité d'impression de certaines pages peut laisser à désirer, surtout si les pages originales ont été dactylographiées à l'aide d'un ruban usé ou si l'université nous a fait parvenir une photocopie de mauvaise qualité.

Les documents qui font déjà l'objet d'un droit d'auteur (articles de revue, examens publiés, etc.) ne sont pas microfilmés.

La reproduction, même partielle, de ce microfilm est soumise à la Loi canadienne sur le droit d'auteur, SRC 1970, c. C-30. Veuillez prendre connaissance des formules d'autorisation qui accompagnent cette thèse.

EVOLUTION OF THE AL AMAR-IDSAS REGION

OF THE ARABIAN SHIELD, KINGDOM OF SAUDI ARABIA

by

Zohair Abdul Haffeez Nawab

Department of Geology

Submitted in partial fulfillment

of the requirements for the degree of

Doctor of Philosophy

Faculty of Graduate Studies

The University of Western Ontario

London, Ontario

March, 1978

FRONT VIEW

The Al Amar-Idsas fault of the Arabian Shield as it appears on the ERTS images.

KILOMETRES

0   100

45°

24°

23°

iv

ABSTRACT

The Precambrian ($\approx$1100-500 Ma) metavolcanic, meta-sediment, and plutonic rocks of the Al Amar-Idsas area are divided into two geologically distinct regions by the Al Amar-Idsas tectonic discontinuity, a major N.N.W.-S.S.E. trending high angle thrust fault. West of this fault, the area is underlain by the metasedimentary Abt Formation which is composed largely of sericite-chlorite schists of andesitic-dacitic affinity, and subordinate amphibolites with both tholeiitic ($FeO^t/MgO = 2$; $TiO_2 = 2\%$) and calc-alkalic ($FeO^t/MgO = 2$; $TiO_2 = 0.8\%$) basaltic characteristics. The Abt schists were intruded by a set of post-tectonic granites $K_2O/(K_2O + Na_2O) = 0.47$ to 0.59 in association with the development of zones of high temperature metamorphism. East of the Al Amar-Idsas fault, the oldest Precambrian rocks are gneissic granodiorite with $K_2O/(K_2O + Na_2O)$ values between 0.16 and 0.4. The gneisses are overlain, unconformably, by a succession of meta-volcanic rocks of calc-alkalic affinity (Meherga formation) intruded by a suite of gabbros, diorites, and quartz-rich and quartz-poor granodiorites. Some of these rocks are rich in Cr, with $K_2O/(K_2O + Na_2O)$ values between 0.27 and 0.41. The lower Halaban metavolcanics (Meherga formation) and associated plutonic rocks are overlain by a succession of soda-rich rhyolites, dacites and pyroclastic rocks (Al Amar formation). In contrast to the post-tectonic

v

granites west of the Al Amar-Idsas fault, those to the east are less potassic with $K_2O/(K_2O + Na_2O)$ values around 0.37.

Although ultramafic rocks occur in the Al Amar-Idsas region and lenses of serpentinite and high Cr-Ni carbonate rocks located along the Al Amar-Idsas fault, a complete ophiolite suite has not as yet been recognized. The possibility remains that the Al Amar-Idsas fault marks the eastern boundary of an incipient back arc basin developed above a westerly dipping subduction zone.

ACKNOWLEDGEMENTS

TERMINOLOGY AND ABBREVIATION

The following terms and abbreviations are used throughout the thesis:

Bir	=	well
B.R.G.M.	=	Bureau de Recherches Geologiques et Minières.
°C	=	centigrade
CIPW	=	Cross, Iddings, Pirsson, and Washington norm system (1902)
C.A.G.	=	Center of Applied Geology
D.I.	=	differentiation index
cm	=	centimeter
c/s	=	counts per second
D.G.M.R.	=	Directorate General of Mineral Resources
ERTS	=	Earth Resources Technology Satellite
I.A.G.	=	Institute of Applied Geology
Jabal	=	mountain
km	=	kilometer
m	=	meter
mm	=	millimeter
my	=	million years
p.p.m.	=	part per million
U.S.G.S.	=	United States Geological Survey
U.W.O.	=	University of Western Ontario
wadi	=	valley
wt %	=	weight percent

TABLE OF CONTENTS

ix

LIST OF TABLES

LIST OF FIGURES

LIST OF PLATES

CHAPTER 1

PREAMBLE

1.1.   Introduction

The Al Amar-Idsas fault, a major physiographic feature
within the eastern edge of the Arabia Shield, has been
interpreted as a collision boundary between a late Protero-
zoic volcanic arc and a more westerly located continental
margin (Al Shanti and Mitchell, 1976). The aim of this
thesis is to evaluate this hypothesis through a compara-
tive study of the metasedimentary and metavolcanic rocks,
and associated ophiolitic and granitic plutonic bodies,
located on either side of the Al Amar-Idsas fault.

The Al Amar-Idsas region is situated in the eastern
part of the Precambrian Arabian Shield in the high plateau
of Najd (Fig. 1). Its geographic limits are:

in the North, parallel 24° 30';

in the South, parallel 22° 30';

in the East, meridian 46° 00';

in the West, meridian 44° 30'.

To the west, the thesis area is bounded by the Khuff
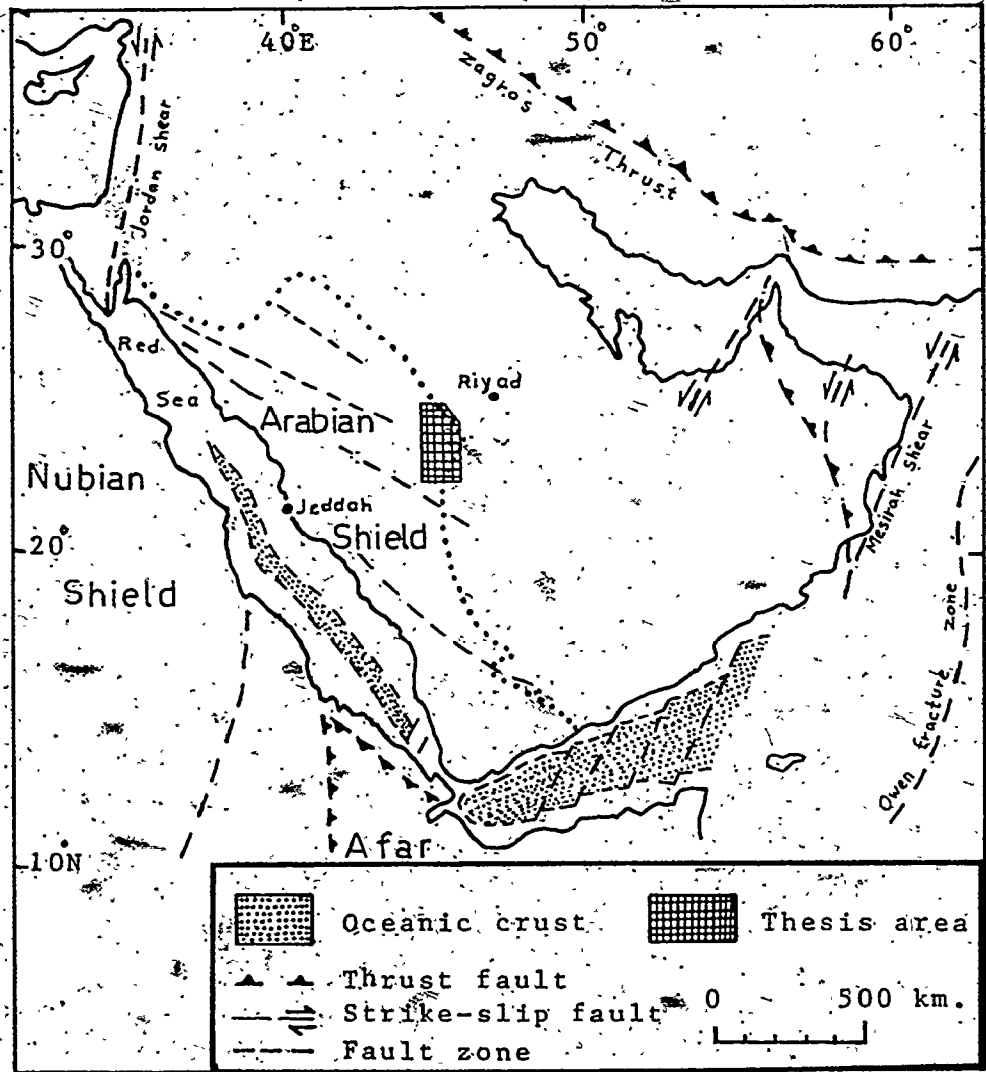
Fig. 1. Location map of the thesis area (after
Gass and Gibson, with modification).

Formation of Permian age.

The centre of the thesis area is about 855 km east of and about 12 hours drive from Jeddah. Access to the thesis area can be gained via the following routes:

A - Jeddah - At Taif   : 150 km of highway;

   At Taif - Afif   : 410 km of highway;

   Afif - Alshara   : 185 km of highway;

   Alshara - Al Amar   : 110 km of unpaved road.

B - Riyadh - Al Quwayiyah   : 200 km of highway;

   Al Quwayiyah - Al Amar   : 36 km of unpaved road.

C - From AdDawadmi, it takes about 2.5 hours to drive about 100 km south to Al Amar along a rough road.

The magnetite deposits of Jabal Idsas are situated near the centre of the area, whereas the Al Amar mine is located about 45 to 50 km north of the Idsas magnetite deposits. A new highway passing through the thesis area 7 km north of Al Amar mine is under construction (1976). This highway will be a segment of the main Riyadh - At Taif highway. The thesis area is crossed from west to east by unpaved roads from which tracks passable to trucks and four wheel drive vehicles lead into the principle wadis.

The Al Amar-Idsas region is characterized by a tropical-arid climate and occurs at an elevation of 700 m above sea level. During the winter months, temperatures fall below freezing point at night (-2° in February) but remain pleasant during the day (20°C). Rainfall is slight,

and prevailing winds are from the north or northeast. In
the summer, the climate is effected by monsoon winds which
blow from the south, sometimes accompanied by haziness and
small scale tornados. The nights are pleasantly cool but
during day the temperature reaches 43°C in the shade.
Humidity is very low both in winter and summer. In addit-
ion to about ten permanent settlements scattered through-
out the area, many semipermanent encampments may also be
found around the several wells within the thesis area.

1.2. Geomorphology

The volcanic rocks of the Halaban Group form a series
of hills of varying height, extending from north to south.
Where the Halaban rocks are metamorphosed and schistose,
the relief is low. In the Idsas mountain range, elevation
may be more than 300 m above the plain.

Marbles tend to occur as medium size hills or mount-
ains, as at Jabal Al Badr Al Aswad, up to 150 m above the
plain.

The north-south trending Al Amar-Idsas fault is bor-
dered to the west by a large wadi about 100 m wide at its
northern end (village of Marjan) and more than 10 km wide
at its southern end.

Silicified carbonates of ultramafic origin distribu-
ted along the Al Amar-Idsas fault form small hills 5 to
40 m high and 10 to 200 m long.

Serpentinite bodies in the central and southern parts

of the thesis area mostly outcrop in the form of small
hillocks, only a few meters high.

The Abt schist forms hills, sometimes even small
mountains, rising about 100 m above the plain (Jabal Tais).
The major wadis within the Abt schist run north and/or
south because they are controlled by north trending foli-
ation.

Gabbros and diorites are distributed along north-
south trends and underlie low to moderate size mountains
rising up to 200 m above the surrounding plains.

Rocks of the gneissic granodiorite unit are found as
small hillocks of weathered rock several meters high and
are located within a large and highly weathered plateau
cut by wadis running from west to east.

The younger granites tend to be unaltered and there-
fore occur as high subrounded mountains rising sharply
from the surrounding plain. In some places, the height of
the mountains (Jabal Batran) is more than 350 m above the
plain.

1.3. Previous work

Rocks of the Al Amar-Idsas region were first repre-
sented on maps of the Arabian Shield by Bramkamp et al.
(1956, 1958). They identified the region as consisting of
igneous and metamorphic rocks, which Bramkamp et al. desig-
nated by the symbols "m" and "s", respectively. The first
modern geological investigation of the Al Amar-Idsas

region was carried out in 1962 by Hunting Survey Corp.,
Ltd., and involved an airborn magnetometer survey of the
Idsas range. The survey was supplemented by a program
of low altitude colour aerial photography of the area in
the vicinity of the Idsas magnetite deposits and the
ancient Fawara and Selib mines. (Aerocarto, 1964). This
work was carried out as a preliminary to a program of
diamond drilling started in 1965 by D.G.M.R. at the Jabal
Idsas magnetite deposits. Airborne magnetic and radio-
metric prospecting surveys were also carried out by the
B.R.G.M. during the period 1965-1966.

Early geological investigations of the Al Amar-Idsas
region were mainly concerned with the geology of specific
mineralized areas of the Al Amar-Idsas region. The con-
tribution of each of these workers will be discussed in
the context of individual rock stratigraphic units de-
scribed in the succeeding chapters.

1.4. Present work

Field work was carried out in the winter of 1976
between February and April. A preliminary analysis of the
thesis area involving more than 12,000 square km, was
accomplished by examination of eight aerial photographs
at a scale of 1:100,000. 460 samples were collected from
325 stations, including 45 field oriented samples for
structural studies, 279 samples for thin section study,
and 170 samples for chemical analyses.

Eight geological traverses were conducted across the thesis area in an east-west direction and approximately 20 to 30 km apart. Sampling was carried out on the basis of structural and lithological changes. The longest traverse was about 70 km long (south of the Al Amar mine) and included 37 sample stations, whereas the shortest traverse was only 10 km long and included only 9 sample stations. 45 samples were collected from silicified carbonate bodies located on a line about 200 km long parallel to the Al Amar-Idsas fault.

CHAPTER 2

REGIONAL GEOLOGY

2.1. Introduction

The thesis area covers more than 12,000 square km of the central part of Saudi Arabia, and located at the eastern edge of the Arabian Shield (Fig. 1). The Arabian Shield and its African counterpart, the Nubian Shield, have been separated by the Red Sea Rift.

During late Proterozoic time (1000 - 540 my), the Arabian Shield underwent a major cycle of deformation and regional metamorphism, referred to as the Hijaz tectonic cycle. Deformation structures produced during this cycle are characterized by north-south trends. Later, during early Paleozoic time, northwest trending structures were generated in association with an important phase of north-west - southeast transcurrent faulting (Najd fault system).

Volcanic activity which occured during the Hijaz cycle was episodic and the various volcanic units are commonly separated by conglomerate, pyroclastic, sedimentary and carbonate rocks (Greenwood et al., 1975). Plu-

8

tonic rocks of the Shield vary in composition and age from diorite, 940 my, through granodiorite, 750 my, to granite, 550 my (Table 1). The basement on which rocks of the Hijaz tectonic cycle are thought to be deposited is possibly represented by the Khamis Mushyt gneiss. a rock unit supposedly older than 1000 my.

Greenwood et al. (1975) proposed that the southwestern part of the Arabian Shield formed by cratonization of intra-oceanic island arcs during the Hijaz tectonic cycle (1000 - 540 my). They postulated the existence of a northeasterly dipping subduction zone, on the basis of a general increase in the potassium content of more northeasterly located younger volcanic and plutonic rocks.

Bakor et al. (1976), Neary et al. (1976), and Nasseef and Gass (1977) have suggested that the ultramafic zones of the Nubian and Arabian Shields of which there are five in the Nubian Shield and at least two in the Arabian Shield, represent relics of closely spaced oceanic crust between island arcs. These island arcs have been formed in a manner analogous to those of the southwestern Pacific region.

Marzouki (1977) concluded that the plutonic rocks of the Al Hadah region are typical of those produced by subduction of oceanic crust under continental crust. Marzouki (1977) also suggested that the evolution of the Arabian Shield involved collision of continental rocks separated

Table 1 – Stratigraphy, orogenic events, and plutonic rocks in the southern part of the Arabian Shield (After Greenwood et al., 1975).

	UNITS	PRINCIPAL LAYERED ROCKS	OROGENIC EVENTS	PLUTONIC ROCKS
HIJAZ TECTONIC CYCLE — THIRD EPISODE	Murdama Group	Conglomerate Graywacke Andesite Rholite Marble	BISHAH – Folds and faults; northerly trends; greenschist metamorphism	Granite and quartz monzonite (570–550 Ma)
	UNCONFORMITY			
SECOND EPISODE	Halaban Group	Conglomerate Graywacke Rhyolite Dacite Andesite Marble	YAFIKH – Folds and faults; northerly trends; greenschist metamorphism	Quartz monzonite (650–600 Ma)
	UNCONFORMITY ?			
	Ablah Group		RANYAH – Folds and faults; northerly and northeasterly trends; late transverse shears; greenschist, amphibolite, and granulite metamorphism	Injection gneiss (785 Ma) / second dioritic series (800 Ma)
	UNCONFORMITY			
FIRST EPISODE	Jiddah Group Bahah Group Baish Group	Conglomerate Graywacke Dacite Andesite Basalt	AQIQ – Folds and faults; northerly trends; greenschist metamorphism	First dioritic series (960 Ma)

by closely spaced ocean basins.

2.2. Regional stratigraphy

The rocks of the Al Amar-Idsas region (Fig. 2) were considered by Bois and Shanti (1970) to be equivalent to the Halaban Group of the central part of the Arabian Shield (Brown and Jackson, 1960). The lithostratigraphic succession established by Bois and Shanti (1970) is based on their study of the As Sakhen area (zones A, B, C; Fig. 3; Table 2). They divided the rocks into two main lithostratigraphic groupings, a lower metavolcanic group, further subdivided into three units, and an upper meta-sedimentary group composed of a lower conglomeratic unit and an upper metagraywacke unit. The ultramafic and associated gabbroic rocks of the Halaban Group were designated as the oldest rocks in the area, although Bois and Shanti (1970) allowed the possibility that the ultramafic rocks might be intrusive bodies formed penecontemporaneously with or even later than the associated volcanic units. These authors considered the rocks of the Al Amar-Idsas region to represent an unbroken lithostratigraphic succession of rocks. According to Bois and Shanti (1970) the lower andesitic volcanics (ha) form a central anticline dividing the younger sedimentary unit into two parts (Fig. 2). Conglomeratic and pyroclastic beds (cg) were found at the base of the sedimentary group.
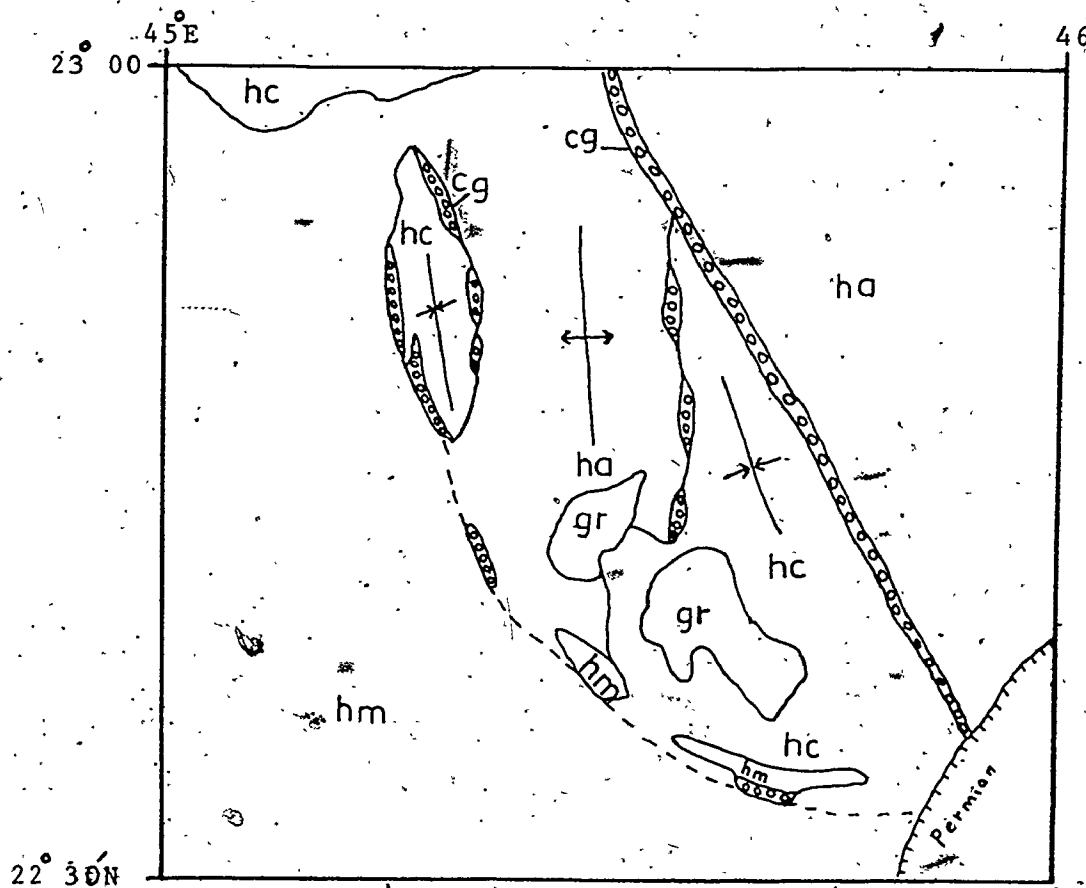
Fig. 2. Sketch map of the As Sakhen area as
mapped by Bois and Shanti (1970).

hm= marble
hc= clastic graywacke
cg= conglomerate
ha= andesitic flow

Table 2 – Lithostratigraphic correlation of different workers in the Al Amar–Idsas region.

Bois and Shanti (1970)	Overstreet et al. (1972) Kahi et al. (1972)	Thekair (1976)	Lithology
Clastic rocks, graywackes, quartzite and sericite-chlorite schist	Abt Formation		Quartz-sericite-chlorite and quartz-chlorite-plagioclase schist, thin layers of graywacke, argillite, calcareous quartzite layers, lenses and beds of marble
	Zreiba Formation		Greenish brown graywacke, pebble conglomerate to boulder conglomerate
	Badriyah Formation		Green-brown-black andesite, andesite lithic tuff, agglomerate, brecciated andesite, hornblende schist
	Abu Sawarir Formation		Green-brown graywacke, siltstone grade to argillite, thin calcareous layers, sericite chlorite schist, quartz-sericite-chlorite schist, lenses of limestone
	Fawara Formation		Gray-blue, brown and black marble, silicified marble, grades downward into calcareous conglomerate
Conglomerate, pyroclastic rocks, and marble	Idsas Formation	Conglomerate	Green-brown graywacke conglomerate, lenses of gray marble
Rhyolitic tuff, ignimbrite flows and marble	Wadi al Jifr Formation	Pyroclastic, agglomerate, and tuff	Red-brown, massive to locally sheared rhyolite, pyroclastic, volcanic breccia
Andesitic flows, tuff and marble	Jabal al Egfool Formation	Andesite flow	Epidiorite, altered diorite and andesite, meta-andesite and chlorite-amphibole schist
	Umm Mushraha Formation		Gray, dark green, fine to coarse-grained amphibole schist, meta-andesite, biotite-hornblende gneiss, gray-brown lenses of silicified marble and dolomite
	Hornblende-biotite granite gneiss	Abt Formation = Quartz-chlorite schist and chlorite-sericite schist Ultramafic and serpentinite.	
Ultramafic and basic rocks			

Murdama Group, Bir Khountina Group, Halaban Group — Overstreet et al. (1972) / Kahi et al. (1972); Basement.

Halaban Group, Basement — Thekair (1976).

Kahr et al. (1972) and Overstreet et al. (1972)
divided the rocks of Jabal Batran and Bir Al Badriyah
quadrangles of the Al Amar-Idsas region (Fig. 3) into four
groups as shown in Table 2. The oldest group were con-
sidered to be granitic gneisses forming a basement to
metavolcanic rocks of the Halaban Group (ua). The Bir
Khountina Group, overlying the Halaban Group, consists of
four formations:

1) Idsas Formation (ic), composed of conglomerate and
chlorite metasediments;

2) Fawara Formation (fm), characterized by the pres-
ence of blue-black marble and dolomitic marble;

3) Abu Sawarir Formation (sg), consisting of green to
brown graywacke and massive siltstone grading to black
argillite; and

4) Badriyah Formation (ba), composed of volcanic
andesites, rhyolites and associated pyroclastic rocks.

In the southern part (Zone B; Fig. 3; Table 2) a
fourth group of metasedimentary rocks was divided into a
lower unit of graywacke and conglomerate with a chlorite-
sericite matrix called the "Zreiba Formation" (zs), and an
upper unit of gray to green graywacke, laminated argillite
and calcareous graywacke, which Overstreet et al. (1972)
correlated with the main outcrop of sericitic schist of
the Abt Formation (ac) located west of the Al Amar-Idsas
fault (Zone E; Fig. 3). Contrary to Bois and Shanti (1970),
Overstreet et al. (1972) considered both the conglomeratic

A	B	C	D	E
Abu Sawarir Schist	Unnamed Schist		Unnamed Schist	Abt Schist
Unnamed Marble			Fawara Marble	
Unnamed Conglomerate	Zreiba Conglomerate	Unnamed Conglomerate	Idsas Conglomerate	
Unnamed Rhyolite	Unnamed Rhyolite	Wadi al Jifr Rhyolite	Unnamed Rhyolite	
Badriyah Andesite	Badriyah Andesite	Jaba al Egfool Andesite	Halaban Andesite	
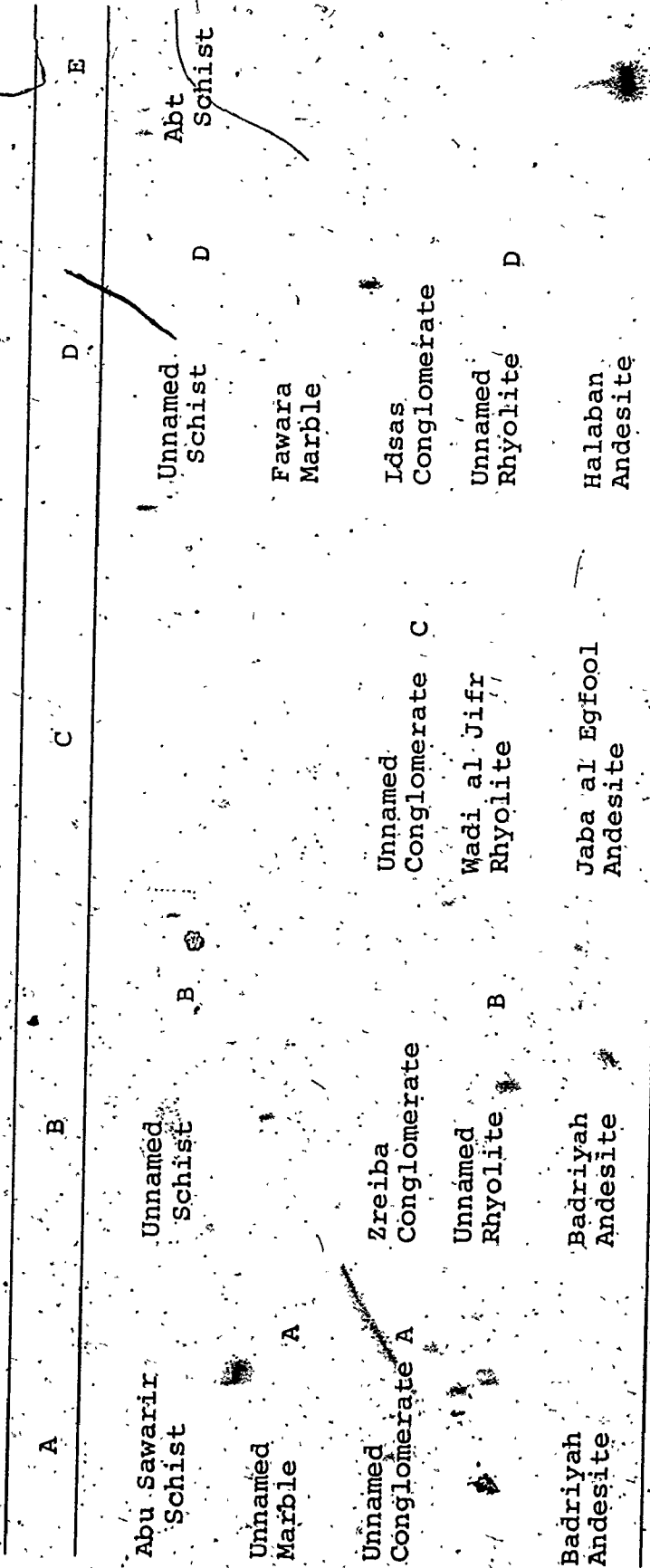
Local stratigraphic succession in zones A, B, C, D, and E of the Al Amar-Idsas region which are shown in Fig. 3.
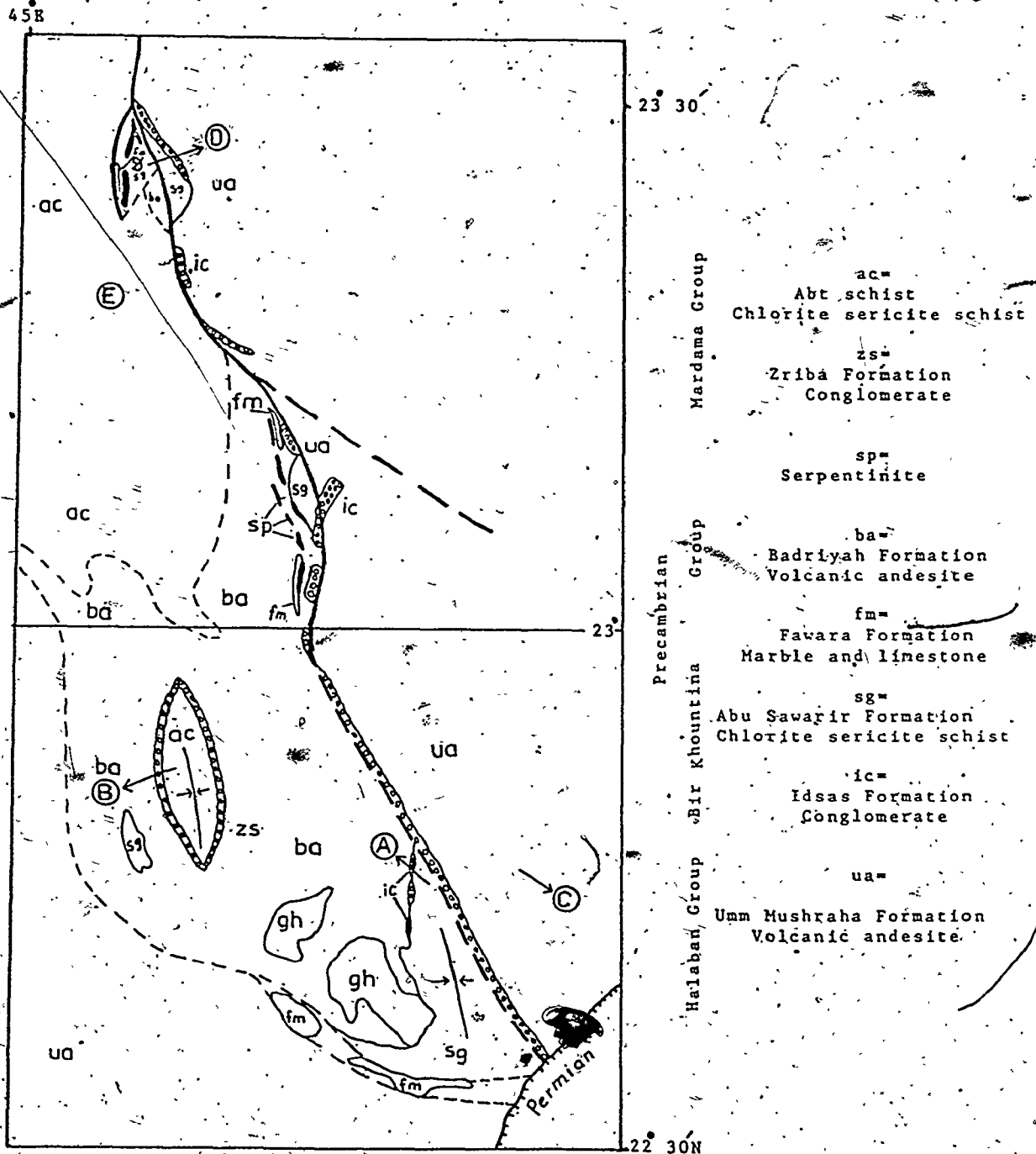
Fig. 3. Sketch map of Jabal Batran quadrangle (Kahr et al., 1972) and Bir Al Badriyah quadrangle (Overstreet et al., 1972). Zones A-B-C-D and E are explained on the facing page.

Idsas (ic) and Zreiba (zs) Formations and the volcanic Halaban and Badriyah units to be independent rather than correlative units.

Thekair (1976) divided the rocks of the Al Amar-Asihailiya district (Zone D; Figs. 3 and 4) of the Al Amar-Idsas region into two groups as shown in Table 2. According to Thekair (1976), the Abt schist (sc) represents the oldest stratigraphic unit in the area and is composed of quartz-chlorite schist and chlorite-sericite schist (sv) of graywacke origin. The rocks of the Halaban Group are considered to be the youngest and are composed of a lower sequence of meta-andesite and dacite and an upper unit consisting of pyroclastics, agglomerate and conglomerate. Gabbros (gm) and diorites (dm) are intrusive equivalents to the older metavolcanic sequence. Thekair's assumption that the Abt schist is older than the Halaban metavolcanics is contrary to the view held by Bois and Shanti (1970), Kahr et al. (1972) and Overstreet et al. (1972).
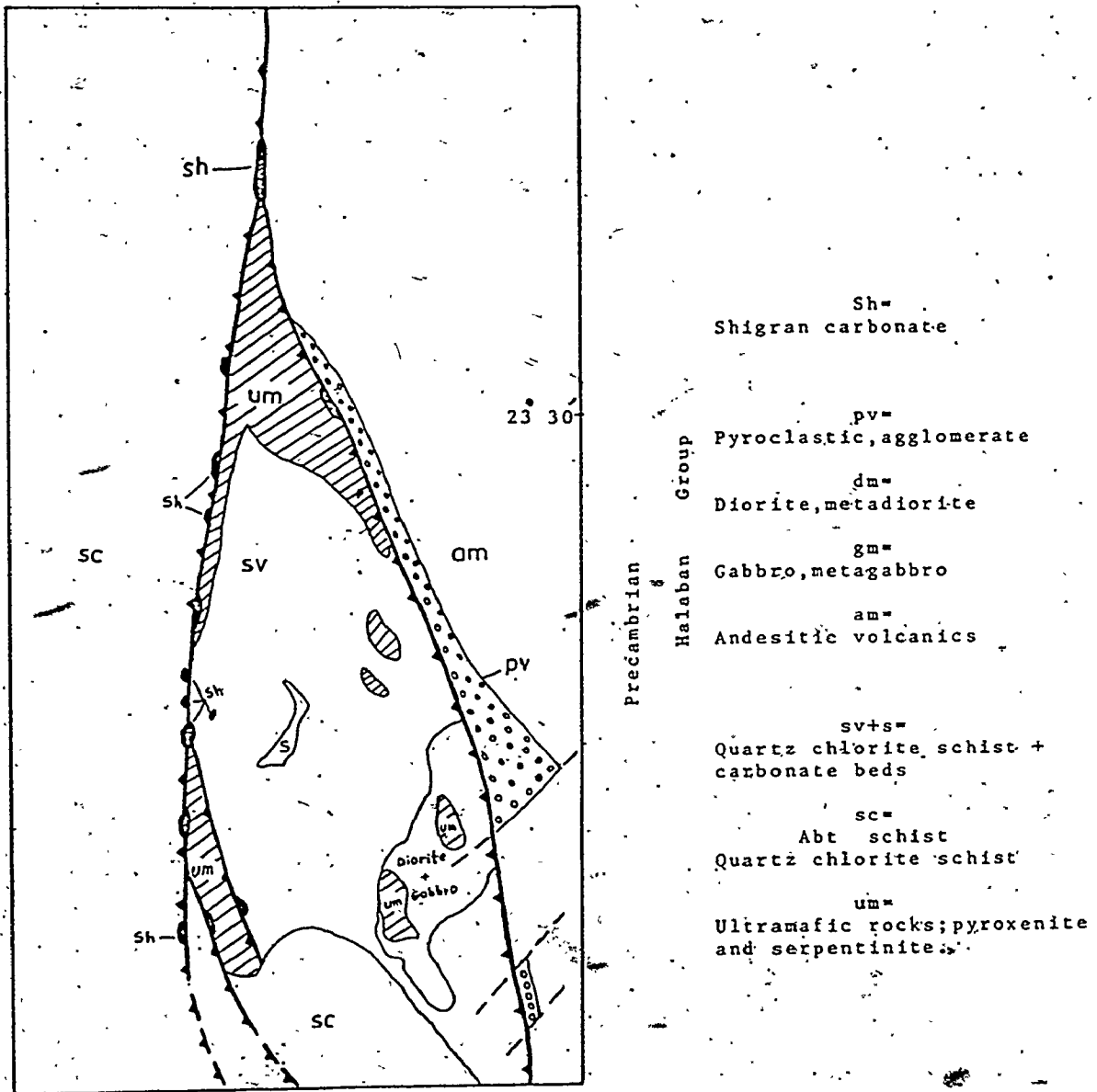
Fig. 4. Sketch map of Jabal Minassa and Shigran fault area (Thekair, 1976).

CHAPTER 3

GEOLOGY AND ROCK UNITS

3.1. Halaban Group

The term "Halaban Andesite" was introduced by G. F.
Brown and R. O. Jackson (1960) to define a mappable unit
in the central and northern part of the Arabian Shield
consisting predominantly of fine-grained felsitic ande-
site. Jackson and others (1963) later utilized the name
"Halaban Formation" to include not only the andesite mapped
by Brown and Jackson (1960), but also other units consist-
ing of sheared and folded, fine-grained felsitic andesite,
agglomerate, quartzite, graywacke and locally interbedded
marble, and rhyolite. J. Delfour (1966) introduced the
term "Halaban Cycle" with reference to rocks in the north-
ern part of the Arabian Shield, and divided the cycle into
two formations:

Formation I (lower Halaban), composed of alternations
of schist; quartzite, and intercalated marble and ultra-
mafic rocks; and

Formation II (upper Halaban), consisting of alterna-
tions of andesitic-basaltic flows, tuffs and agglomerates.

Bois and Shanti (1970) correlated the volcanic rocks
of the Al Amar-Idsas region with those of the central part
of the Arabian Shield and raised the Halaban Formation to
Group status.

As a result of their work in the Jabal Batran quad-
rangle, Kahr et al. (1972) referred the metavolcanic rocks
of this area to the Halaban Group and considered them as
consisting of an unknown thickness of metamorphosed ande-
sitic volcanics, graywacke and marble, intruded by hypa-
byssal plutonic mafic and ultramafic rocks. Overstreet
et al. (1972) consider the Halaban Group to unconformably
overlie hornblende-biotite granite gneisses of the base-
ment complex. They have also shown that the andesitic
volcanic and associated sedimentary rocks are strongly
altered by regional and contact metamorphism and therefore
predate much of the plutonic activity in the area.

The Halaban Group in the Al Amar-Idsas region forms
a belt of mountains 4 to 20 km wide and more than 200 km
long, located to the east of the Al Amar-Idsas fault (Fig.
5). North of Jabal Chelir in the southeastern part of the
thesis area, the Halaban Group appears to unconformably
overlie gneissic granodiorites.

The lower part of the Halaban Group, here designated
as the "Meherga formation" after the village of Meherga,
consists of basic volcanics overlain by a succession of
thin basaltic flows alternating with thick andesitic
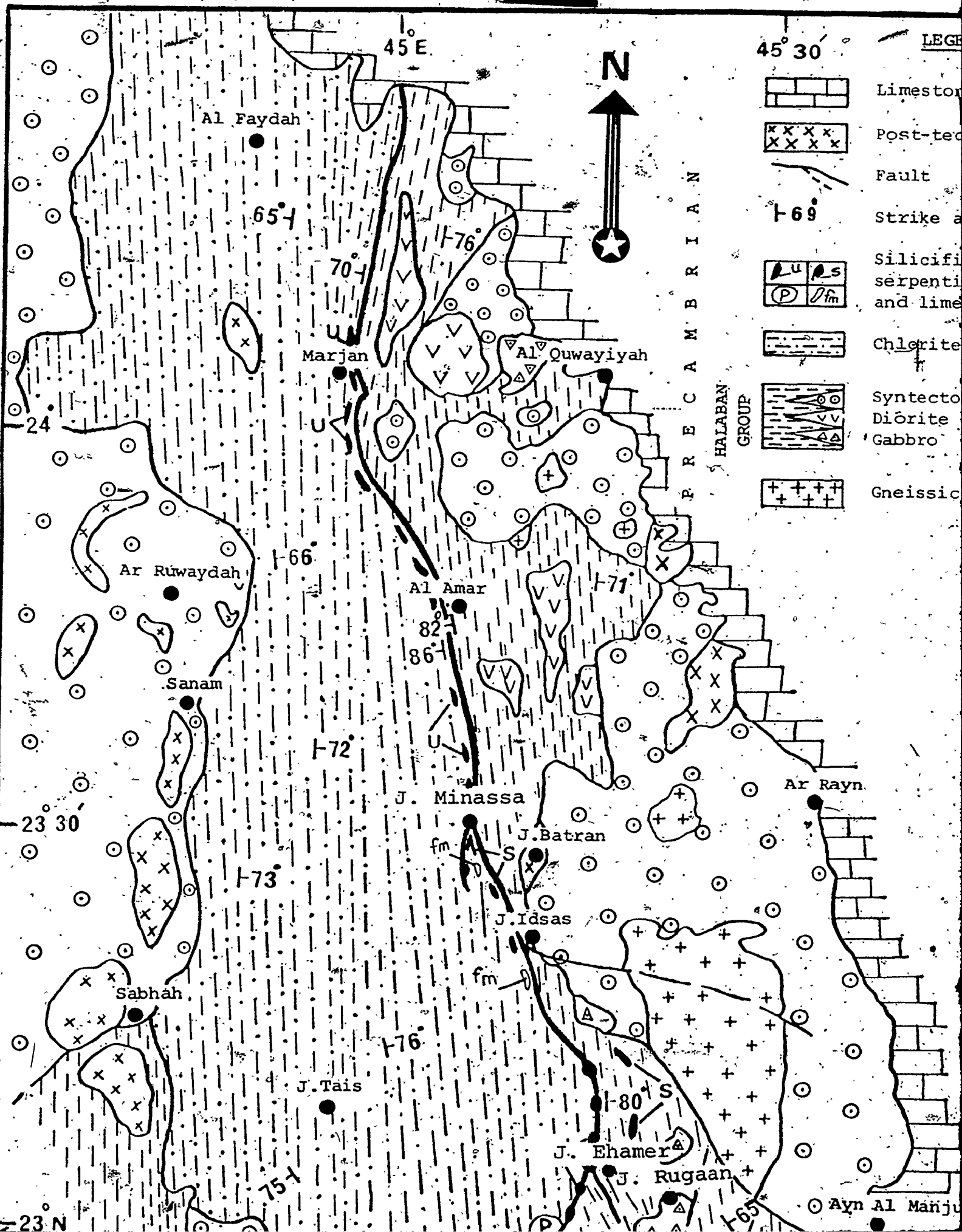
Geological map showing the Halaban Group region between 45°E and 45°30′, from 23°N to 24°N.

Labeled localities: Al Faydah, Marjan, Al Quwayiyah, Ar Ruwaydah, Al Amar, Sanam, J. Minassa, J. Batran, Ar Rayn, J. Idsas, Sabhah, J. Tais, J. Ehamer, J. Rugaan, Ayn Al Manju.

LEGEND

Limestone (Khuff Form.)

Post-tectonic granite

Fault

⊢69° Strike and dip (foliation)

Silicified ultramafic (u); serpentinite (s); pyroxenite (p) and limestone (fm)

Chlorite schist (Abt Form.)

Syntectonic granodiorite Diorite Gabbro

Gneissic granodiorite

GEOLOGIC MAP OF
THE AL AMAR-IDSAS REGION
By
Zohair A. Nawab, 1978

0   25km.
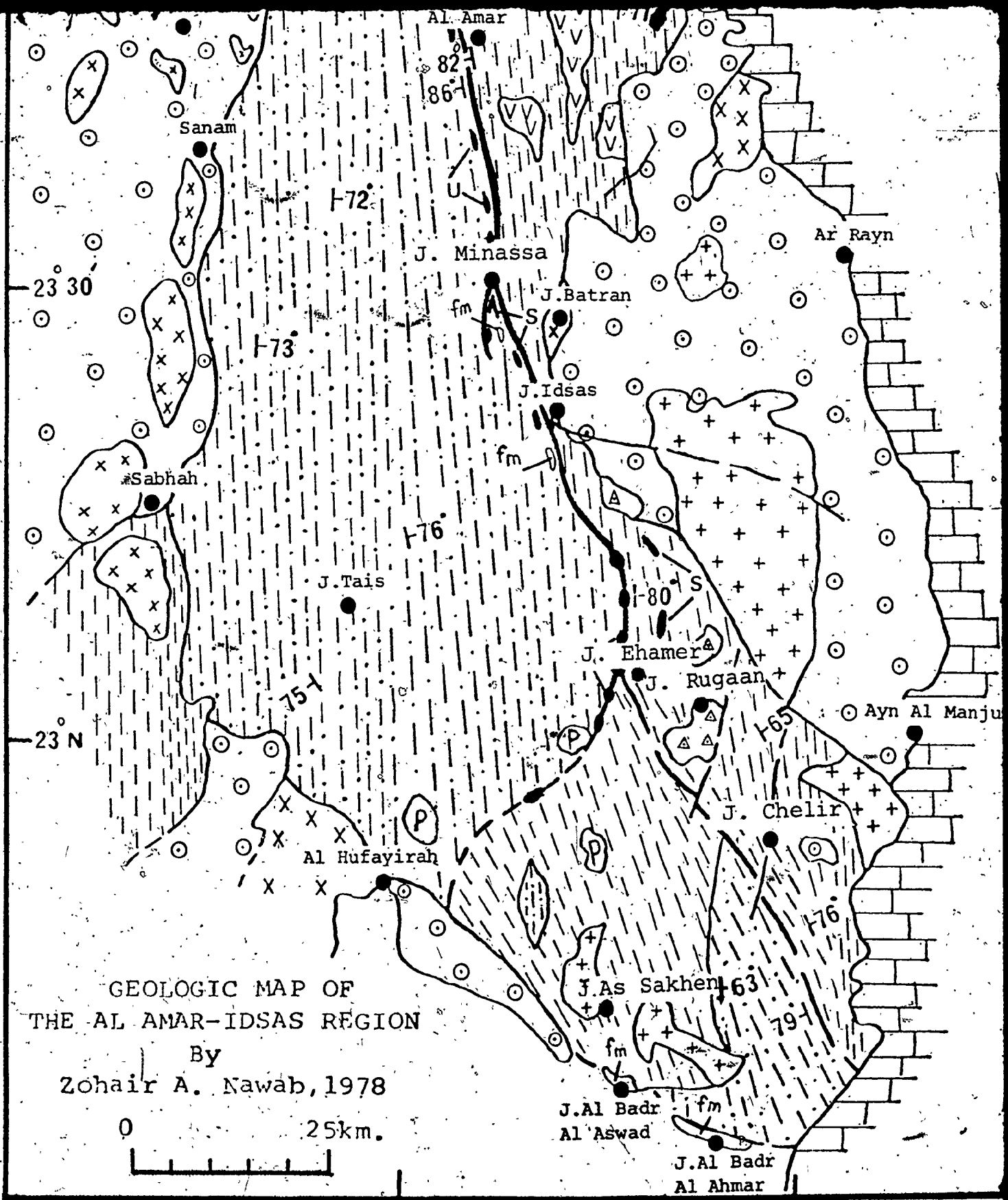
Figure 5- Geologic map of the Al Amar-Idsas region.
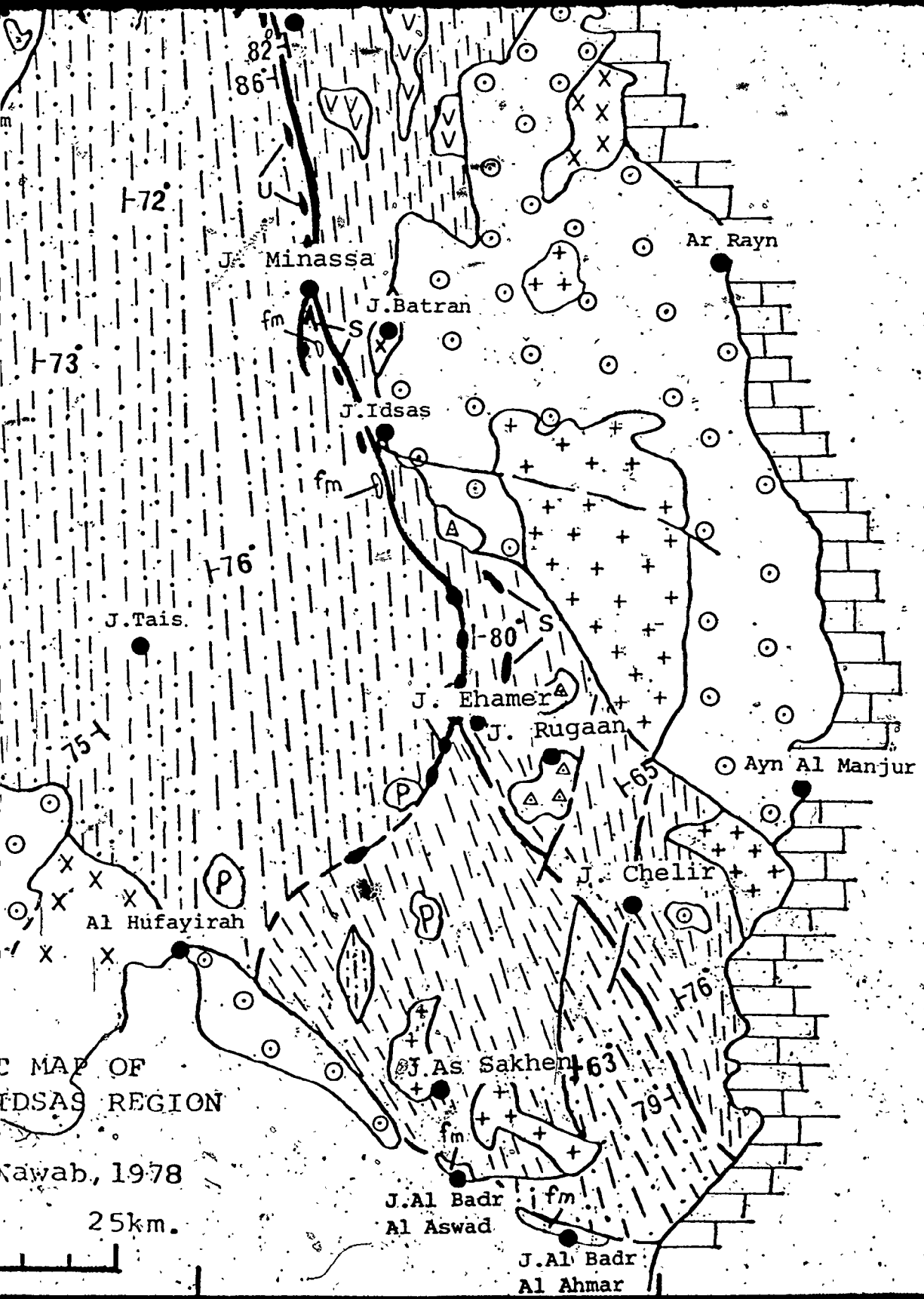
Figure 5- Geologic map of the Al Amar-Idsas region.

flows.*.   Rocks of the Meherga formation are metamorphosed
to amphibolite grade (Plate 1-A).

The upper part of the Halaban Group, designated as
the "Al Amar formation" after the village of Al Amar,
occupies a limited area in the central and southern parts
of the thesis area and is composed of slightly altered to
weakly metamorphosed andesitic and rhyolitic volcanic
rocks. Andesite dominates in the lower part of the suc-
cession and rhyolite dominates in the upper part together
with pyroclastic, agglomerate, volcanic breccia and con-
glomerate.

Gabbro, diorite and granitic rocks commonly occur as
intrusions within the volcanic rocks of the Halaban Group.
The gabbros are dominant in the southern part of the area,
whereas the granites are more common in the northern and
central parts.

Magnetite deposits west of Jabal Idsas are associated
with jointed, fractured and strongly sheared andesites.
The magnetite forms lenticular masses in which the long
axes are parallel to the hinges of small folds in the
andesitic unit. Large bodies of magnetite have not been
found; the magnetite usually occur as grains and inter-
stitial fillings in the andesitic unit (Kahr et al., 1972).

---

*The terms basalt and andesite are field terms used to
  describe quartz poor and quartz rich mafic volcanic
  rocks respectively.

Abdul-Aziz (1974) concluded that the magnetite crystallized
initially from a late stage immiscible liquid-derived from
an iron-titanium rich gabbroic magma, but that it was
subsequently mobilized during deformation and metamorphism.
Cu-Zn-Au ore bodies within the Halaban were explained by
Al Shanti and Mitchell (1976) as volcanogenic stratiform
deposits mobilized and redeposited in fractures within
volcanic breccias and acidic rocks of the Halaban Group.

3.1.1. Meherga formation

The volcanic rocks of the Meherga formation include
both basaltic and andesitic rocks. The 'basalts', forming
layers up to 2 m thick, alternate with beds of slate,
siliceous schist, pyroclastics and some marbles. The
basaltic rocks where metamorphosed to amphibolite are fine
to medium-grained and dark green in colour (Plate 1-B).
In the southern part of the area however the 'basalts' are
sometimes blackish green in colour and contain white pheno-
crysts of feldspar about 0.5 cm long. Locally, the
amphibolites are deformed and have the appearance either
of medium-grained diorite or chlorite schist depending
upon the degree of deformation. Vesicules are sometimes
abundant (Plate 1-C and 1-D) and small veins of calcite
are common.

The 'andesites' form a unit with a maximum thickness
of 10 km. They are invariably metamorphosed and sometimes
highly altered (e.g. the southern and south-central parts

of the thesis area).

In the lower part of the Meherga formation, meta-morphism increases to amphibolite grade. The more meta-morphosed rocks have a well developed foliation trending north-south and dipping steeply 75° due east. Vertical joints in the volcanics trend north (5° to 10°) west.

Badriyah Formation

In the south-central part of the Al Amar-Idsas region, in the area between Jabal Idsas and Jabal Rugaan, ande-sitic rocks occur in contact with and east of the Abt Formation (Fig. 3). This belt of volcanic rocks was mapped by Overstreet et al. (1972) and Kahr et al. (1972) as the "Badriyah Formation" of the Bir Khountina Group (Fig. 3). In the southern part of the thesis area, the Badriyah Formation is in contact with another more easterly located metasedimentary sequence, presented by Overstreet et al. (1972) and Kahr et al. (1972) as the "Abu Sawarir Formation" of the Bir Khountina Group, but considered by Bois and Shanti (1970) and Thekair (1976) as correlative with the Abt schist. The Badriyah Formation is not in physical contact with the Meherga formation of the lower Halaban Group; they are separated by the Al Amar-Idsas fault. However both groups of rocks are petrographically similar and the Badriyah Formation is intruded by gabbroic, dioritic, and granodioritic rocks similar to those cutting the Meherga formation.

If the Abt and the Abu Sawarir Formations are coeval, then the Badriyah Formation may be older than both and is perhaps.stratigraphically equivalent to the Meherga formation.

3.1.1.1. Petrography*

The 'basalts' of the Meherga and Badriyah formations are composed of plagioclase, hornblende, chlorite and minor amounts of biotite, quartz, sericite, epidote, sphene and ilmenite. 'Andesites' are composed of the same minerals as the 'basalts' but also have calcite and hematite. In contrast to the 'basalts' the 'andesites' contain little if any biotite.

Plagioclase occurs as euhedral crystals of andesine and labradorite, about 1 mm long and 0.5 mm wide. The twinning is of albite type. The plagioclase crystals are sometimes zoned and altered to sericite, epidote and/or calcite especially at their centres. Fine-grained plagioclase makes up about 25% to 60% of the matrix of the basalt and andesite respectively. Tiny crystals are sometimes folded and twisted inside large crystals of quartz (Sample 246, Plate 1-E), indicating that some of the quartz crystals are porphyroblastic. Spherulites about 1 mm in

---

*The petrographic descriptions in this thesis are the result of the study of many thin sections. The minerals described under this chapter and the other chapters are not necessarily to be associated together in the same thin section.

PLATE 1

A - Amphibole schist of the lower Halaban Group (Meherga formation).

B - Handspecimen of the amphibole schist. The grains are oriented in one direction.

C - Vesicules in a handspecimen of basaltic andesite. The vesicules are pure white in colour when filled with calcite.

D - Basaltic andesitic unite of the Meherga formation contain abundant of vesicules (south of the hammer head).

E - Fine to medium-grained chlorite (CL) schist. Grains of plagioclase are enclosed by large crystals of quartz (QZ) in the southeastern corner of the picture.

F - Fine-grained chlorite (CL) schist with spherulites about 1 mm in radius and made up of plagioclase (PL) and quartz (QZ).

P L A T E   1

amph.

A

B

0   5 Cm

0   5 Cm

C

D

E   .5 m m.

F   .5 m m.
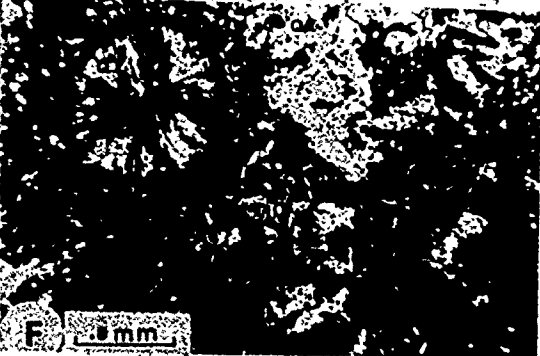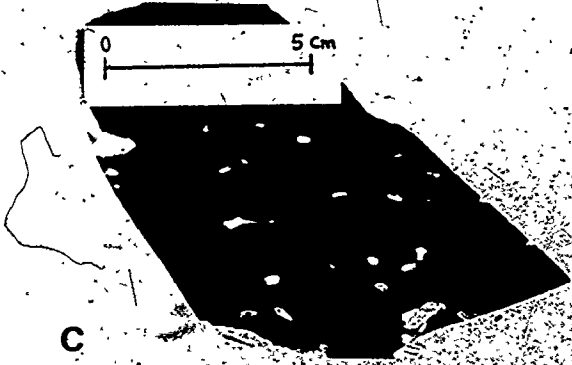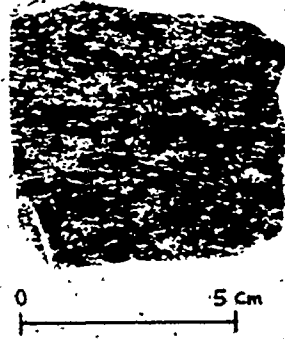
radius are made up of plagioclase and quartz (Plate 1-F). The spherulites may be formed by fast crystallization of feldspars and quartz around nuclei in a viscous magma before its eruption as a flow (Williams et al., 1954, p. 24).

Hornblende crystals are anhedral to prismatic in shape, about 2 mm long and 0.5 mm wide. They are light brown to greenish brown to light green in colour and exhibit two sets of cleavage (Plate 2-A). In sample (283), the hornblende has evidently grown at the expense of pyroxene. Hornblende shows subophitic texture (Plate 2-B), and sometimes is partly replaced by magnetite.

Pyroxene occurs as anhedral to subhedral crystals of hypersthene, about 0.8 mm in diameter in both 'basalt' and 'andesite' (Samples 228, 181). They have a parallel extinction and slight pleochroism. A few fine-grains of pyroxene are present in the matrix. Most of the pyroxene crystals are altered to chlorite.

Biotite tabular crystals of light to dark brown biotite about 0.7 mm long and 0.4 mm wide are common in the 'basalts'.

Chlorite is very abundant and forms prismatic oriented laths or clots possibly replacing hornblende.

Quartz occurs both as oriented anhedral, medium-grained crystals about 0.4 mm in diameter, invariably exhibiting undulatory extinction, and as interstitial, fine-grained crystals about 0.1 mm in diameter (Plate 2-C). The latter

are thought to have formed by metamorphic recrystallisation of the former. The quartz grains form about 2% of the constituent of the basaltic and not more than 10% of the andesitic rocks.

Calcite crystals are subhedral, about 1.2 mm long and 0.6 mm wide. They are products of altered plagioclase.

Epidote is present as anhedral crystals within the plagioclases about 1 mm to 0.5 mm in diameter.

Sericite is very fine-grained, has a high birefrengences, and is usually present in the cores of plagioclase crystals.

Sphene, ilmenite, magnetite and hematite occur as minor components of both 'basalts' and 'andesites'.

3.1.2. Al Amar formation

The Al Amar volcanic sequence is about 5 km thick and composed dominantly of rhyolite. Downwards, the rhyolites are intercalated with andesitic rocks whereas upwards, the rhyolite passes into agglomerates, pyroclastics, volcanic breccias (Plate 2-D) and isolated beds of conglomerate. The Al Amar rhyolites are absent from the area north and south of Jabal Idsas as a result of deformation and/or erosion. In the northern part of the thesis area, the rhyolites are fine-grained, massive and jointed. Where weathered, they are brownish to black in colour but on fresh surfaces they are buff to pink. In the southern part, the rhyolites are often sheared, and in many places

contains abundant disseminated pyrite. In these cases they are gray to light green in colour on both weathered and fresh surfaces.

The rhyolitic and andesitic units of the Al Amar formation unconformably overlie the Meherga formation and associated gabbro-diorite-granodiorite intrusions. Locally, in the northern part of the thesis area, rhyolitic rocks rest unconformably on diorite-granodiorite plutonic rocks. In the southern part of the area, andesites of the Al Amar formation unconformably overlie gnessic granodiorite.

A conglomeratic layer at the top of the Al Amar formation contains clasts of the gneissic granodiorite of the basement complex and of the Halaban Group and associated plutonic rocks, including pebbles of gabbro, diorite, granite and magnetite. The conglomeratic pebbles are about 0.5 cm in size, but locally boulders of gneissic granodiorites up to 10 cm across are present (Plate 2-E). The conglomeratic layer is usually sheared and its matrix is composed of chlorite and calcite.

3.1.2.1. Petrography

The Al Amar rhyolite which is the dominant rock type in the upper Halaban volcanics is soda rich ($Na_2O/K_2O \approx$ 1.8 wt. ratio) and is composed of quartz, plagioclase, and secondary chlorite, epidote, sericite, zircon, and

hematite (Plate 2-F).

Plagioclase occurs as euhedral crystals of oligoclase (An_{16}); the crystals are about 1 mm long and 0.7 mm wide and commonly untwinned and zoned. Quartz occurs frequently as fracture fillings within the plagioclase crystals which are commonly partially altered to epidote and sericite. Fine-grained plagioclase makes about 50% of the rhyolite matrix.

Quartz is found as euhedral to subhedral phenocrysts often exhibiting corrosion features. The grains are about 0.8 mm in diameter and invariably show undulatory extinction. Locally as a result of deformation they are crushed and have sharp edges. Fine-grained quartz makes up about 40% of the rhyolite matrix. Small veins of quartz fill fractures in the matrix and phenocrysts.

Chlorite is present as prismatic crystals about 0.6 mm long and 0.1 mm wide. These crystals are grayish green to dark green in colour. The shape of chlorite crystals indicates that they formed at the expense of hornblende. Fine-grained chlorite crystals are also present in the groundmass.

Epidote occurs either as anhedral crystals about 0.5 mm in diameter replacing plagioclase or as fine grains in the matrix.

Sericite is very fine-grained, has a high birefrengence and occurs as an alteration product of about 10% of the plagioclase.

PLATE 2

A - Xenoblastic crystals of hornblende (AM) in the amphi-
    bole schist. The crystals are about 2 mm long, 0.5 mm
    wide, and characterized by two sets of cleavage.

B - Prismatic crystals of hornblende (AM) show subophitic
    texture. The hornblende crystal grown partially at
    the expense of pyroxene (PY).

C - Fine-grained recrystallized quartz (QZ).

D - Outcrop of volcanic breccia. The fragments are angu-
    lar and about 2 to 5 cm long.

E - Outcrop of conglomerate. The pebbles are about 0.5 cm
    across. West of the hammer head a pebble about 10 cm
    is present.

F - Medium-grained quartz (QZ) of the rhyodacite of the
    Al Amar formation. The quartz crystals are euhedral
    to subhedral in shape.

PLATE 2

A .smm

B .smm

C .2mm

D

E

F .smm
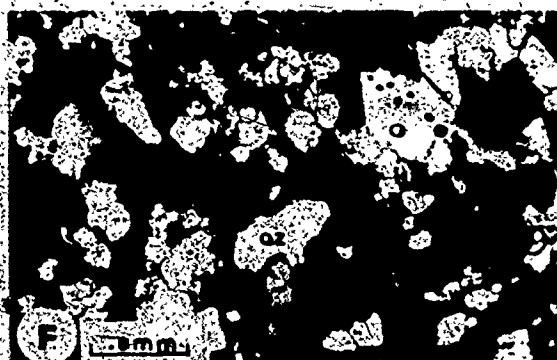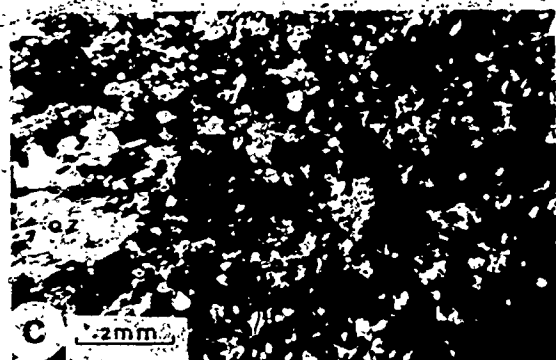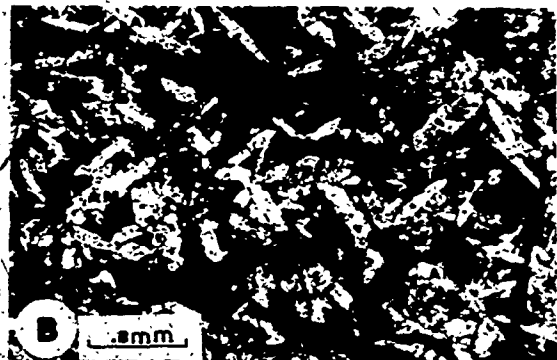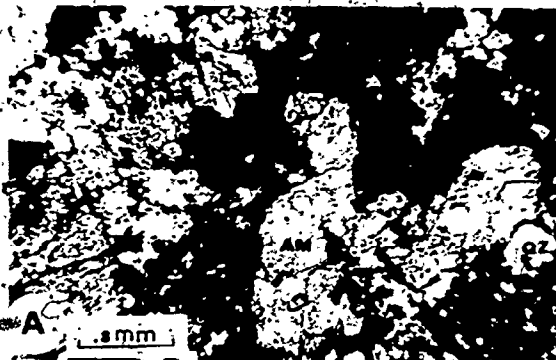
Zircon occurs as very small euhedral crystals enclosed in quartz grains.

Iron oxides are developed by alteration of mafic minerals.

3.1.3. Structure

Nebert (1970) in his study of the area between Al Amar in the west and Al Quwayiyah in the east found that the structure of the Halaban Group was largely obscured by extensive intrusions of granitic rock. In the Mizil and other areas, however, plots of bedding and axial-planar foliations revealed the existence of three sets of complementary tight anticlines and synclines trending north and northeast. In the cores of the anticlines, granite is always present, whereas basic igneous rocks invariably occupy the cores of the synclines (Fig. 6). The general strike and dip of the foliation in rocks of the Halaban Group varies between N 20°W/70°W and N 20°E/72°E and the folds plunge 10° to 30° to the north.

Three well defined fracture systems occur in the Halaban Group, the orientation of the two dominant systems being N 42°W/51°NE and N 68°E/71°NW. Other fractures strike N 63°W/36°SW. Two sets of faults are present in the southern part of the thesis area. The older set is related to the Al Amar-Idsas fault and strikes mainly N 5°-10°E; the younger set intersects the older fault at angles ranging from 40° to 60° and strikes N 10°-20°E. A
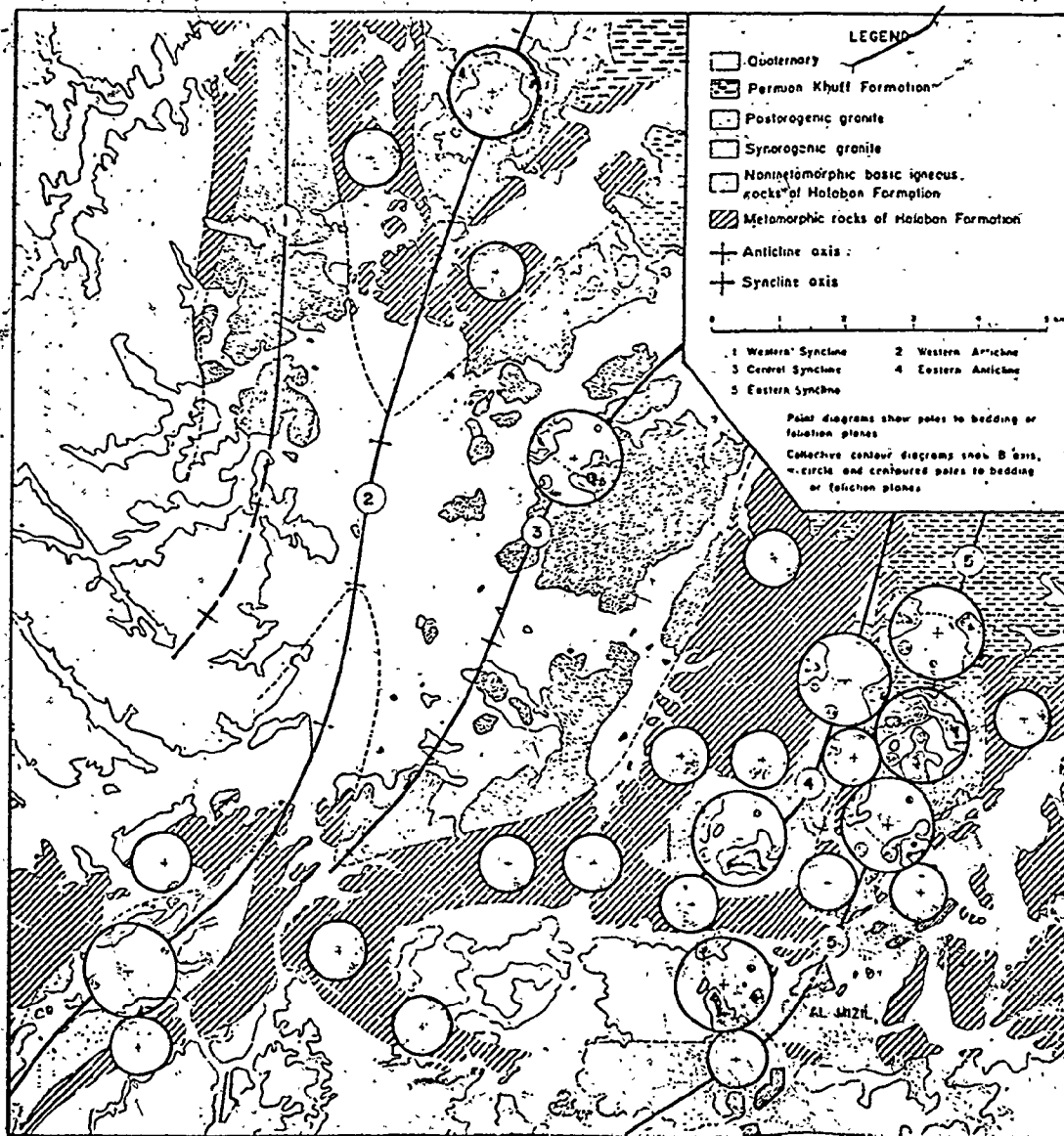
Fig. 6. Point diagrams of poles to bedding or foliation of
the Halaban rocks (Nebert, 1970)

branch of the Al Amar-Idsas fault passes through the

gneissic granodiorites of the basement complex and appears

'to displace a dike cutting the granodiorite, southeast of

Jabal Idsas, for about 1.5-km. The younger faults dis-

place the older fault for about 3 km in the southern part

of the thesis area.

3.1.4. Chemistry

Chromium content of basaltic rocks invariably de-

creases with fractionation. Taylor (1966) showed that the

chromium content of ultrabasic rocks is 2000 p.p.m., ba-

salts contain approximately 200 p.p.m., and andesites

usually less than 50 p.p.m. Chromium crystalizes early

as chromite, and is also contained in pyroxene and to a

much lesser extent in olivine. Nickel, zirconium, yttrium,

titanium, and phosphorous in the Halaban volcanic rocks

are plotted* against chromium in Figure 7. Nickel de-

creases regularly with decreasing chromium, as would be

expected in magmatic fractionation processes involving

crystallization of olivine and chromite, and the Ni versus

Cr trend in the Halaban volcanic rocks is therefore con-

sidered to be a primary igneous variation.

Plots of zirconium, titanium, phosphorous, and yttrium

against chromium permits distinction of four

---

*All variation diagrams in this thesis are:
1) plotted on natural logarithmic scales because this dis-
plays the real fractionation trends more clearly;
2) major oxides are recalculated to 100% (anhydrous).
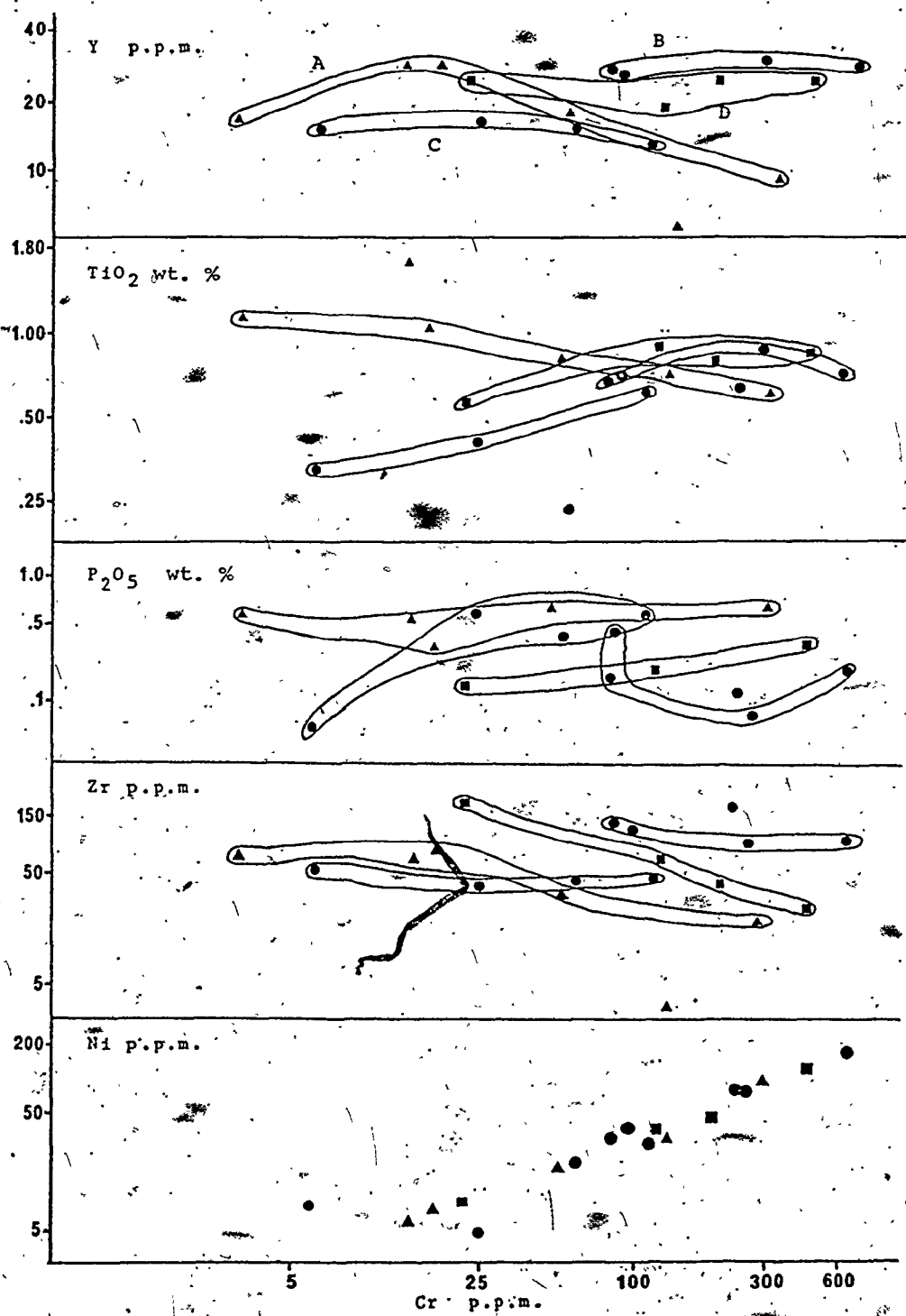
Fig. 7. Plot of Cr against Ni, Zr, P₂O₅, TiO₂, and Y of the Halaban rocks. Some points are anomalous and therefore they were excluded from the groups.

groups* (Fig. 7):

Group A – mafic rocks of the Halaban Group distinguished by a tendency for titanium to increase with fractionation.

Group B – mafic rocks of the Halaban Group characterized by high values of yttrium and zirconium.

Group C – mafic rocks of the Halaban Group with low values of titanium, nickel, yttrium, and zirconium and high values of phosphorous relative to the volcanic rocks of group B.

Group D – mafic rocks of the "Badriyah Formation" with trace element contents intermediate between groups B and C.

There are no obvious trends in the plots of barium, strontium, and rubidium against chromium (Fig. 8), probably reflecting the mobile nature of these elements during low grade metamorphism and alteration.

One of the most common diagrams used to distinguish basaltic rocks is the total alkalies versus silica. However, problems arise in the use of this diagram when the rocks being plotted have been subjected to low-grade metamorphism. Under these circumstances, most major elements and many trace elements are mobile during alteration

---

*The trends of all variation diagrams in this thesis are not based on statistical technique or regression equation. They are interpretations of the data as elements behave during a normal fractionation process and also based on grouping together the samples that belong to the same unit in the field.
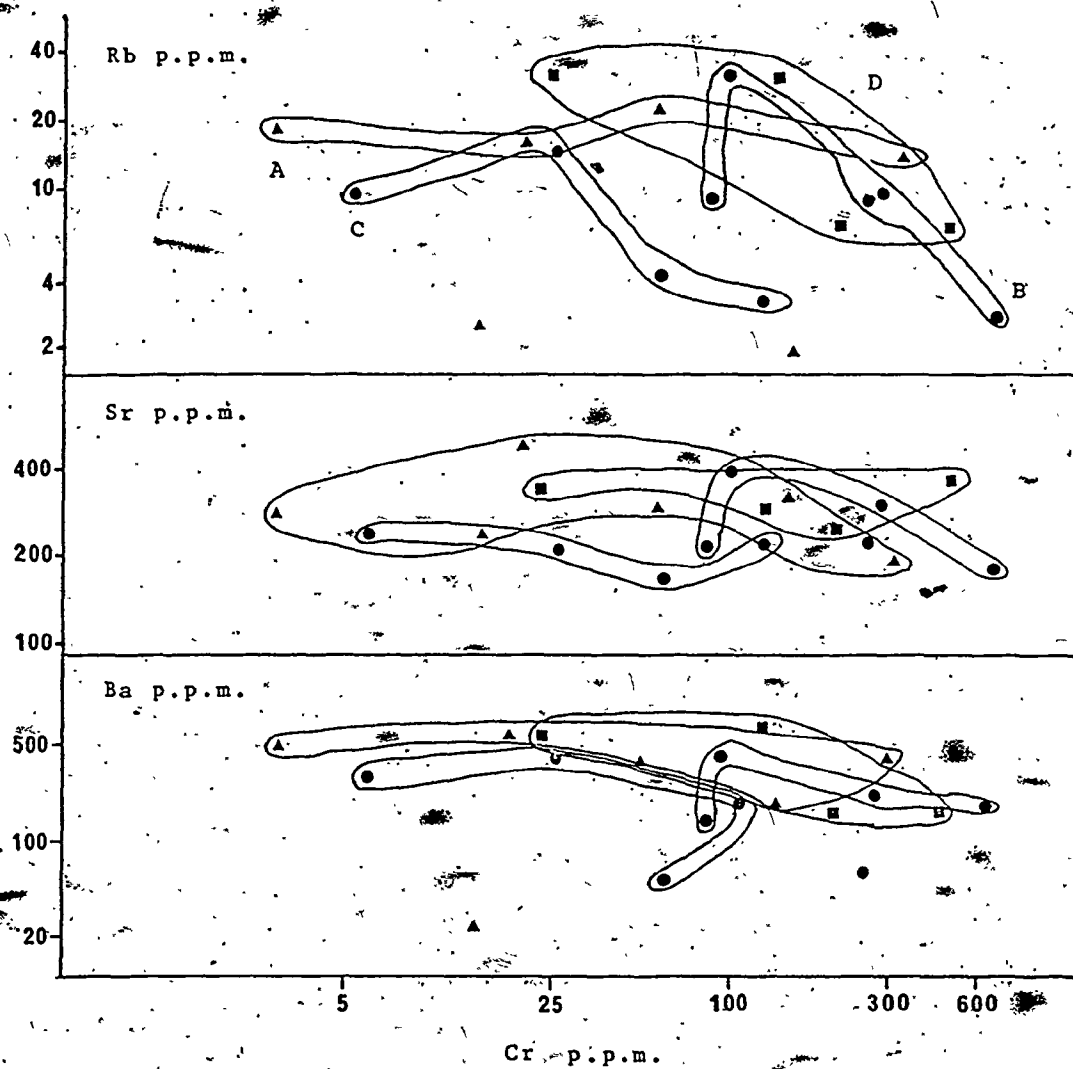
Fig. 8. Plot of Cr against Ba, Sr, and Rb of the Halaban rocks.

(Cann, 1969). However, trace elements such as phosphorous, titanium, zirconium, yttrium and niobium are considered by Nicholls et al. (1971) to be relatively immobile during alteration, a point of view also subscribed to by Cann (1970), Hart (1973), Pearce (1975), Wood et al. (1976), and Coish (1977).

To test the mobility of various elements of the Halaban Group, the trace and major element concentrations of the Halaban intermediate and basic volcanics have been plotted against their zirconium content in Figs. 9, 10, 11, and 12. Chromium, nickel, and titanium tend to decrease whereas yttrium increases with increasing zirconium (Fig. 9) as would be expected in fractional crystallization. Figure 10 reveals no obvious trends. There is no marked tendency for silica to vary with zirconium in any of the four groups with the possible exception of the rocks of group D (Figures 11, 12). Total alkalies tend to increase with increasing zirconium in groups B and C, whereas overall contents of aluminium, total iron, manganese, calcium, and magnesium tend either to decrease or show no systematic variation. Although the trends for most major elements is not very clear, the division of the Halaban volcanic rocks into four groups is nevertheless still evident.

Plots of major oxides versus silica indicate that total iron, magnesium and calcium decrease with increas-
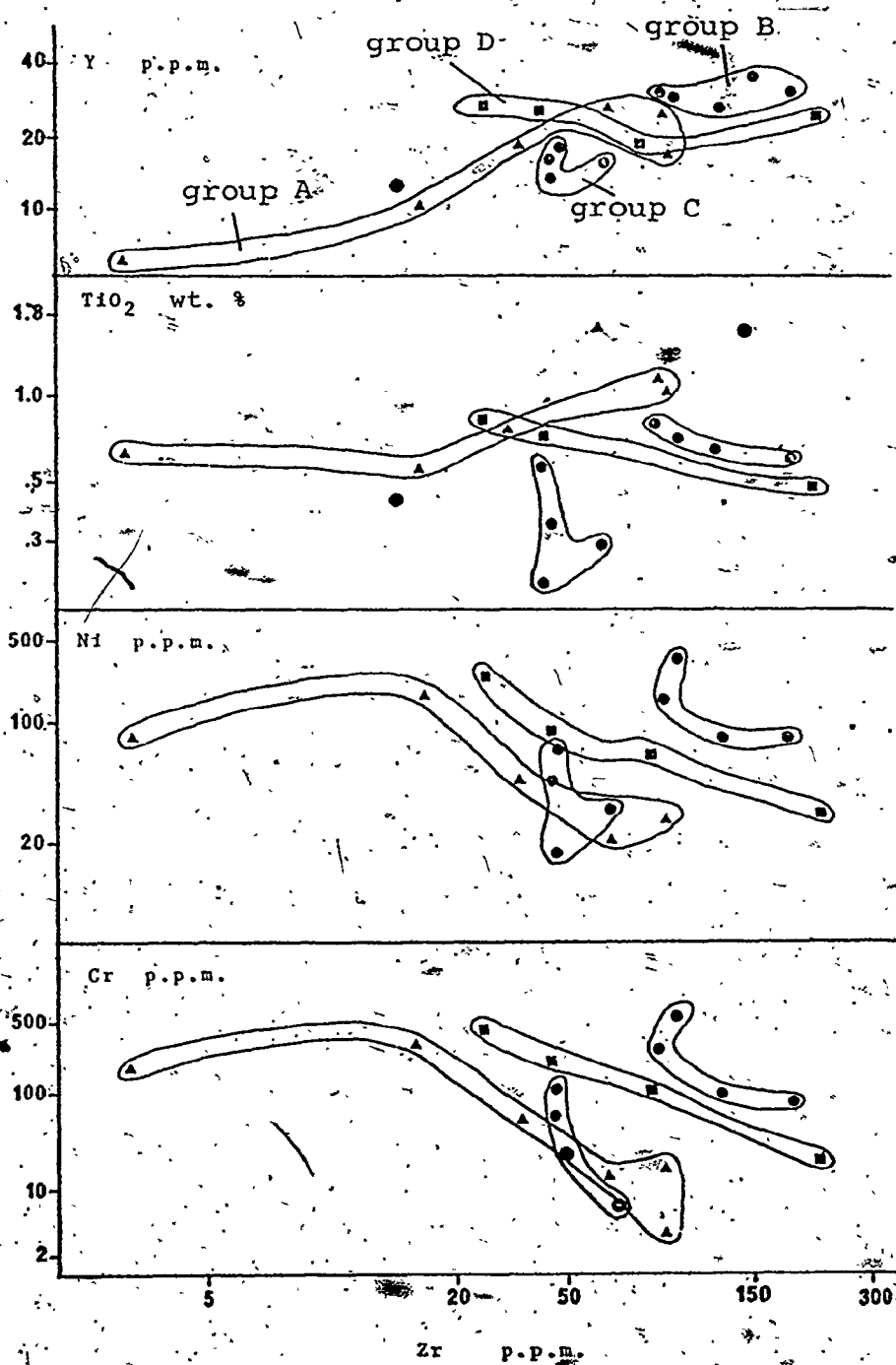
Fig. 9. Zr plotted against Cr, Ni, TiO$_2$, and Y of the Halaban rocks.
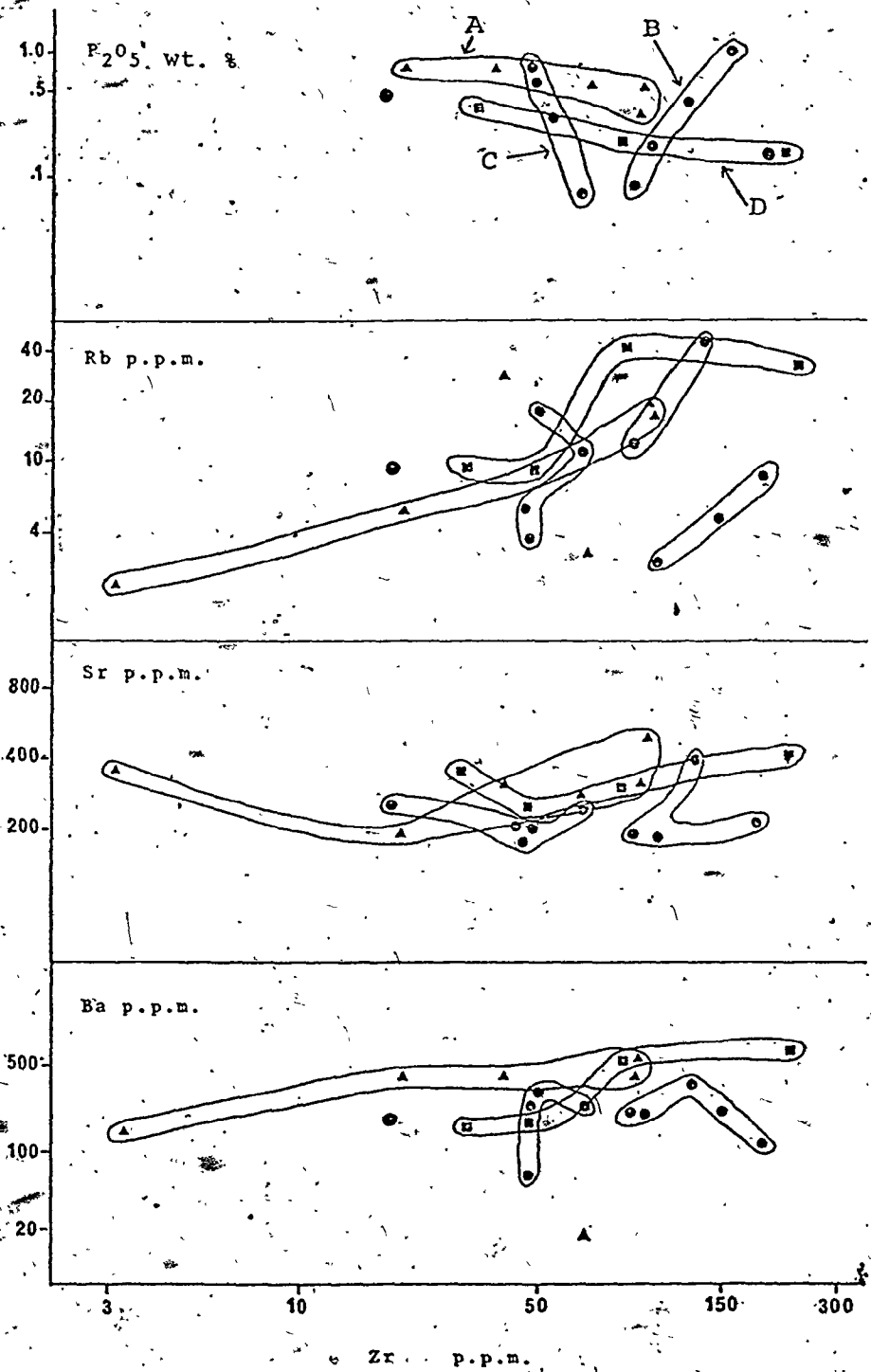
Fig. 10. Zr plotted against Ba, Sr, Rb, and P$_2$O$_5$ of the Halaban rocks.
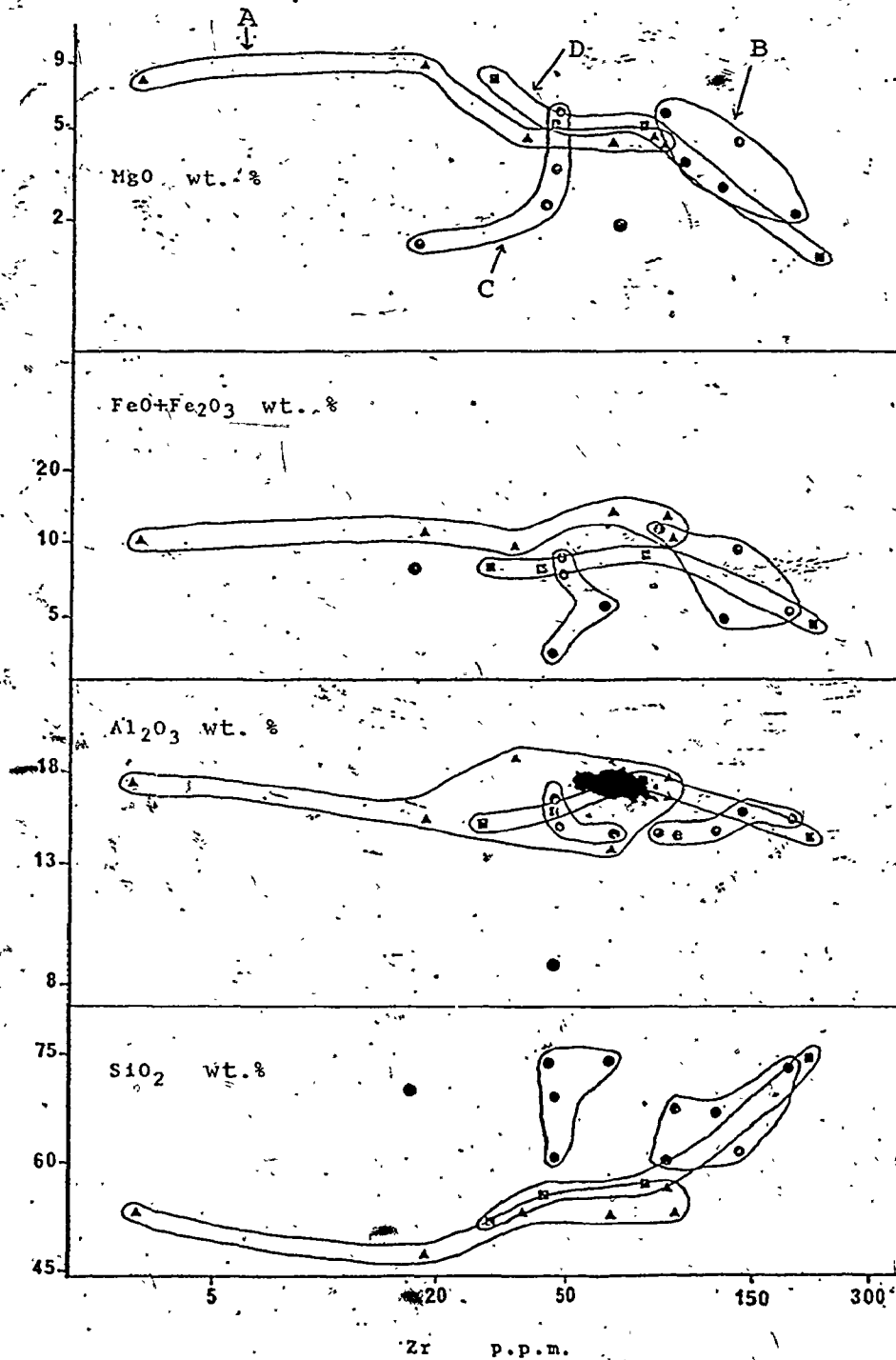
Fig. 11. Plot of Zr against SiO$_2$, Al$_2$O$_3$, FeO+
Fe$_2$O$_3$, and MgO of the Halaban rocks.
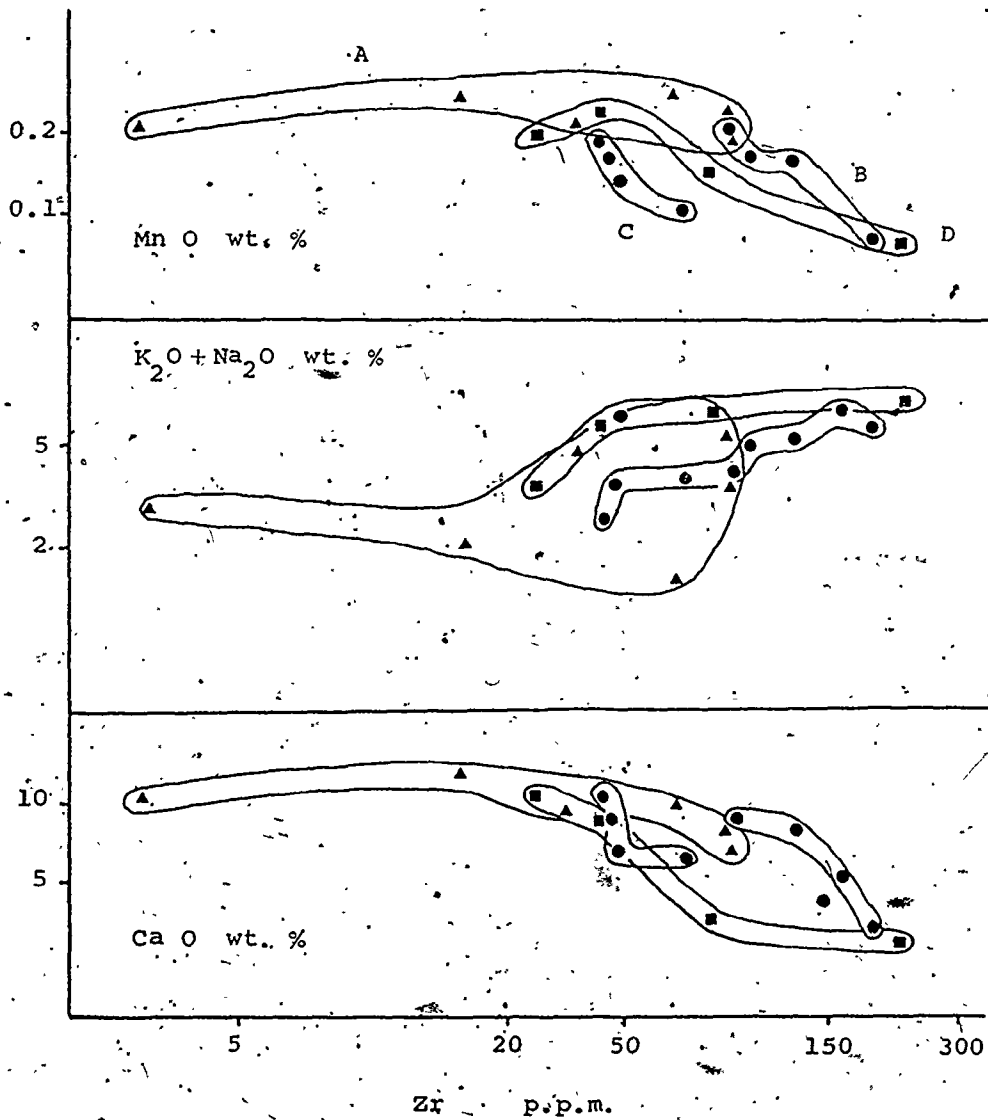
Fig. 12. Plot of Zr against CaO, K_2O+Na_2O, and MnO of the Halaban rocks.

ing silica; whereas total alkalies show little change (Fig. 13).

Rubidium is one of the large cation elements which tend to increase with fractionation (Taylor et al., 1969). Rubidium enters preferentially the potassium position in mica first, and K-feldspars second (Taylor, 1966). Figure 14A reveals a strong covariance between potassium and rubidium.

Barium tends to concentrate during the late stages of fractionation due to its large size. Barium enters K sites of potassic-feldspars and therefore tends to covary with rubidium (Fig. 14B).

Kuno (1966) plotted total alkalies versus silica oxide to divide basic magmas into three types: alkali basalt; high alumina basalt; and tholeiitic basalt. Figure 15 indicates that 'basalt' samples (group A) are located in the alkali basalt and high alumina basalt fields the same as the rocks of group D. Groups B and C both are located within the field of tholeiitic basalt except for one sample which is located in the field of high alumina basalt. The value of this diagram is however doubtful due to the altered nature of the rocks.

The differentiation index, used as a measure of rock basicity (Figure 16), reveals that silica increases with differentiation. Hutchison (1974) stated that average rock types have the following differentiation indices:
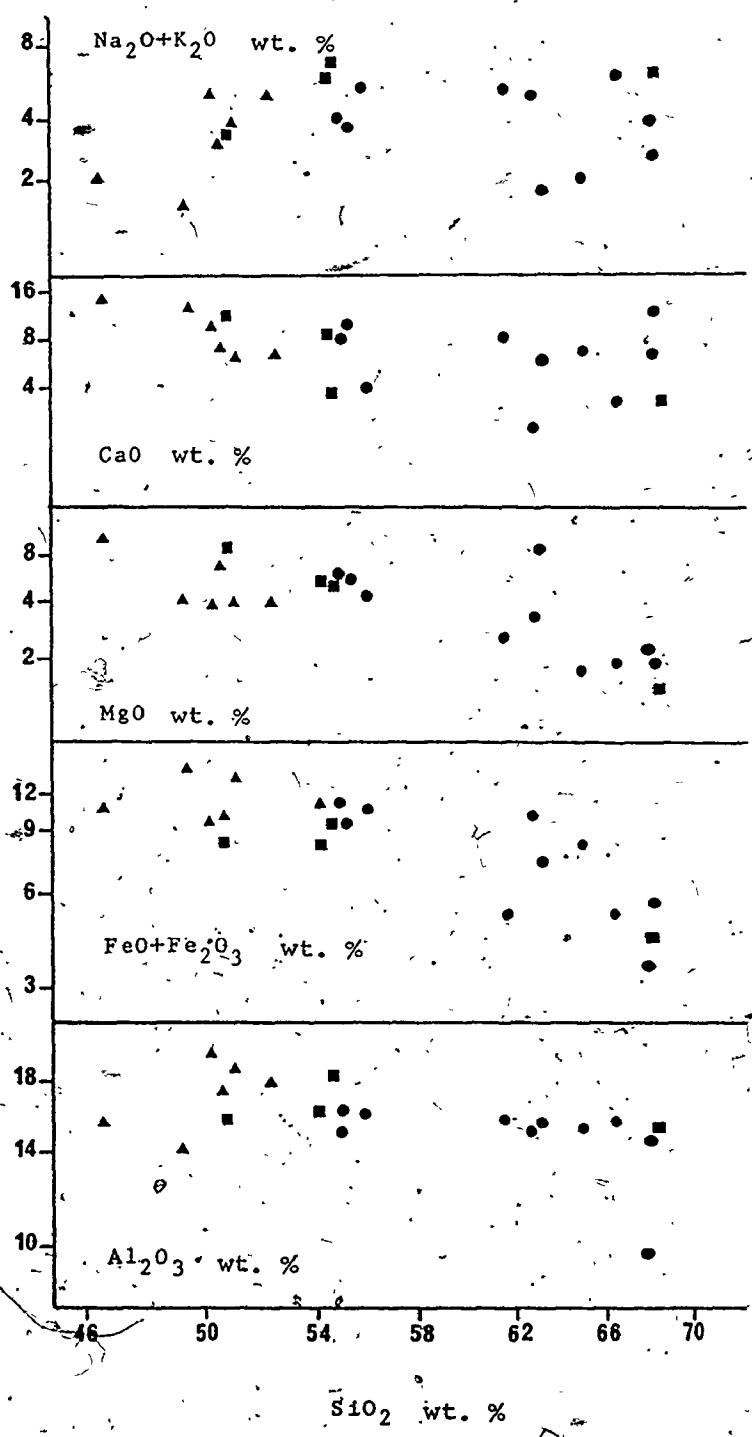
Fig. 13.   Plot of SiO_2 versus Al_2O_3,
$FeO+Fe_2O_3$, MgO, CaO, and
Na_2O+K_2O of the Halaban
rocks.
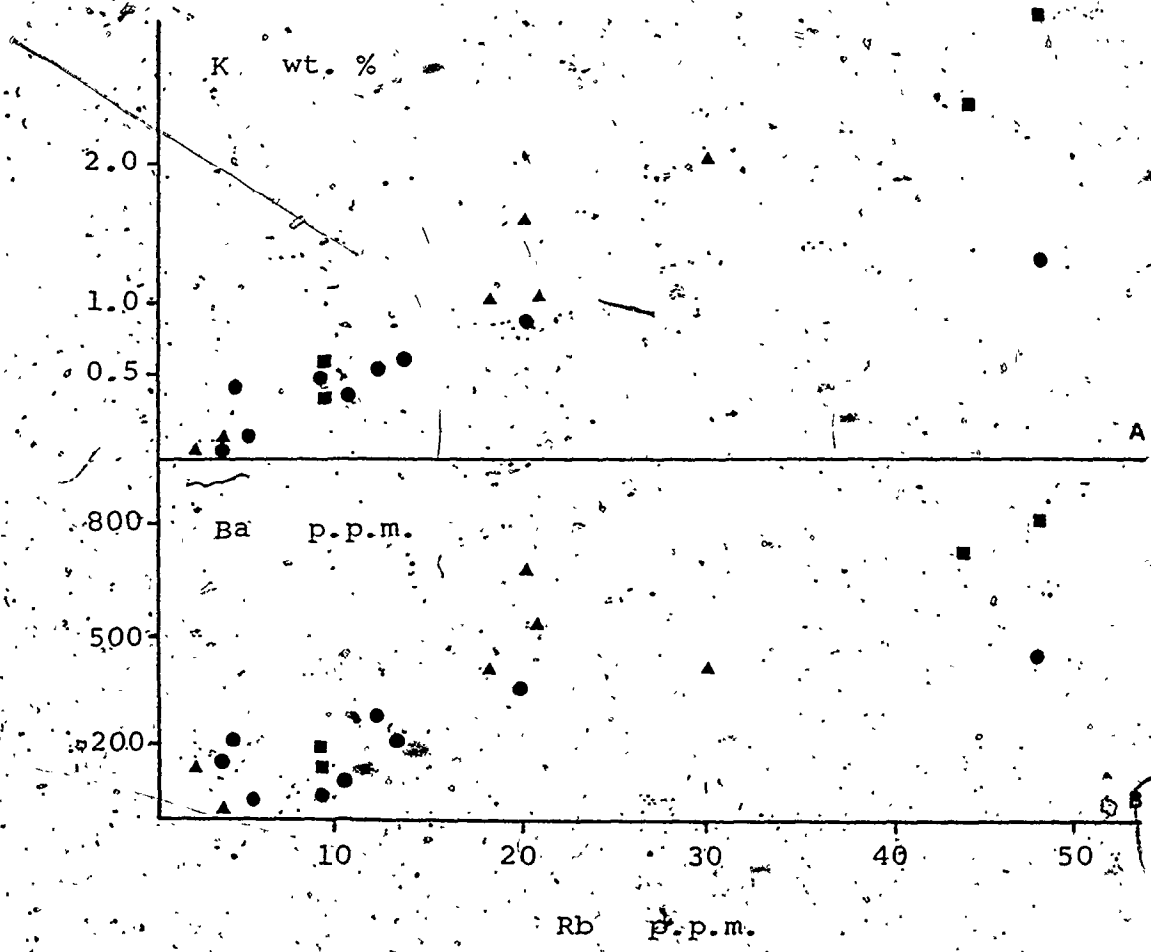
Fig. 14. (A) Variation diagram of Rb versus K, and
(B) Rb versus Ba of the Halaban rocks.
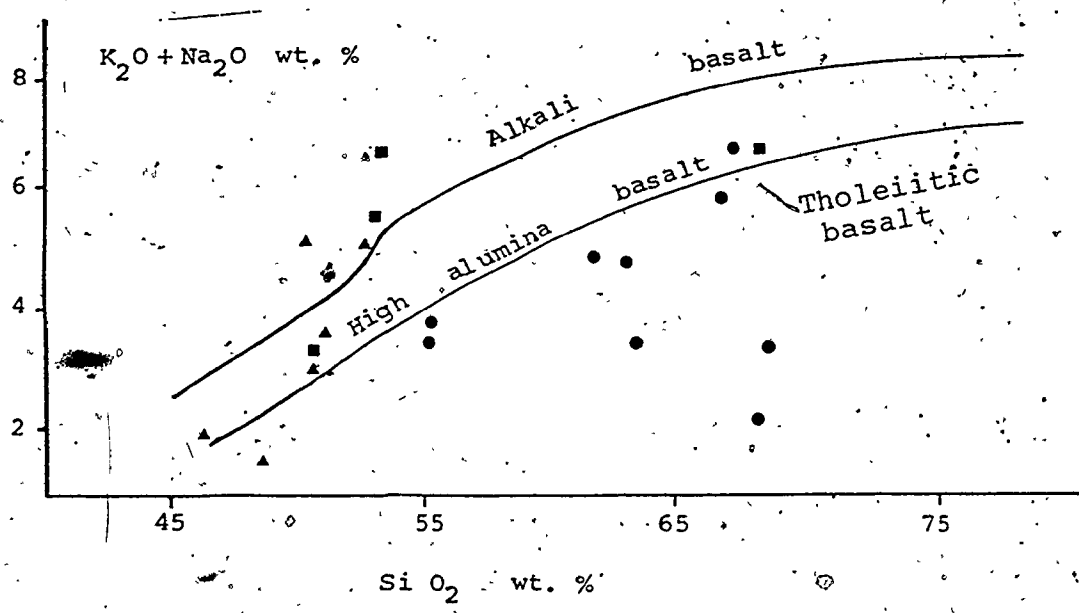
Fig. 15. Kuno's diagram (total alkalies versus silica) applied to classify the Halaban volcanics into the alkali basalt, high alumina basalt, and tholeiitic basalt fields.
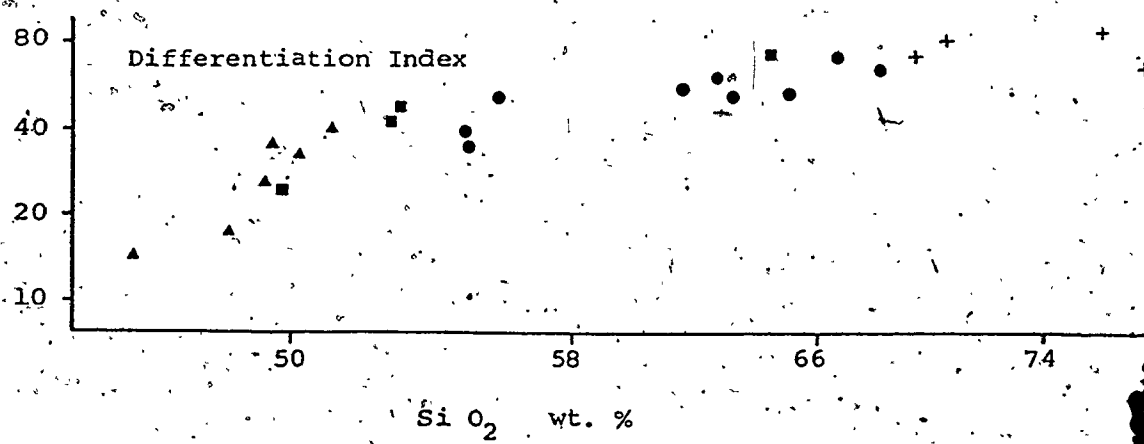
Fig. 16. Plot of the differentiation index (D.I.) versus silica content of the Halaban rocks.

Alkali granite = 93; granite = 80; granodiorite = 67;
diorite = 48; andesite = 53; gabbro = 30; basalt = 35 and
peridotite = 6.

The general trend of the volcanic rocks of the
Halaban Group plotted on an A-F-M diagram (Fig. 17; A =
total alkalies, $F = Fe_2O_3 \times 0.8998 + FeO$, $M = MgO$) co-
incides with the general trend of the calc-alkali suites.
The volcanic rocks exhibit little iron enrichment rela-
tive to magnesium with increasing total alkali and silica
content. On Figure 17, one rhyolite sample (zn 253) plots
well away from other rhyolites. It is characterized by
high values of silica (78.17), total iron (4.74), mangan-
ese (0.20), calcium (5.08) and phosphorus (0.65) and a low
value of aluminium (8.32). This sample is located on an
east-west fault close to a body of mafic igneous rock.

TiO_2 is plotted against FeO^t/MgO on Figure 18 for the
volcanic rocks of the Halaban group. Group A of the
Halaban rocks, characterized by a well defined trend along
which titanium increases with increasing FeO^t/MgO. Group
B marked by increase of titanium then very slight decrease
as FeO^t/MgO increased. Group C starts with increase in
titanium then rapid decrease with increasing FeO^t/MgO.
Group D is characterized by decreasing titanium with in-
creasing FeO^t/MgO.

Average abundances and ranges of major oxides, minor
elements, and CIPW norm values of the Halaban Group are
given in Table 3. Chemical analyses of rock samples belong
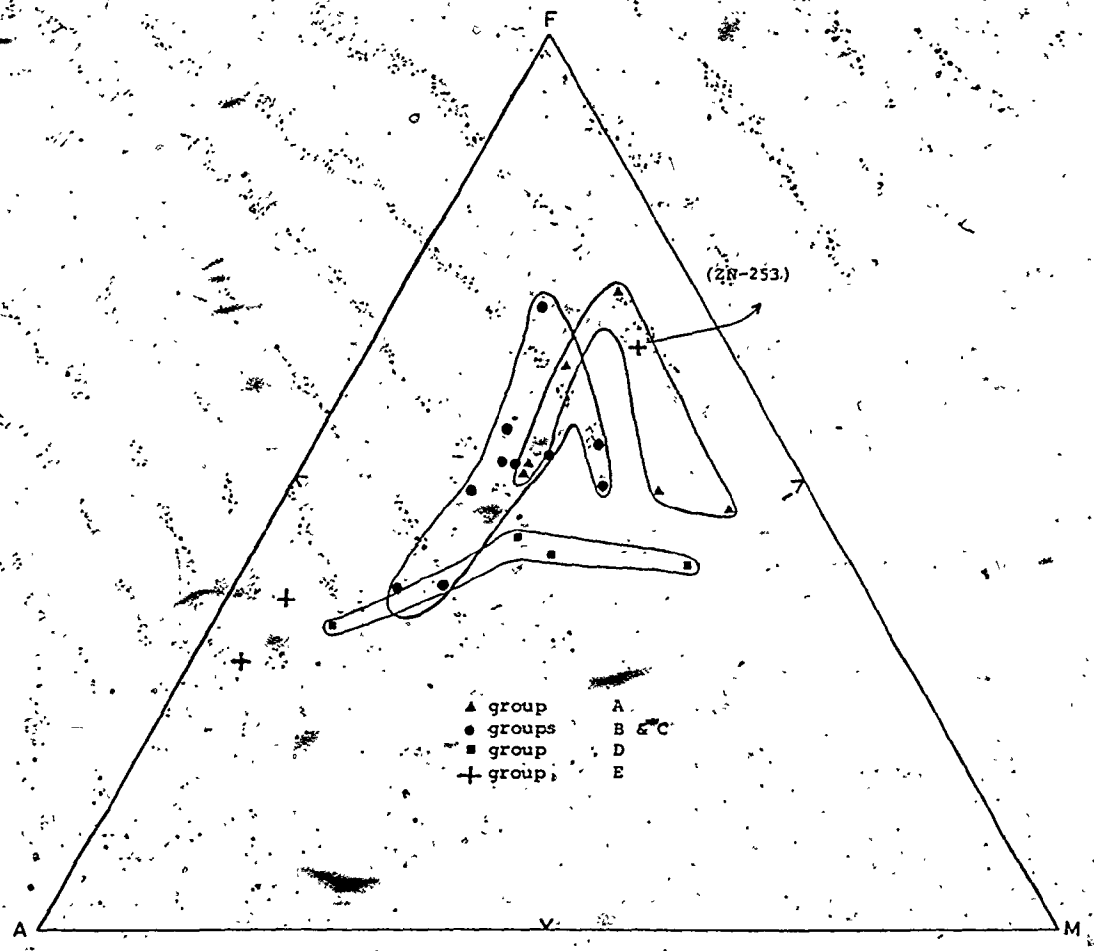
Fig. 17. A-F-M diagram of the calc-alkalic and tholeiitic
rocks of the Halaban rocks.
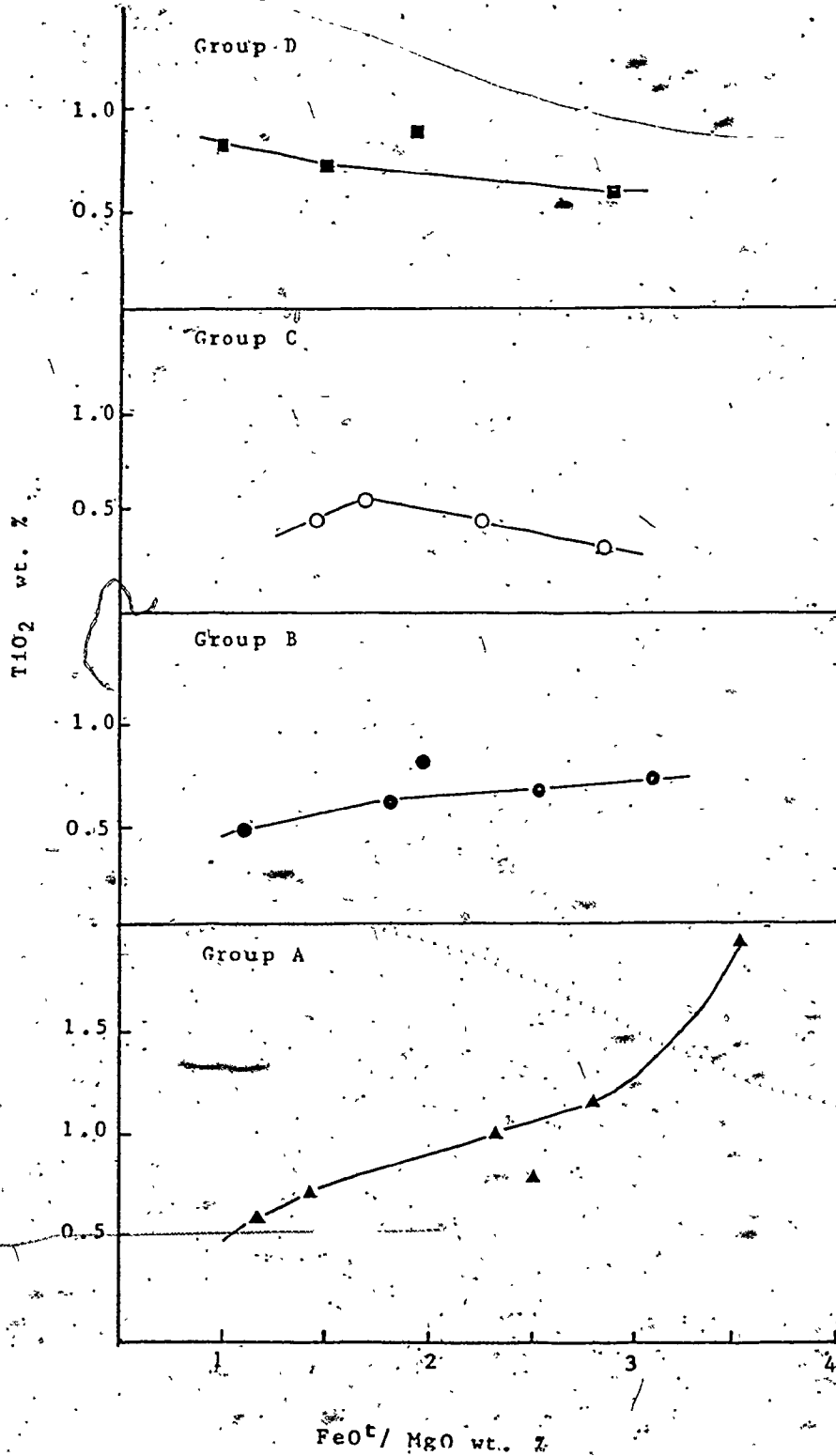
Fig. 18. Plot of TiO$_2$ against (FeO^t/MgO) of the different units in the Halaban Group.

Table 3 — Average and range of chemical composition and CIPW norm values of the Halaban volcanic rocks.

	Group A		Group B		Group C		Group D		Group E	
	Ave. I	Range	Ave. II	Range	Ave. III	Range	Ave. IV	Range	Ave. V	Range
SiO_2	48.08	46.05 - 50.59	60.51	54.42 - 64.67	61.91	55.18 - 67.49	55.71	49.95 - 65.99	74.63	69.55 - 78.17
TiO_2	1.01	0.58 - 1.83	0.66	0.53 - 0.83	0.40	0.30 - 0.54	0.74	0.57 - 0.87	0.31	0.21 - 0.43
Al_2O_3	16.52	13.05 - 19.80	14.78	14.48 - 15.09	13.53	8.58 - 15.88	16.04	14.24 - 18.10	11.63	8.32 - 14.71
Fe_2O_3	2.46	2.22 - 2.75	2.02	1.57 - 2.49	2.00	1.68 - 2.34	2.13	1.79 - 2.31	1.77	1.67 - 1.83
FeO	8.73	7.50 - 11.05	4.76	0.60 - 8.82	4.31	1.60 - 6.93	5.60	2.55 - 7.29	2.49	1.54 - 2.99
MnO	0.23	0.19 - 0.30	0.12	0.02 - 0.20	0.14	0.10 - 0.17	0.17	0.08 - 0.25	0.16	0.14 - 0.20
MgO	5.53	3.97 - 9.52	3.12	1.96 - 5.71	3.21	1.80 - 5.65	5.23	1.43 - 8.56	1.06	0.55 - 1.91
CaO	9.85	6.10 - 14.20	5.52	2.28 - 8.30	8.33	5.95 - 12.27	6.87	3.46 - 11.47	2.39	0.62 - 5.08
Na_2O	2.29	0.90 - 3.29	4.47	2.96 - 5.78	2.63	2.10 - 3.14	3.80	2.61 - 5.16	4.36	0.01 - 6.60
K_2O	1.01	0.06 - 2.01	0.61	0.07 - 1.36	0.57	0.15 - 0.98	1.68	0.45 - 3.13	0.41	0.07 - 0.64
P_2O_5	0.45	0.00 - 0.68	0.20	0.08 - 0.47	0.42	0.06 - 0.66	0.18	0.15 - 0.33	0.23	0.01 - 0.65
Total	96.16		96.77		97.45		98.22		99.44	
$\frac{FeO^+}{MgO}$	1.98		2.11		1.90		1.44		3.85	
Norms (CIPW)										
Q	2.05	.0 - 6.30	15.92	6.06 - 21.17	24.77	7.31 - 33.16	6.35	.0 - 24.59	40.45	23.08 - 62.57
or	6.21	0.35 - 11.97	3.73	0.42 - 8.53	3.37	0.96 - 5.80	10.19	2.65 - 19.01	2.42	0.42 - 3.82
ab	20.15	7.69 - 30.20	39.12	25.27 - 50.54	22.68	19.29 - 26.50	32.58	22.40 - 43.33	37.23	0.03 - 56.40
an	31.69	27.26 - 34.99	17.24	10.45 - 24.65	23.13	14.70 - 27.82	20.07	14.24 - 29.09	10.39	3.03 - 7.15
cor	0.58	.00 - 3.48	0.66	0.00 - 3.03	0.27	0.00 - 1.07	0.76	.0 - 3.02	0.22	0.02 - 0.57
di	13.11	.00 - 26.30	7.64	0.00 - 13.78	7.71	0.00 - 15.65	10.59	.0 - 21.28	0.00	0.00 - 0.00
hy	15.20	6.19 - 27.22	7.32	0.00 - 21.01	10.35	0.00 - 19.18	10.20	.0 - 24.36	5.56	2.75 - 8.32
ol	4.28	.00 - 12.75	0.00	0.00 - 0.00	0.00	0.00 - 0.00	3.99	.0 - 9.55	0.00	0.00 - 0.00
mt	3.71	3.24 - 4.26	2.65	0.48 - 3.64	2.96	2.64 - 3.38	3.14	2.68 - 3.44	2.58	2.44 - 2.68
il	2.00	1.11 - 3.72	1.29	1.04 - 1.59	0.68	0.43 - 1.02	1.47	1.12 - 1.69	0.60	0.40 - 0.82
ap	1.13	.00 - 1.62	0.48	0.19 - 1.18	1.01	0.14 - 1.56	0.43	.0 - 0.80	0.55	0.02 - 1.54
Trace elements (P.P.M.)										
Cr	86	3 - 307	256		51	6 - 117	189	21 - 436	1	0 - 1
Ba	377	21 - 697	213		235	54 - 371	504	180 - 861	194	63 - 285
Ni	24	0 - 82	84		15	4 - 31	51	9 - 121	5	0 - 10
Nb	3	0 - 7	8		5	3 - 7	6	6 - 7	10	8 - 12
Zr	51	3 - 94	132		49	42 - 63	90	29 - 213	246	104 - 318
Y	18	6 - 28	36		16	14 - 18	24	19 - 26	65	27 - 88
Sr	336	197 - 591	252		226	177 - 253	353	266 - 437	148	82 - 277
Rb	16	2 - 30	17			4 - 20	28	9 - 48	7	2 - 13

I = 6 samples.   II = 5 samples.   III = 4 samples.   IV = 4 samples.   V = 3 samples.

FeO^+ = total iron $(Fe_2O_3 \times 0.8998 + FeO)$.

to Halaban Group are given in Appendix 2.

3.2. Metagraywacke units

3.2.1. Abt schist

The Abt schist as described by Bramkamp et al. (1956, Map I-212A; 1958, Map I-207A; 1963, Map I-206A) and Jackson et al. (1963, Map I-211A) is composed of sericite-chlorite schist, derived mostly from sedimentary rocks, and minor amount of marble. The name Abt schist first appears on geologic map I-270A, scale of 1:2,000,000, of the Arabian Peninsula published by the U.S. Geol. Survey and Arabian American Oil Company (1963). The same unit mapped by Mytton (1966) on Mineral Investigations Map MI-4, scale of 1:100,000, as "sc" is described as consisting chiefly of quartz-biotite schist, chlorite-biotite schist and sericite-biotite schist with abundant pinch and swell layers of quartz lying within the regional foliation. Nebert (1970) mapped the Abt schist as well foliated paraschist striking between NNW and NW and dipping steeply 90° to 60° east or west. Al Shanti (1973) mapped the Abt schist as tightly folded chlorite schist with bedding and foliation mostly dipping to the east.

3.2.1.1. Geology and petrography

The Abt schist in the thesis area forms a belt of low hills, about 30 to 40 km wide and 200 km long,

located between the Al Amar-Idsas fault in the east and a
belt of post-tectonic granites in the west (Fig. 5). The
Abt schist reaches a maximum width of about 40 km in
the central part of its outcrop area and a minimum of 3 km
in the southern part. Sedimentary features such as cross
bedding (Plate 3-A) are still preserved. To the north,
the Abt schist is separated from the Halaban Group by the
Al Amar-Idsas fault, while in the central part, it appears
to be in tectonic contact with volcanic rocks of the
Badriyah Formation (Overstreet et. al., 1972). To the
northwest, the Abt schists are underlain either strati-
graphically or tectonically by the Ar Radainyah formation,
an eastward dipping succession of quartzo-feldspathic
rocks and calcareous units, including marble, character-
istic of shore line facies (Al Shanti, 1973).

The western and southwestern parts of the Abt schist
are characterized by a higher metamorphic grade in the
vicinity of large, elongated post-tectonic granites. Three
metamorphic zones developed from west to east, they are:
    a - biotite-hornblende schist: A medium-grained, dark
green to brown coloured rock, composed of plagioclase,
biotite, chlorite and epidote. Quartz occurs as anhedral,
oriented grains exhibiting undulatory extinction, and as
interstitial, fine-grained crystals formed by recrystal-
lization of the former. Hornblende occurs as subhedral
crystals, brown to brownish green in colour; some horn-

blendes appear to have grown at the expense of pyroxene. Anhedral crystals of garnet are locally present, and ilmenite and hematite are found as opaque minerals (Plate 3-B).

b - chlorite-biotite schist: Fine to medium grained, light green to light brown in colour; composed of quartz, plagioclase, epidote, chlorite, tabular crystals of light to dark green biotite and accessory ilmenite and sphene (Plate 3-C).

c - sericite-chlorite schist: A very fine-grained light gray to light green coloured rock (Plate 3-D); composed of quartz exhibiting undulatory extinction, chlorite as tiny oriented laths, sericite, epidote as equigranular crystals, plagioclase as altered crystals. calcite either as grains or tiny veinlet, and ilmenite as an accessory mineral.

Some biotite-chlorite rich layers of the Abt schist in the central and northern parts of the thesis area may have been originally mafic lava, and the numerous quartz-calcite sericite layers may have been calcareous shale and tuffaceous marl (Plate 3-E).

Abu Sawarir Formation

In the southern part of the thesis area, Overstreet et al. (1972) recognized a weakly metamorphosed to un-metamorphosed, medium to coarse-grained graywacke and calcareous graywacke, grayish green in colour with sedi-

mentary features such as cross bedding and graded bedding still preserved. Overstreet et al. (1972) called this unit the "Abu Sawarir" Formation of the lower Bir Khontina Group (unit sg; Fig. 3).

Bois and Shanti (1970) correlated the Abu Sawarir Formation with the Abt schist in the north (unit hc; Fig. 2). Thekair (1976), in the area south of Jabal Minassa, correlated the schist sequence east of the ultramafic belts, mapped as unit sv, with the Abt schist (unit sc; Fig. 4).

3.2.1.2. Marble units

Eijkelboom et al. (1966) mapped these marble units as making up the upper part of an unmetamorphosed volcanic sequence located along the Al Amar-Idsas fault. Kahr et al. (1972) introduced the term "Fawara Formation" to include limestone, dolomite, marble and silicified carbonates although they admitted that not all of these carbonate rocks are similar.

The carbonate rocks were subsequently divided by Thekair (1976) into three groups; one group, which he designated as the Sihailiya carbonate, he considered to be sedimentary. The two other categories of carbonate rocks were referred to as the Halaban carbonate and the Shigran carbonate. The latter are altered ultramafic rocks and will be discussed later.

The Fawara Formation (Sihailiya carbonate) are black,

blue, and brown marbles of sedimentary origin which in the
central and southern parts of the thesis area separate
graywackes of the Abt schist (Abu Sawarir Formation) from
the volcanics of the Meherga formation (Badriyah Formation).
The marbles form isolated lenses and ridges of various
size and shape. The thickness of the lenses ranges from
1 m to 1 km, their length from 20 m to about 7 km and their
height from 10 m to about 200 m above the plain level.
The contact of the marbles with the surrounding country
rock may be sharp or gradational.

In the central and southeastern parts of the Al Amar-
Idsas region, the marbles have sharp contacts with amphi-
bole schist and calcareous sandstone beds respectively.
In the southern part, gradational contacts are found be-
tween the marbles and surrounding calcareous clastics and
tuffaceous rocks of the Abt schist (Abu Sawarir Formation).
At Jabal Al Badr Al Ahmar in the southern part, the marble
is underlain by a thin bed of conglomerate (Plate 3-F)
whose interstices are filled by carbonate materials. These
marbles are reddish brown in colour on both fresh and
weathered surfaces. They are medium to fine-grained,
thinly bedded and gently folded. Coarse to medium-grains
of white calcite are present. Cavities are filled with
precipitated calcite, first coating the walls, then fill-
ing the spaces. At Jabal Al Badr Al Aswad, about 7 km
north of Jabal Al Badr Al Ahmar, the marble is black in

PLATE 3

A - Graywacke of the Abt Formation contain cross bedding, a sedimentary feature.

B - Biotite-hornblende schist consist of biotite (B), hornblende (HD), chlorite (CL), sphene (SPH) and ilmenite.

C - Chlorite-biotite (B) schist consist of quartz, albite, chlorite (CL), epidote and ilmenite. The grains are very fine.

D - Handspecimen of the chlorite-sericite schist with tiny veinlets of calcite perpendicular to the foliation planes.

E - Handspecimen of folded calcareous and quartz layers of the Abt Formation.

F - Conglomeratic bed underlain Jabal Al Badr Al Ahmar marble. The pebbles are cemented by carbonate materials.

PLATE 3

A

B   .8mm

C   .8mm

0   5 Cm

D

0   5 Cm

E

0   5 Cm

F
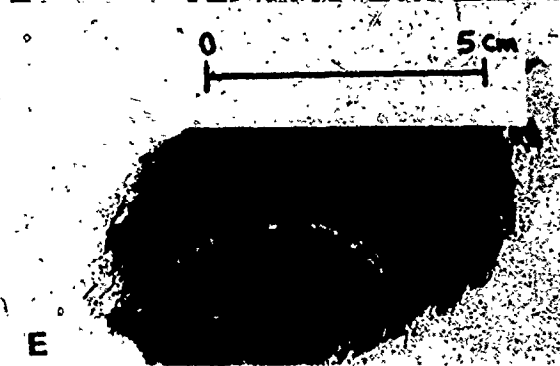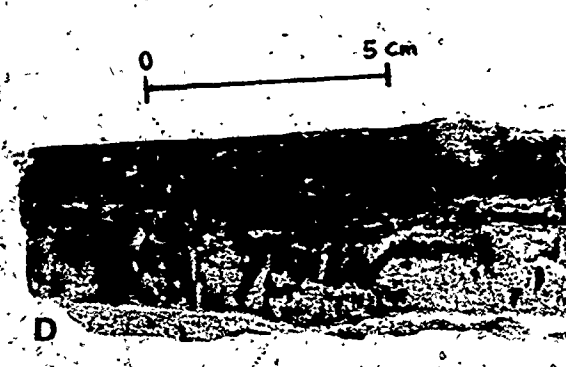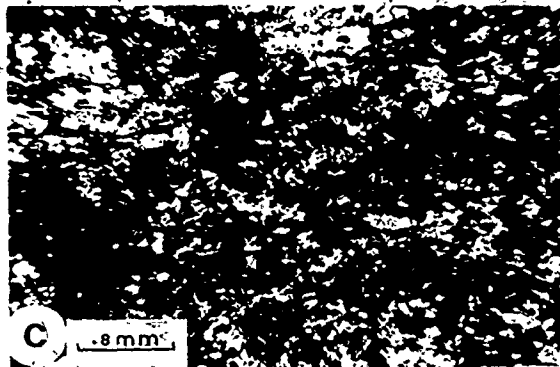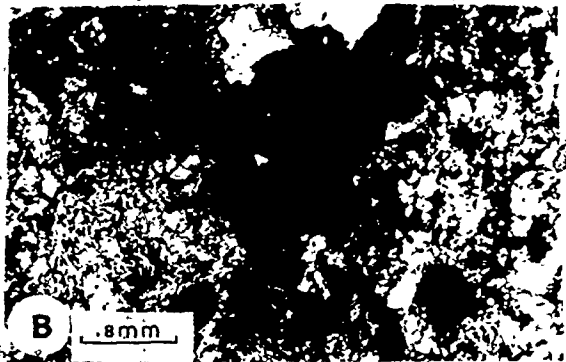
colour on both fresh and weathered surfaces. The marbles which are locally folded are thick bedded (about 2 m) and very fine-grained (Plate 4-A). In the central part of the thesis area, the marbles are buff, pale brown and gray in colour on weathered surfaces but dark gray to black-blue in colour on fresh surfaces. The marbles of the central part are massive; although locally they are bedded, gently folded and contain abundant calcite veins.

All the marbles are composed of very fine-grained calcite and variable amounts of secondary crystalline quartz. TheKair (1976) found using x-ray diffraction methods that dolomite is the predominant component of these marbles.

Table 4 illustrates the average and range of chemical composition of five marble samples. The variation in silica, magnesium and calcium content reflects the degree of hydrothermal activity along the fault plane at the base of the carbonates. Chemical analyses of individual samples are given in Appendix 3.

3.2.1.3. Structure

The Abt schist is tightly folded; bedding and foliation both dipping steeply east or west. The general strike of the foliation varies between N 10°E and N 30°W and dip between 55° east or west, and 90° (Plate 4-B). There are three fracture cleavage systems in the Abt schist Forma-

Table 4 - Average and range of chemical composition
of the marbles.

	Ave. I	Range		Ave.	Range	
SiO$_2$	13.41	2.30 - 30.43	Cu	2	0 -	6
TiO$_2$	.07	.02 - .09	Ba	29	2 -	81
Al$_2$O$_3$	.41	.06 - 1.06	Ni	11	0 -	58
Fe$_2$O$_3$	.72	.10 - 1.64	Nb	2	0 -	5
FeO	.33	.15 - .82	Zr	6	0 -	17
MnO	.07	.02 - .23	Y	3	0 -	5
MgO	14.23	.59 - 22.41	Sr	448	53 - 1808	
CaO	34.21	22.97 - 54.22	Rb	4	1 -	9
Na$_2$O						
K$_2$O	.02	0 - .10				
P$_2$O$_5$	.02	0 - .06				
L.O.I.	37.35	30.62 - 42.44				
Total	100.84					

I = average of 5 samples.

tion: N 45°W/75°SW; N 65°E/70°SE; and less commonly N 35°E/55°NW. The latter system of fractures is usually filled with calcite minerals (Plate 4-C). Locally the Abt schist exhibits a secondary crenulation (Plate 4-D). Crenulation represents inhomogenous deformation and changes in the total volume of the rocks (Hobbs et al., 1976, p. 40).

Aerial photographic studies indicates the presence of many lineaments within the Abt schist. In the field however it is difficult to determine the nature of the lineaments because of the low relief and extreme weathering of the fine-grained schists. On the east, the Abt schist is bordered by the Al Amar-Idsas fault, at least two branches of which pass through the Abt schist in the central and southern parts of its outcrop area. Plates 4-E and 4-F show faults in the Abt schist displacing andesite dikes about 5 cm and 1 m, respectively. The nature of the folds present in the Abt schist are illustrated in Plate 5-A, 5-B, 5-C, and 5-D. Most commonly, the folds are inclined although the other types of folds are also present. A plot of poles of bedding and foliation (Fig. 19) shows that the axial planes of folds in the Abt schist tend to strike north-south, dipping 75° to 80° west whereas the folds plunge about 10° to the south-southwest.

Quartz veins are abundant throughout the Abt schist.
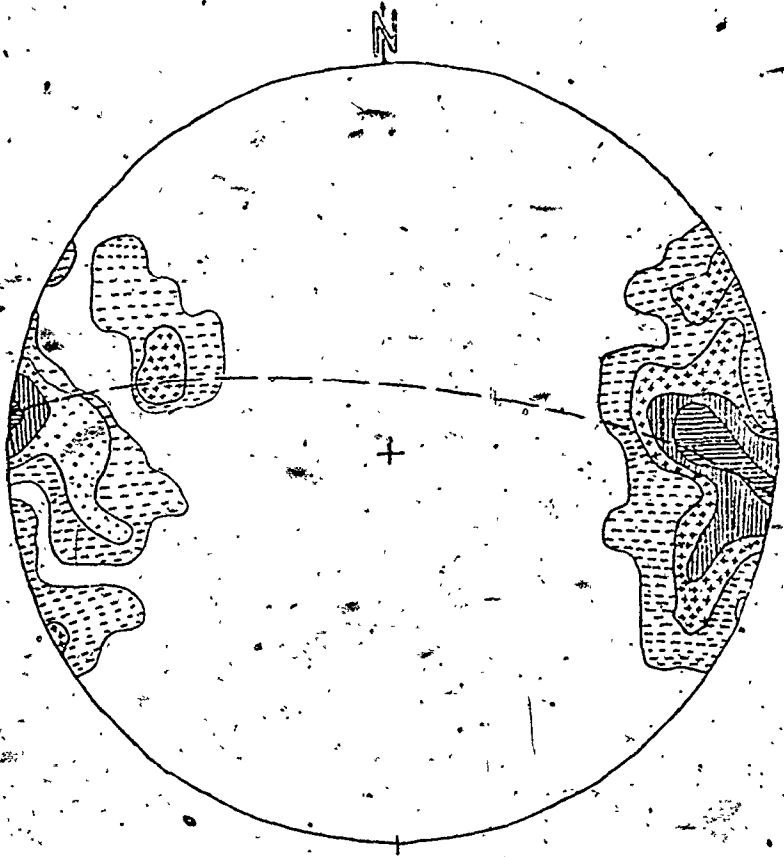
Fig. 19. Sterogram of poles to bedding
and foliation of the Abt
Formation.

PLATE 4

A - Beds of marble about 2 m thick at Jabal Al Badr
    Al Aswad.

B - Typical foliation of the Abt schist trending N 10°E
    and dip 75°E.

C - Fractural cleavage in the quartz-chlorite schist.
    Calcite minerals filled the fractures.

D - Crenulation developed in the chlorite-sericite schist
    as a result of deformation.

E - Fault in the Abt schist displaced a small layer of
    andesitic vein-type about 5-10 cm.

F - Fault in the Abt schist displaced andesitic dike about
    1 m.

PLATE 4
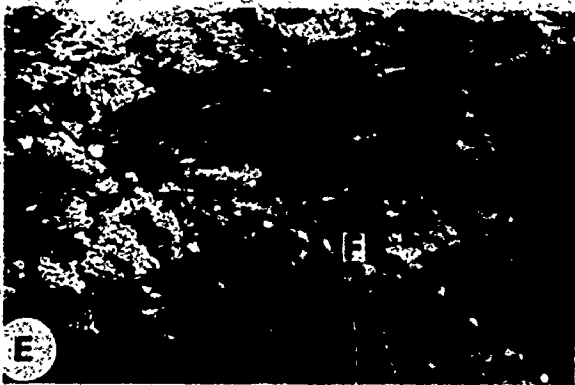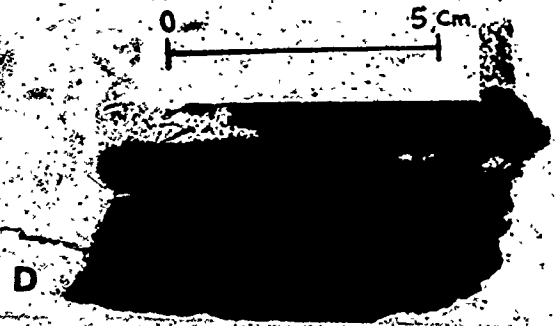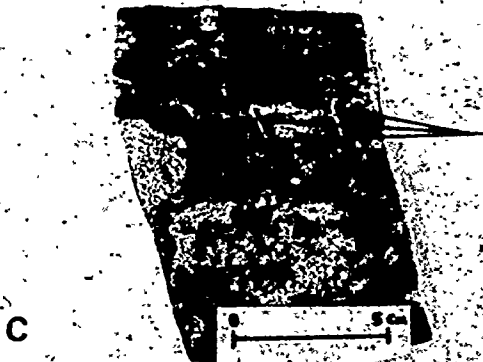
The oldest quartz veins are those striking north-south parallel to the foliation. They are refolded the same as the schist (Plate 5-E and 5-F); younger quartz veins however cut across the foliation and bedding surfaces. The quartz veins vary in thickness between a few millimeters and 1 m, and in length from 0.5 to 300 m. Pods of quartz are also present (Plate 6-A). Most of the quartz veins are white in colour, clear and milky quartz veins being rare. Calcite veins are less common than quartz veins but in many localities both quartz and calcite are present in the same veins (Plate 6-B).

3.2.1.4. Chemistry

Average abundances and ranges of major oxides, minor elements, and CIPW norm values of the Abt schist are given in Table 5. Two of the amphibole schist samples (269A; 276) are basaltic, having relatively high nickel and titanium contents with the TiO_2 values comparable numerically to their FeO^+/MgO ratios. The remainder of the samples (249, 283, 278A) are characterized by low titanium contents relative to FeO^+/MgO and appear to be low potassic calc-alkaline rocks. The more silicic rocks (SiO_2 = 62 wt % to 73 wt %) are low in titanium relative to FeO^+/MgO but appear to be enriched in nickel and chromium relative to island-arc andesites from Tonga (Ewart et al., 1972).

The general trend of the Abt schist rocks in an A-F-M

PLATE 5

A, B, C - Illustrate different scale of folds in the
chlorite-sericite schist of the Abt Formation.

D - Quartz, albite, and chlorite crystals deformed
and folded in a thin section of quartz-sericite
schist of the Abt Formation.

E - Quartz veins are abundant in the chlorite schist
of the Abt Formation.

F - Quartz vein deformed and folded within the Abt
Formation.

PLATE 5
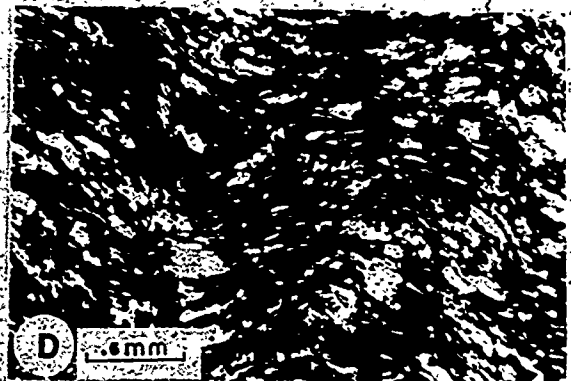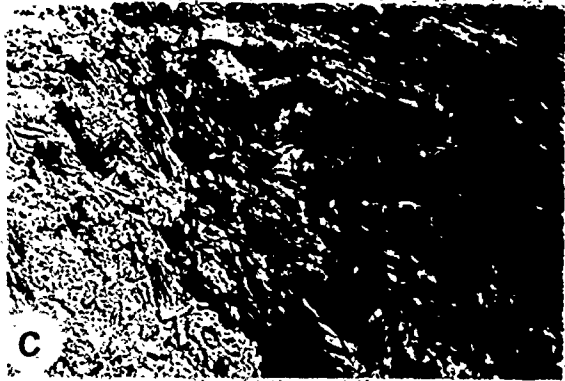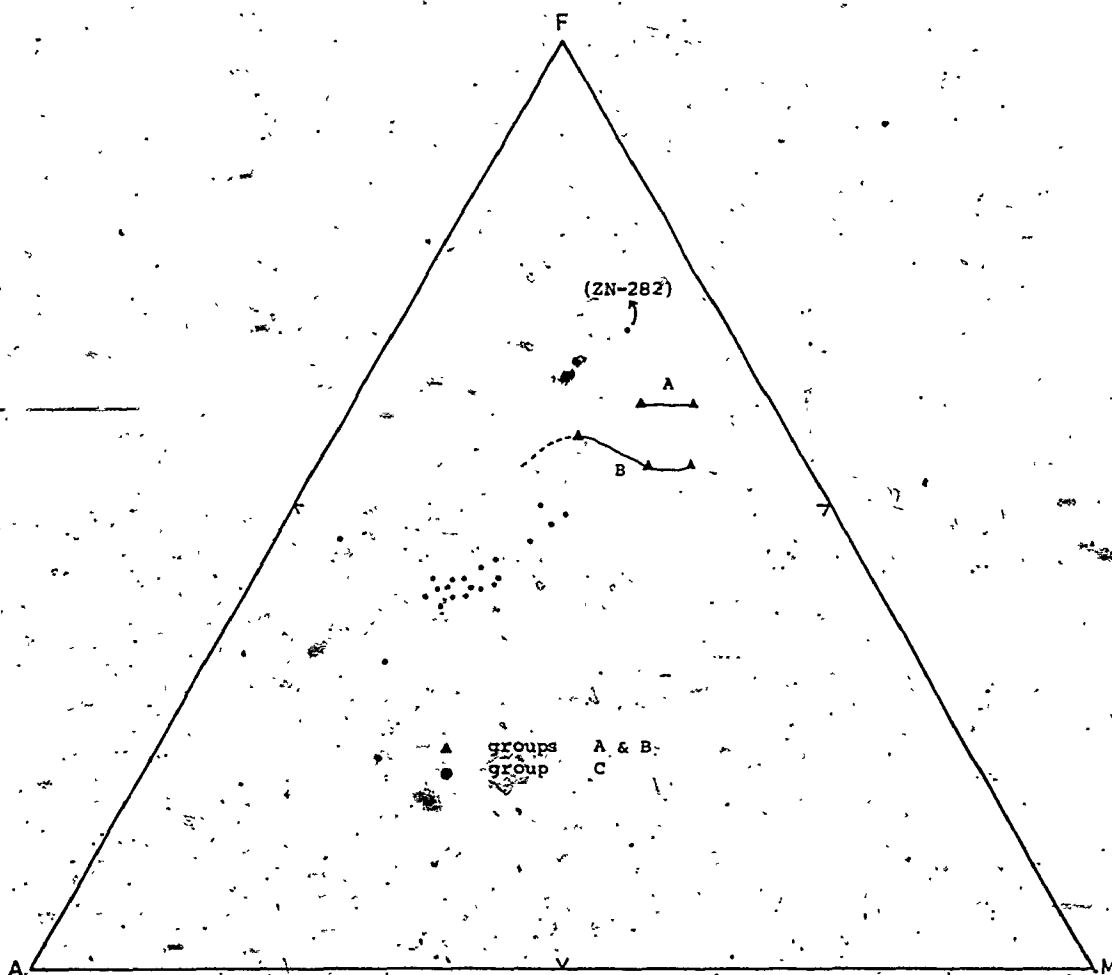
Fig. 20. A-F-M diagram of the calc-alkalic to tholeiitic rocks of the Abt Formation.

Table 5 – Average and range of chemical composition and CIPW norm values of the Abt Formation.

	Group A		Group B		Group C	
	Ave.[I]	Range	Ave.[II]	Range	Ave.[III]	Range
SiO_2	46.54	47.33 – 45.75	45.55	40.24 – 49.63	65.39	58.50 – 73.01
TiO_2	2.00	1.92 – 2.08	0.83	0.62 – 1.09	0.64	0.21 – 0.81
Al_2O_3	14.46	14.19 – 14.73	16.35	11.87 – 19.46	14.27	10.61 – 16.03
Fe_2O_3	2.88	2.87 – 2.89	2.35	2.16 – 2.54	1.88	0.60 – 2.50
FeO	12.38	12.25 – 12.50	7.86	6.62 – 9.38	3.72	0.88 – 8.99
MnO	0.24	0.24 – 0.24	0.20	0.17 – 0.22	0.12	0.03 – 0.56
MgO	6.93	6.47 – 7.39	5.37	3.67 – 6.75	2.50	0.54 – 4.16
CaO	10.89	10.53 – 11.24	12.20	10.04 – 16.34	3.47	1.99 – 5.72
Na_2O	2.05	2.58 – 1.52	1.90	0.82 – 2.48	3.55	0.98 – 6.89
K_2O	0.25	0.33 – 0.17	1.01	0.93 – 1.10	1.54	0.38 – 5.56
P_2O_5	0.20	0.19 – 0.20	0.31	0.28 – 0.34	0.31	0.08 – 0.72
Total	99.07		93.93		97.39	
$\frac{FeO^t}{MgO}$	2.16		1.86		2.16	
$\frac{*K_2O}{K_2O+Na_2O}$	0.11		0.35		0.30	

Norms (CIPW)

Q	–	0.00 – 0.00	0.61	0.00 – 1.84	27.40	12.37 – 35.27
or	1.50	1.97 – 1.02	6.47	6.08 – 7.17	9.73	2.23 – 33.06
ab	17.54	22.06 – 13.02	14.24	0.70 – 21.41	30.69	8.69 – 59.37
an	29.86	26.44 – 33.28	34.92	30.25 – 39.22	13.99	7.04 – 22.77
cor	–	0.00 – 0.00	–	0.00 – 0.00	1.79	0.00 – 6.54
di	19.51	20.89 – 18.12	23.46	7.79 – 50.58	1.30	0.00 – 8.35
hy	16.27	11.27 – 21.27	6.88	0.00 – 4.48	10.33	2.13 – 19.19
ol	6.81	9.03 – 4.58	5.96	0.00 – 15.61	–	0.00 – 0.00
mt	4.22	4.20 – 4.24	3.62	3.46 – 3.75	2.80	0.89 – 3.61
il	3.84	3.68 – 4.00	1.66	1.37 – 2.11	1.20	0.41 – 1.58
ap	0.47	0.45 – 0.48	0.80	0.68 – 0.89	0.75	0.19 – 1.84
ne	–	0.00 – 0.00	1.30	0.00 – 3.90	–	0.00 – 0.00

Trace elements (P.P.M.)

Cr	79	64 – 94	89	42 – 128	102	0 – 287
Ba	113	90 – 136	236	161 – 367	393	44 – 765
Ni	44	40 – 47	17	12 – 25	32	0 – 89
Nb	4	3 – 4	1	0 – 2	8	0 – 13
Zr	94	90 – 98	50	29 – 84	159	72 – 207
Y	19	19 – 19	15	13 – 18	27	1 – 40
Sr	322	174 – 469	460	245 – 290	315	39 – 693
Rb	6	5 – 7	18	12 – 26	38	5 – 89

FeO^t = total iron $(Fe_2O_3 \times 0.8998 + FeO)$.

K_2O and Na_2O recalculated at SiO_2 = 65 wt. %.

I = 2 samples   II = 3 samples   III = 29 samples

diagram (Fig. 20; A = alkalies, $F = Fe_2O_3 \times 0.8998 + FeO$, M = MgO) is of calc-alkaline type. There is little iron enrichment relative to magnesium with increasing total alkali and silica content. Sample 282, which plots away from the sedimentary group of the Abt schist on the A-F-M diagram, was collected from an area which has been affected by an east-west fault, and as a result may have been depleted in aluminium, total alkalies, barium, niobium and strontium and enriched in total iron, manganese, magnesium and calcium.

Chromium content of the Abt schist is plotted against their trace element concentrations in Figures 21, 22, 23, and 24. The two mafic groups are outlined. In the tholeiitic basalt group (samples 269A; 276) there are no changes in the overall trends except that strontium increases and total alkalies decrease with fractionation. In the calc-alkali basalt group (samples 249; 283; 278A) titanium, yttrium, zirconium, barium, silica and aluminium increase with fractionation but rubidium and magnesium decrease with fractionation, whereas nickel, phosphorous, total iron, and manganese show either no or very slight variation with fractionation. Compared with the mafic calc alkaline rocks, the Abt metasedimentary schist is enriched in zirconium, yttrium, barium, rubidium, total alkalies and silica and depleted in total iron, magnesium, calcium, manganese, phosphorous and possibly titanium. The enrich-
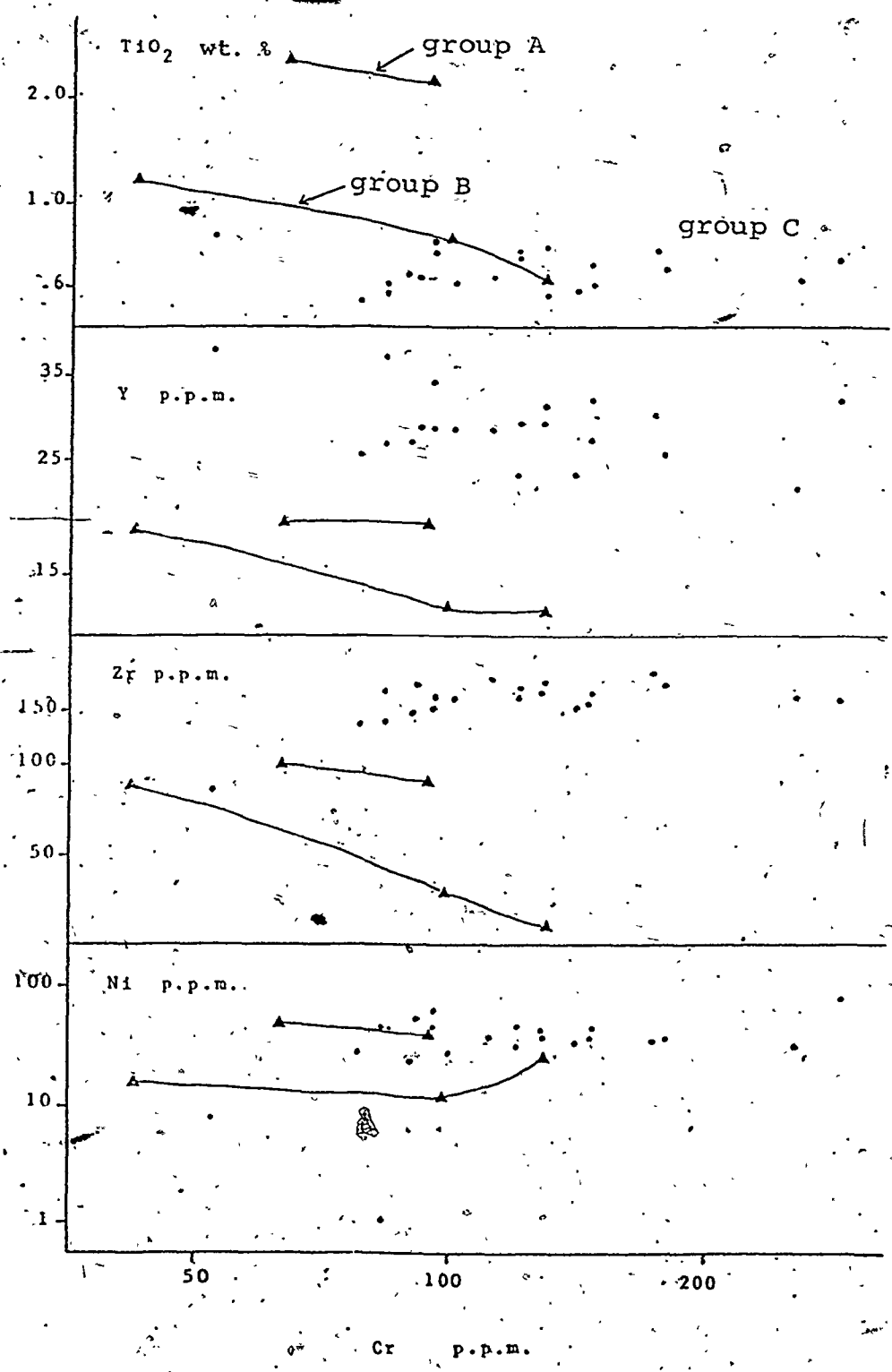
Fig. 21. Plot of Cr against Ni, Zr, Y, and TiO_2 of the different groups of the Abt Formation.
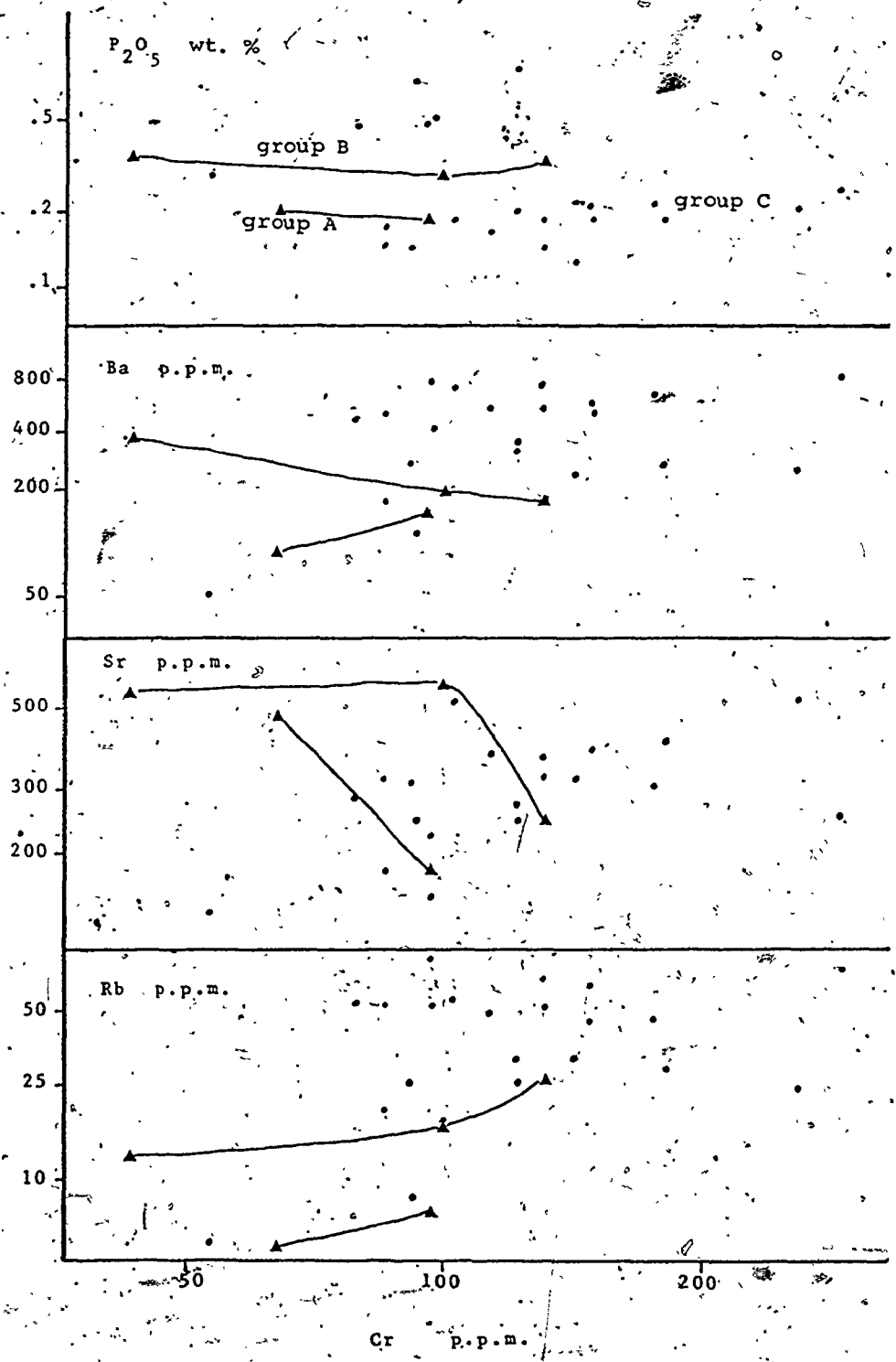
Fig. 22. Plot of Cr against Rb, Sr, Ba, and
P_2O_5 of the different groups of the
Abt schist.
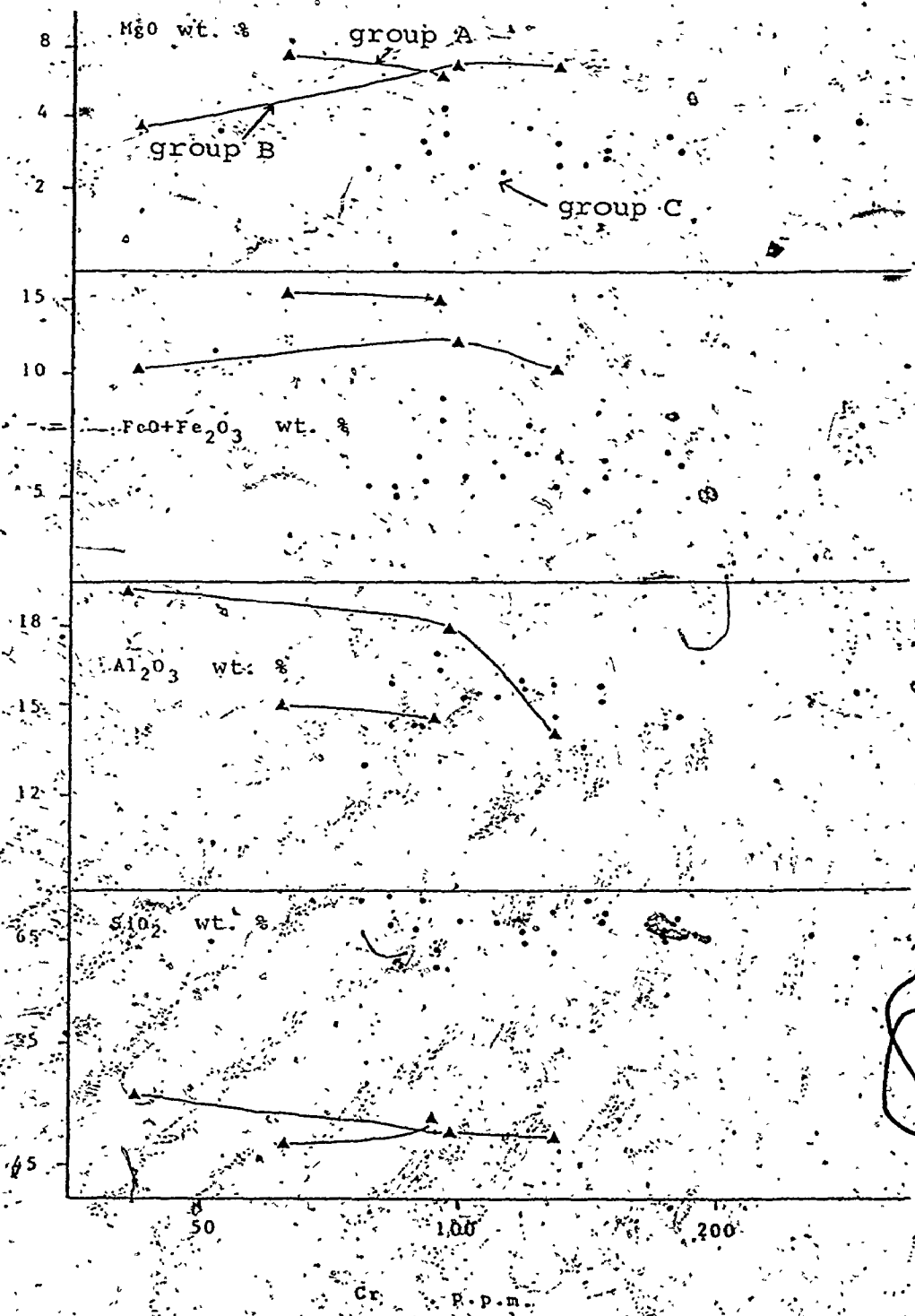
Fig. 23. Plot of Cr against SiO_2, Al_2O_3, FeO+ Fe_2O_3, and MgO of the different groups of the Abt schist.

2

1.0
1.1
1.25 1.4 1.6
2.8 2.5
3.2 2.2
3.6
4.0 2.0
1.8
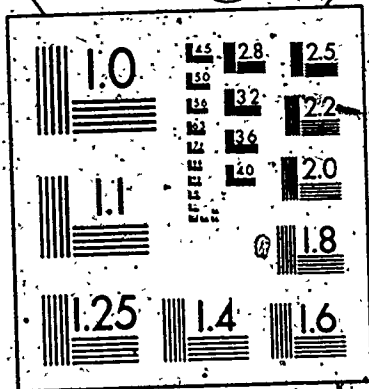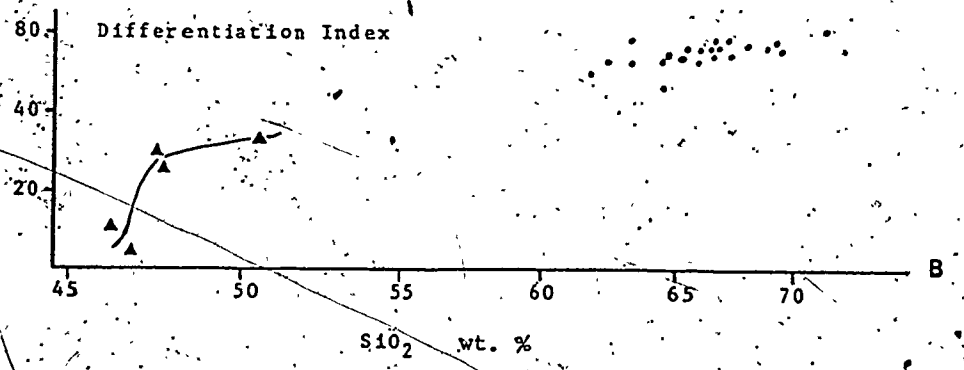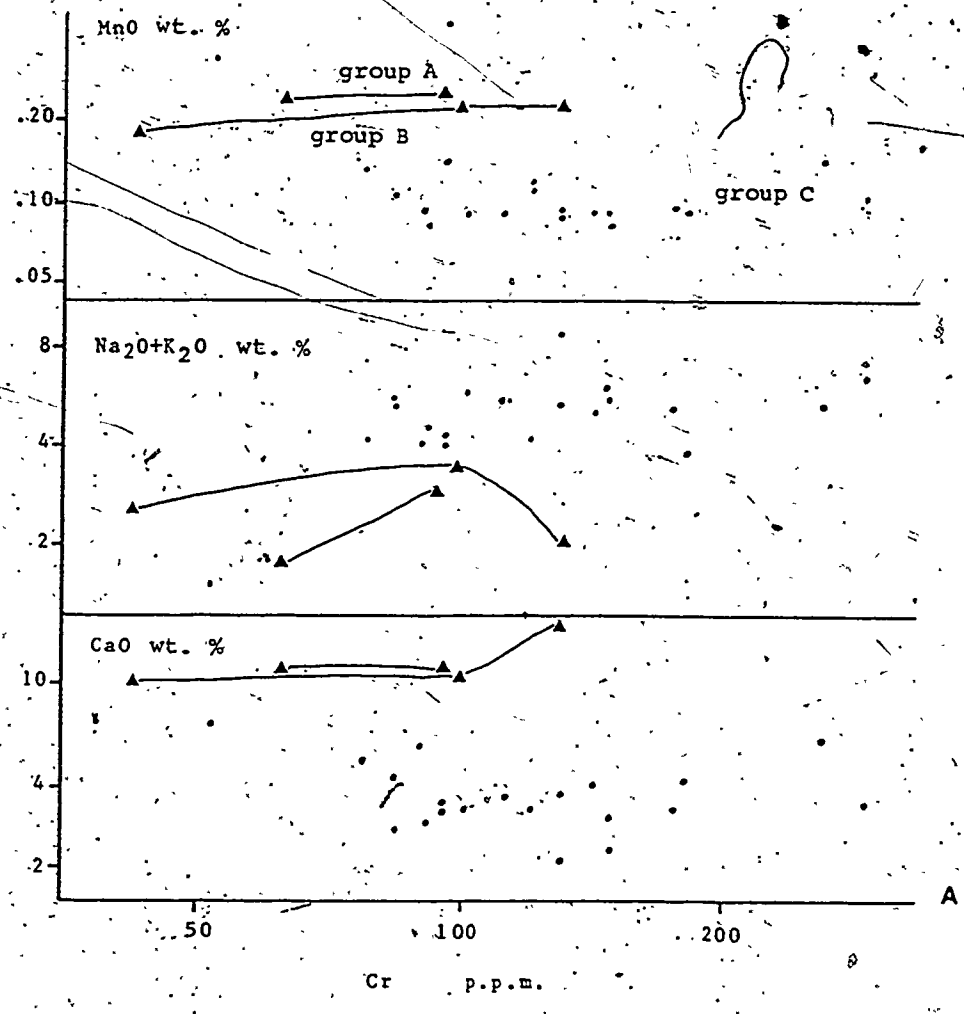
Fig. 24. (A) Plot of Cr against CaO, Na$_2$O+K$_2$O, and MnO, and (B) differentiation index versus SiO$_2$ of the Abt Formation.
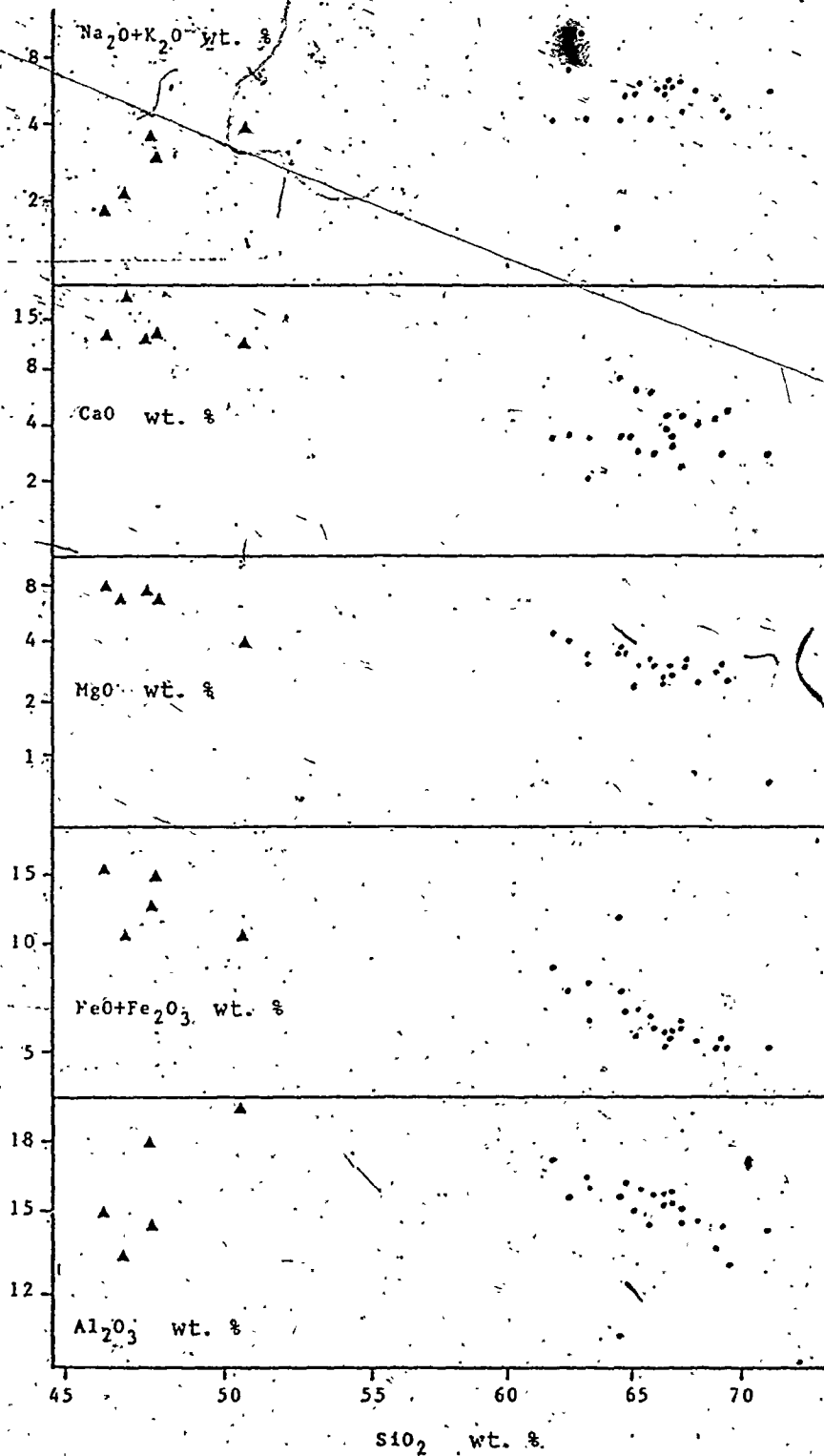
Fig. 25. Plot of SiO_2 against Al_2O_3, FeO+
Fe_2O_3, MgO, CaO, and Na_2O+K_2O of
the Abt Formation.

ment of the sediments in silica, zirconium, yttrium,
rubidium, and total alkalies relative to the calc-alkaline
mafic schists possibly reflects mixing of material from
both island arc and continental sources.

Major oxides of the Abt schists are plotted against
their silica content (Fig. 25). Alumina increases in the
basic rocks with increase in silica. On the other hand,
alumina decreases in the sedimentary rocks of the Abt
schist with increasing silica. Iron and magnesium decrease
in both, the basic and sedimentary groups with increasing
silica. Calcium does not vary with silica increase in the
basic rocks whereas in the sedimentary rocks, calcium
varies widely. Total alkalies tend to increase in the
basic rocks of the Abt Formation with increasing silica.

The gap between the basic and silicic rocks in terms
of silica (Fig. 25) suggests a different source for the
metavolcanic and metasedimentary Abt schist groups.

Chemical analyses of rock samples from the Abt
Formation are given in Appendix 4.

3.3. Shigran carbonates

The Shigran carbonates were mapped by Eijkelboom
(1966 A 12) as beds or lenses of brown silicified marble
occurring in association with ultramafic rocks located
along the Al Amar-Idsas fault. Eijkelboom (1966 A 14)
considered the brown marble to be of sedimentary origin

and compared it with the Farida marble of the Murdama
Group. Bois and Shanti (1970) interpreted the Shigran
carbonates to be the dolomitized and silicified parts of
serpentinite and pyroxenite bodies, whereas Kahr et al.
(1972) and Overstreet et al. (1972) included both the
brown marble associated with ultramafics and the clearly
sedimentary marbles overlaying the Halaban Group within
a single lithostratigraphic unit the "Fawara Formation".
The carbonate rocks of this unit were however divided by
Thekair (1976) into three categories:

    a - Halaban Carbonate of sedimentary origin,

    b - Sihailiya Carbonate of sedimentary origin,

    c - Shigran Carbonate of magmatic origin.

3.3.1. Geology

The term "Shigran" (introduced by Thekair, 1976) was
derived from Jabal Ashigran in the central part of the
thesis area. The most obvious feature of the Shigran
carbonates is their alignment along the Al Amar-Idsas fault
and its central and southern branches. In the northern
part, the carbonates are found between the volcanic rocks
of the Al Amar formation to the east and the sedimentary
Abt schist to the west. To the south the carbonates are
found not only along branches of the Al Amar-Idsas fault
(e.g. Shigran fault) but also occur within the Abt
schist.

The Shigran carbonates form isolated, elongated lenses.

and/or sheet-like bodies rising above plain level (Plate
6-C). The carbonates vary in size from 10 m to 1.25 km
long and 20 m to 200 m thick. Shigran carbonates are
abundant in the central part of the Al Amar-Idsas region
between Marjan village and Jabal Rugaan, and are less
frequently encountered to the north of Marjan village and
to the south of Jabal Rugaan.

Bois and Shanti (1970) and Kahr et al. (1972) speci-
fically pointed out the spatial relationship between the
brown marble and the ultramafic rocks west of Jabal Batran.
Thekair (1976) reported that ultramafic rocks are associ-
ated with Shigran carbonates only south of latitude 23°
34'N.

In the northern part of the Al Amar-Idsas region, the
Shigran carbonates are in contact with pyroclastic rocks
(Plate 6-D) and/or conglomerates along their eastern side
and chlorite-sericite schist on their western side. In
the central part of the region, the carbonates are in
contact with conglomerate and/or pyroclastic and ultra-
mafic rocks on their eastern side, and chlorite-sericite
schist along their western side. Occasionally, Shigran
carbonates are entirely enclosed within the Abt schist.
Thekair (1976) found the contact between Shigran carbon-
ates and the ultramafic rocks to be gradational. Further-
more, he found that the carbonates contain small patches
of serpentinite as well as veinlets of serpentine about

1 mm to 1 cm thick. The contact of the Shigran carbonates (Plate 6-E) are frequently brecciated, the breccia zones ranging in thickness between 5 cm and 15 m. The brecciated zone west of the carbonate consists of crushed and sheared chlorite-sericite schist, Shigran carbonate, quartz, and calcite. On the other hand the brecciated zone along the eastern margin of the carbonate consist of Shigran carbonate, serpentine, rhyolite, conglomerate and/or pyroclastic materials.

Calcite veins are abundant in the Shigran carbonate. They vary in size and shape, but some are evidently fracture fillings about 5 mm to 7 cm wide and 10 cm to 1 m long. Otherwise, calcite occurs as lenses or pods. Quartz veins, which are also common, cut across each other in all directions, the dominant vein type being parallel to the long axis of the Shigran carbonate lenses. Barite veins are also present in the northern part of the thesis area about 10 km south of Marjan village. Where associated with carbonates, the barite veins are about 5 to 10 cm wide and 0.5 to 4 m long. Some veins have good crystals developed along one side.

Thékair (1976) found that Shigran carbonate consists of: carbonate, quartz, serpentine, magnetite, chromite, chlorite, talc and sulfides. He also identified using x-ray diffraction methods, magnesite, dolomite, calcite and antigorite.

PLATE 6

A - Pod of quartz about 15 cm wide, 7 cm thick, and 25 cm
    long.

B - Quartz vein between two calcite veins in the Abt
    Formation.

C - Isolated lenses of Shigran carbonate along the Al
    Amar-Idsas fault.

D - Shigran carbonate in contact with pyroclastic unit
    below (at the hammer head) and chlorite-sericite schist
    on top.

E - Typical example of silicified Shigran carbonate.
    Several veins of quartz, calcite, and hematite are
    present.

PLATE 6
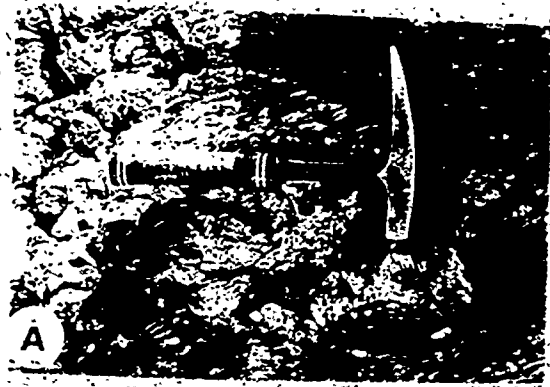
The average chemical compositions and norm values of Shigran carbonates are given in Table 6. For total rock analyses of Shigran carbonates and barite veins, see Appendix 5.

3.4. Ultramafic rocks

The ultramafic bodies of the thesis area have been studied or commented upon by: Schaffner (1955; 1956b), Maclean (1958a; 1958b), Directorate General of Mineral Resources (1959), Kahr (1962), Herness and Kahr (1963), Eijkelboom (1966 A 14; 1966 A 15), Lambolez (1968), Bois and Shanti (1970), Kahr et al. (1972); Overstreet et al. (1972), Mukandy (1975), Thekair (1976), Zubeir (1976) and Al Shanti and Michell (1976). The most comprehensive description of the ultramafic rocks is by Bois and Shanti (1970) who concluded that the ultramafic rocks associated with amphibolitic gneiss, gabbro and altered green schist in the southwestern part of the area formed part of an ophiolitic suite of rocks.

3.4.1. Geology

The ultramafic bodies are mainly serpentinite and to lesser extent pyroxenite and/or peridotite (Plate 7-A). They are mostly located south of Jabal Minassa along the Al Amar-Idsas fault and its branching faults. North of Jabal Minassa, intrusive complexes of gabbro and diorite are common, but ultramafic bodies have not been reported.

In the area between Jabal Minassa and Jabal Rugaan exten-
sively developed ultramafic bodies vary in dimension from
10 m to 4 km long, 2 m to 1 km wide and 0.5 to 5 m above
plain level. Few ultramafic bodies are exposed in the
mountains north of the magnetite deposit of Jabal Idsas.
Ultramafics associated with Shigran carbonates tend to lie
east of the carbonates. However, many ultramafic bodies,
are enclosed within the Abt schist about 20 km west of
Jabal Rugaan and without any relationship to Shigran
carbonates.

The serpentinized rocks are locally carbonatized and
silicified (Plate 7-B) along fracture and fault zones
where most of the serpentinite bodies are mylonitized and
crushed. At Jabal Minassa, unaltered pyroxenite is pre-
served in the cores of serpentinite rocks.

Magnesite veins are present in the southern part,
north of Jabal Ahaamer (Plate 7-C) and occur in associ-
ation with ultramafic bodies. The veins are notable for
the cauliflower-like form of the magnesite and they are
about 10 to 30 cm wide and 5 to 100 m long.

The average chemical composition of the ultramafic
rocks is given in Table 6, and total rock analyses of the
ultramafics, pyroxenite and magnesite are given in
Appendix 6.

3.5. Al Amar-Idsas fault

The Al Amar-Idsas fault has long been recognized as

Table 6 – Average and range of chemical composition and CIPW norm values of the Shigran carbonates and ultramafic rocks.

	Shigran Carbonate		Ultramafic	
	Ave.[I]	Range	Ave.[II]	Range
SiO_2	32.91	24.25 – 41.48	33.57	15.18 – 41.69
TiO_2	.05	.02 – .13	.12	.05 – .21
Al_2O_3	.89	.23 – 1.93	3.49	.60 – 10.81
Fe_2O_3	1.96	1.88 – 2.15	2.34	1.95 – 2.76
FeO	4.10	3.41 – 5.80	7.67	4.01 – 11.29
MnO	.16	.09 – .19	.15	.08 – .22
MgO	21.75	6.64 – 35.19	26.39	5.49 – 39.22
CaO	10.54	.58 – 24.07	10.93	.02 – 35.57
Na_2O	–		.03	.0 – .18
K_2O	.04	.0 – .22	.04	.0 – .11
P_2O_5	–		.06	.0 – .50
L.O.I.	28.08	21.81 – 33.53	15.99	6.37 – 29.30
Total	100.48		100.78	
FeO^+/MgO	.27		.37	

Norms (CIPW)

Q	.30	.0 – 2.91		
or	.09	.0 – .68	.29	.0 – .69
ab			.34	.0 – 1.62
an	2.76	1.38 – 6.69	10.54	.11 – 31.82
cor			.22	.0 – 1.10
di	33.06	12.67 – 68.67	7.84	.0 – 17.13
hy	8.51	.0 – 32.15	17.14	2.72 – 37.50
ol	23.90	.0 – 56.60	59.52	27.14 – 85.22
mt	2.92	3.71 – 3.97	3.92	3.57 – 4.36
il	.11	.07 – .33	.21	.13 – .31
ap	–		–	

Trace elements (P.P.M.)

Cr	2273	1598 – 3886	1869	409 – 3019
Ba	235	0 – 1552	85	10 – 296
Ni	1553	737 – 2466	1256	205 – 2729
Nb	8	0 – 21	6	0 – 22
Zr	1	0 – 9	2	0 – 7
Y	1	0 – 3	11	0 – 73
Sr	325	38 – 533	126	3 – 404
Rb	4	1 – 9	2	0 – 5

I = 8 samples.   II = 8 samples.

an important tectonic boundary although the nature of the fault has been the subject of widely varying interpretations. Bramkamp et al. (1956, Map I-212A; 1958, Map I-207A) considered the fault to be a normal fault, but Bramkamp et al. (1963, Map I-206A), Jackson et al. (1963, Map I-211A) and Bouladon (1968) represented the Al Amar-Idsas fault as a thrust fault. Eijkelboom (1966 A 12, 1966 A 13 and 1966 A 14) interpreted the fault as normal fault with recent movement along the fault plane. Later, Eijkelboom et al. (1970, Map MI-18) postulated the fault to be a thrust fault involving eastward displacement of the Abt schist over the Halaban, followed by block faulting to give the present differences in elevations on either side of the fault. Mytton (1966, Map MI-4) represented the fault as a major fault extending north-south. Bois and Shanti (1970) found that the fault in the southern most part of the area is intersected and offset by numerous secondary faults. Nebert (1970) considered the fault to be a deep normal fault which has been reactivated several times, the latest phase of movements taking place during Quaternary time. Brown (1970) pointed out that the fault toward the north appears to be a dextral strike-slip fault and to have a displacement of about 60 km.

On the tectonic map of the Arabian Peninsula however Brown (1972) represented the fault as a thrust fault. Kahr et al. (1972) described the Al Amar-Idsas fault in

the Jabal Batran quadrangle as an imbricate overthrust
fault consisting of three imbricate blocks thrust westward
over the Abt schist. In the southern part of the Jabal
Batran quadrangle, they (Kahr et al., 1972) found the
overthrust fault graded into a southeast striking tear
fault. Thekair (1976) stated that the fault started as a
thrust fault involving eastward thrusting of the Abt
schist, but later was reactivated as a strike-slip fault.

Al Shanti and Mitchell (1976) considered the Al Amar-
Idsas fault to be a major tectonic line marking the boun-
dary between two plates. Moore (1976) concluded that the
Al Amar-Idsas fault is a strike-slip fault of Proterozoic
origin, reactivated and dislocated by later sinistral
strike-slip faulting during development of the early
Paleozoic Najd fault system. Moore (1976) also pointed
out that the fault is a "copper-lead line" dividing a
"Pb-Ag" province to the west from a "Cu-Zn-Au" province
to the east.

3.5.1. Observations

The Al Amar-Idsas fault is a well-defined topographic
feature that can be seen clearly on aerial photographs and
ERTS images (Plate 7-D). It is exposed in the extreme
eastern corner of the Arabian Shield and extends approxim-
ately for more than 220 km before disappearing to the
north and south beneath the Permian Khuff Formation (Fig.

5). North of Jabal Minassa, the Al Amar-Idsas fault is well defined as a single boundary line whereas, south of Jabal Minassa, the fault is splayed (Fig. 26).

The strike and dip of Al Amar-Idsas fault changes along a north-south line as follows:

at latitude 24" 20' strike N 10° E dip 75° NW,

at latitude 24° 05' strike N-S dip 70° W,

at latitude 23° 55' strike N 25° W dip 56° SW,

at latitude 23° 15' strike N 30° W dip 85° NE,

at latitude 22° 50' strike N 35° W dip 67° NE.

The fault can be divided into three segments (Fig. 26).

1) north of Jabal Minassa the fault sharply separates Halaban volcanic rocks to the east from Abt schist metasedimentary rocks to the west;

2) between Jabal Minassa and Jabal Ehamer, the fault splits south of Jabal Minassa into two parts, one the Shigran fault passing through the Abt schist, the other, representing the main fault, cutting the Halaban volcanic rocks. South of Jabal Idsas, one branch of the main fault strikes southeast through the volcanic and igneous rocks; the other branch, striking south separates the volcanic rocks to the east from the metasedimentary rocks to the west;

3) south of Jabal Ehamer, the fault changes strike from south to southeast and separates conglomeratic rocks

The Al Amar – Idsas Fault
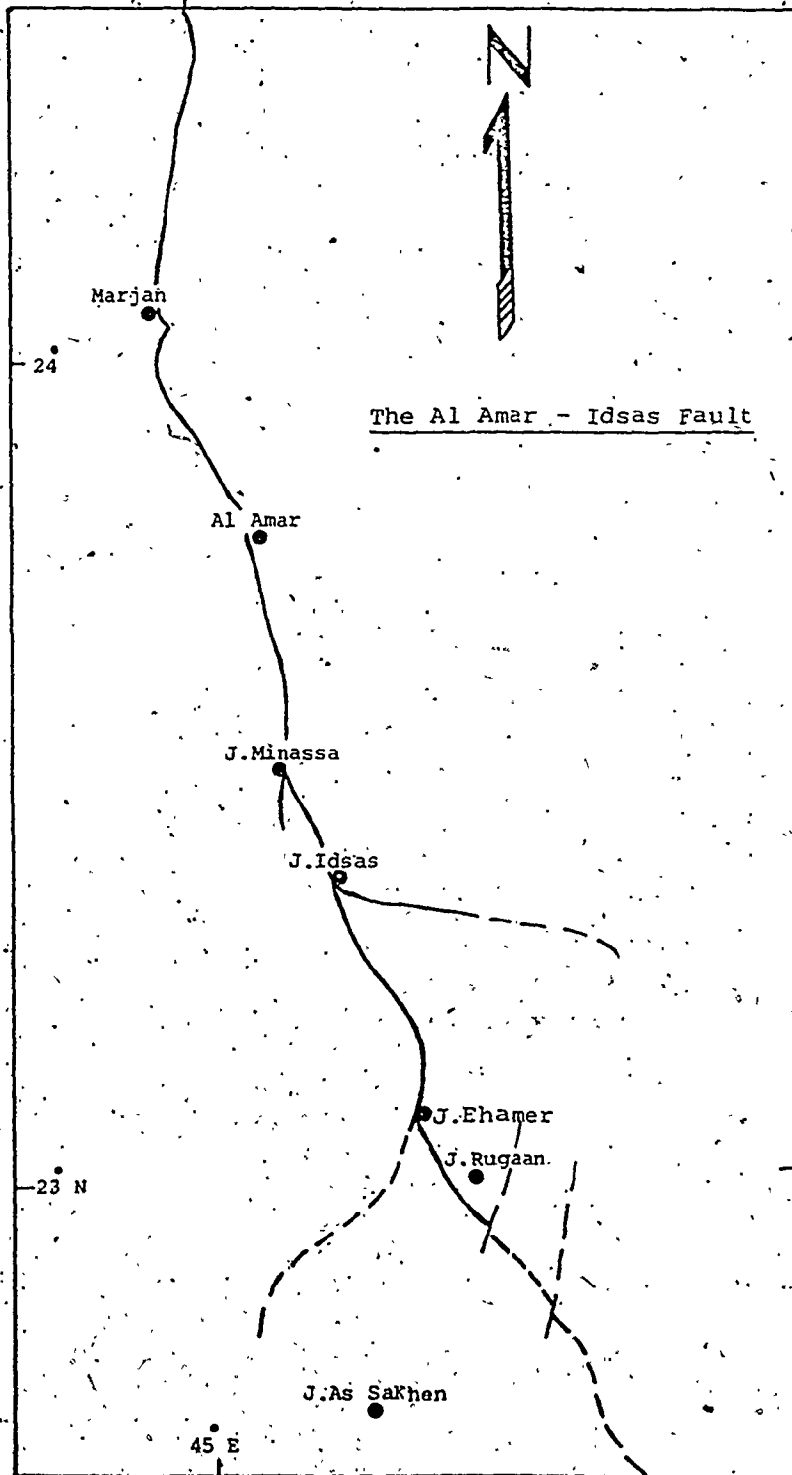
Fig. 26.   Sketch map of the Al Amar–Idsas
fault.

to the east from scattered exposures of the Abt schist
(Abu Sawarir Formation of Overstreet et al., 1972) to
the west.

Surficial deposits and Quaternary sands extensively
cover areas through which the fault passes in the south
central part of the region.

The Al Amar-Idsas fault is the locus of occurrence
of the Shigran carbonates. Slickensides occur in quartz
veins along the Al Amar-Idsas fault plain (Plate 7-E).

3.5.2. Interpretation

The Al Amar-Idsas fault is here interpreted as a
westerly directed thrust fault which later became the
locus of strike-slip faulting. The direction antithetic
to the dip of the fault plain cannot be considered to
represent the thrust direction. Thrusting is associated
with regional deformation involving folding of the Abt
metasedimentary rocks and their conversion to sericite-
chlorite schists.

The shape and nature of the Al Amar-Idsas fault was
compared by Thekair (1976) to other major strike-slip
faults such as San Andreas fault of California and the
Alpine fault of New Zealand.

Reactivation of the Al Amar-Idsas fault over a pro-
longed period of time is indicated by the relationship
between different types of veins and the slickensides they

PLATE 7

A - Ultramafic bodies of serpentine and pyroxene are
    slightly altered.

B - Serpentinite body highly carbonatized and silicified
    particularly along fracture zones.

C - Handspecimen of magnesite vein north of Jabal Ehamer.

D - Al Amar-Idsas fault as it appears on the ERTS images.

E - Slickenside occur in quartz vein at the bottom of the
    picture and to the east of the hammer arm.

PLATE 7
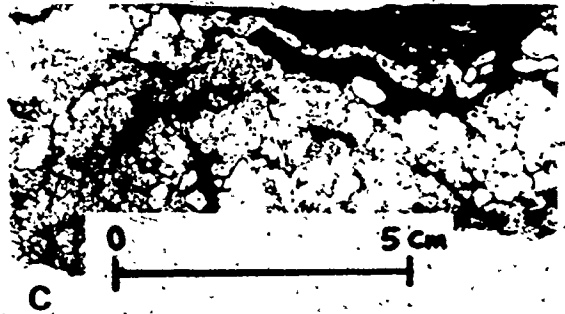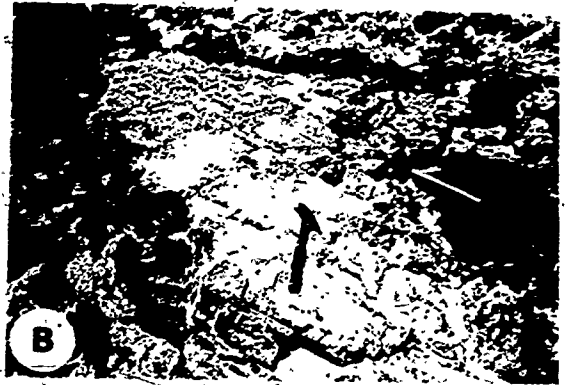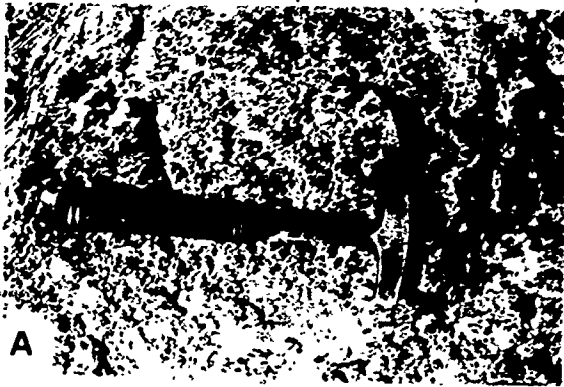
bear. Moore (1976) stated that the fault was reactivated during development of the Najd fault system, whereas Nebert (1970) suggested that Al Amar-Idsas fault may have undergone reactivation even during Quaternary time.

3.6. Plutonic rocks

3.6.1. Classification

On Streckeisen's diagram (1976) the plutonic rocks of the Al Amar-Idsas region are located within the gabbro-diorite, tonalite, granodiorite and granite fields (Fig. 27).

The Al Amar-Idsas plutonic rocks can be considered on the basis of element abundances to form four groups: 1) a low K_2O gabbroic-dioritic group, 2) a high K_2O dioritic group, 3) a granodioritic-tonalitic group, and 4) a granitic-adamellitic group.

In terms of field relationships, however, the plutonic rocks of Al Amar-Idsas region fall into four groups:

1) gneissic granodiorite, the oldest unit,

2) gabbro-diorite complexes, pre-Al Amar formation,

3) syntectonic granodiorite, pre-Al Amar formation, - and

4) post-tectonic granite representing the youngest suite of intrusion in the Al Amar-Idsas region.
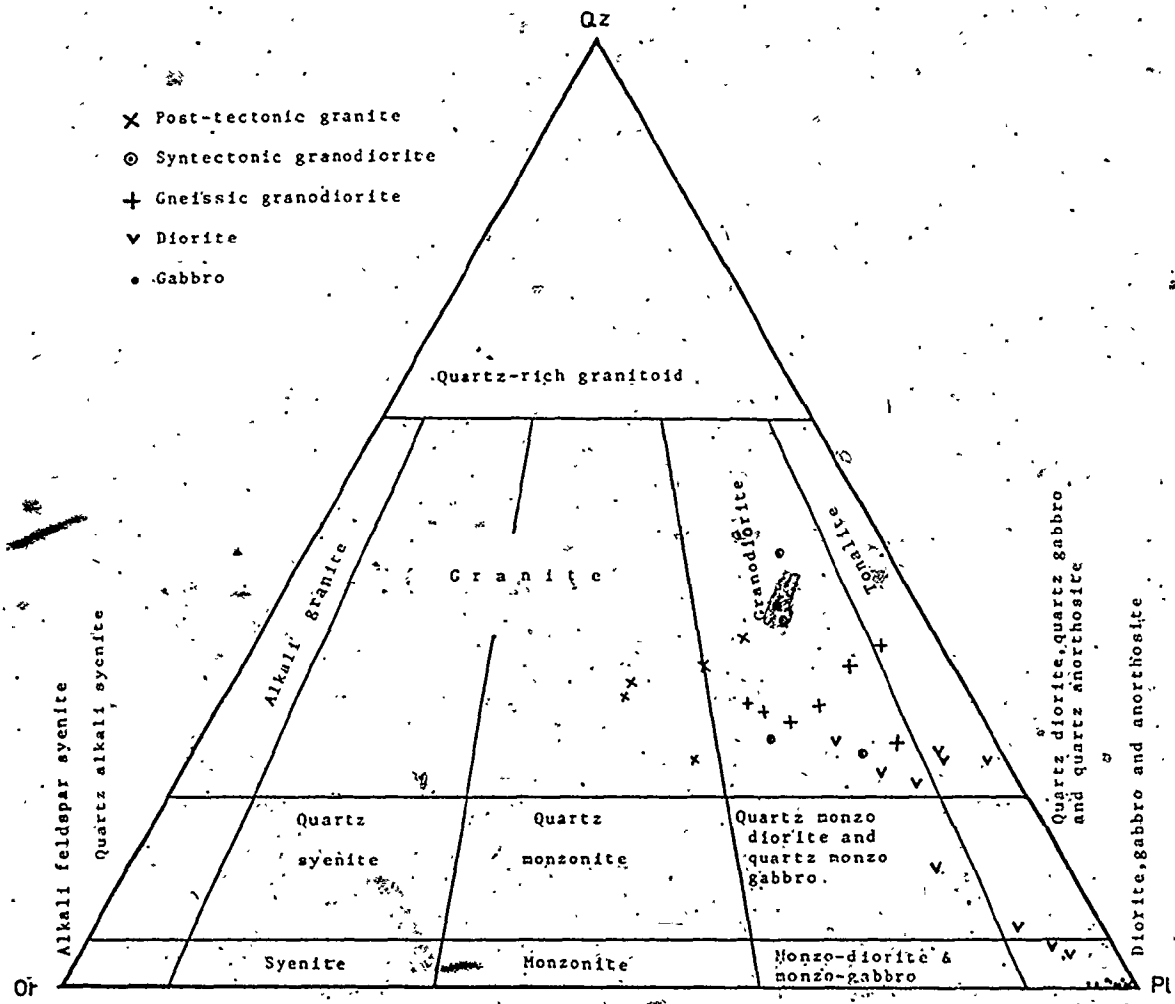
Fig. 27. Streckeisen's diagram (Or-Qz-Pl) applied to classify the plutonic rocks of the Al Amar-Idsas region.

3.6.2. Gneissic granodiorite

Kahr et al. (1972) and Overstreet et al. (1972) considered the gneissic granodiorite of the Al Amar area to be the oldest rocks in the thesis area. They mapped it as a polydeformed, gray, massive hornblende-biotite gneiss highly variable in terms of its mineral composition, grain size and texture. Bois and Shanti (1970) described the gneissic granodiorite as large intrusions of laminated, coarse-grained hornblende-biotite granodiorite containing inclusions of mafic and metamorphosed sedimentary rocks. The main foliation has a north-south trend and dips steeply either to the west or east.

3.6.2.1. Geology

The gneissic granodiorite underlies parts of the area east of the Al Amar-Idsas fault (Fig. 5) where it forms both large and small hills. When a gneissic structure is not well developed in the rocks, foliation is the prominent feature (Plate 8-A). The gneissic granodiorite seems to form the land surface on which the later volcanic and sedimentary rocks of the Halaban Group were deposited. Small, white or pink aplitic dikes intrude the gneissic granodiorite and tend to grade into felsitic and/or quartz veins. To the contrary, dikes genetically related to the gneissic granodiorite have not been observed to cut younger rock units. East of Jabal Batran, the gneissic granodiorite contains a diverse set of inclusions of meta-

sediment considered by Kahr et al. (1972) to be the oldest
sediment in the area (Plate 8-B). Rb/Sr isotopic age data
(Brown in Overstreet et al., 1972) indicate that the
gneissic granodiorites east of Jabal Idsas are as old as
1010 my.

The gneissic granodiorite has three sets of joints:
N 30° E/40° SE; N 05° W/15° W.; and N 55° W/63° NE. The
gneissic granodiorites are cut by at least two sets of
faults. The older, a branch of the main Al Amar-Idsas
fault south of Jabal Idsas, strikes southeastward; the
younger, which displaces the Al Amar-Idsas fault to the
south of Jabal Rugaan, strikes north-south.

3.6.2.2. Petrography

The gneissic granodiorite varies in composition from
biotite-gneiss to hornblende-gneiss and locally to horn-
blende-biotite gneiss. They are medium to coarse-grained
rocks, composed of about 45% feldspar, 30% biotite, 20%
quartz, and 5% hornblende.

The texture of the gneissic granodiorite is hypido-
morphic-granular, medium-grained (Plate 8-C). The mafic
minerals, feldspars, and quartz exhibit a dimensional
preferred orientation.

Plagioclase crystals are euhedral in shape, about 1.5 mm
long and 0.8 mm wide. The twinning is of albite type and
some of the crystals have normal zoning. The central part

of the plagioclase is commonly altered to sericite.

Orthoclase forms subhedral crystals, about 1 mm in diameter. A few small crystals of perthite are present in some thin sections and the orthoclase sometimes rims crystals of plagioclase. In general the orthoclase is altered to kaolin.

Quartz forms anhedral grains about 0.8 mm in diameter. The quartz has undulatory extinction and occupies irregular spaces between the other constituents. Some grains are broken and filled with calcite minerals. The quartz crystals are locally dusty, and contain inclusions of apatite and zircon.

Biotite is the characteristic mafic mineral of the gneissic granodiorite. It forms unaltered, light to dark brown, euhedral crystals, about 1 mm long and 0.5 mm wide, with a preferred orientation. Pleochroic haloes are sometimes present in the biotite.

Hornblende crystals are prismatic, euhedral to subhedral in shape, about 1 mm long and light brown to light green in colour. Where altered, hornblende has been changed to chlorite.

Muscovite is present as very small crystals, about 0.2 mm long. They are found mainly bordering quartz crystals.

Zircon and apatite are found as very small inclusions in quartz grains, whereas leucoxene is present as an alteration product of ilmenite.

3.6.2.3. Chemistry

Seven chemical analyses were made of the gneissic granodiorite (Appendix 7).

On a normative Q-Or-Pl diagram (Fig. 28) the gneissic granodiorite samples plot as a series of points extending from the tonalite field to the granodiorite field. On an A-F-M diagram (Fig. 29; A = alkalies, F = Fe_2O_3 x 0.8998 + FeO, M = MgO) the samples define a curved trend line along which alkalies progressively increase relative to iron and magnesium.

The average and range of composition of the gneissic granodiorite are given in Table 7. The rocks are character- ized by low to intermediate silica content and highly vari- able calcium content. Barium and strontium have higher values than do average granitic rocks, while chromium, zirconium and rubidium have generally lower than average values.

Since chromium is usually a stable element during metamorphism, trace element contents of the gneissic grano- diorites have been plotted* against their chromium content (Figs. 30, 31). Taken as a group, only titanium, phos- phorous, and zirconium appear to vary systematically with chromium content. Nickel, yttrium, barium, strontium, and

---

*All variation diagrams in this thesis are:
1) Plotted on natural logarithmic scales because this dis- plays the real fractionation trends more clearly
2) major oxides are recalculated to 100% (anhydrous).

Table 7 - Average and range of chemical composition and CIPW norm values of the gneissic granodiorites.

	Ave.[I]	Range		Norms (CIPW)	
				Ave.	Range
SiO_2	71.54	70.47 - 73.32			
TiO_2	0.27	0.14 - 0.32	Q	28.82	24.85 - 33.55
Al_2O_3	14.70	13.29 - 16.85	or	13.27	5.27 - 20.04
Fe_2O_3	1.40	0.20 - 1.67	ab	40.96	38.06 - 46.27
FeO	0.83	0.30 - 1.50	an	11.73	8.66 - 15.92
MnO	0.05	0.04 - 0.07	cor	-	
MgO	0.70	0.16 - 1.10	di	1.20	0.09 - 2.98
CaO	2.63	1.82 - 3.48	hy	1.65	1.39 - 2.95
Na_2O	4.76	4.26 - 5.51	he	0.56	0.21 - 1.30
K_2O	2.23	0.87 - 3.34	mt	1.21	0.29 - 2.48
P_2O_5	0.08	0.04 - 0.10	il	0.52	0.27 - 0.62
Total	99.19		ap	0.15	0.10 - 0.24

$FeO^+/MgO = 2.99$

$*K_2O/(K_2O+Na_2O) = .32$

Trace element (P.P.M.)

Cr	5	1 - 16
Ba	781	254 - 1408
Ni	15	12 - 17
Nb	9	7 - 13
Zr	105	60 - 167
Y	14	3 - 31
Sr	528	320 - 811
Rb	44	14 - 73

I = 7 samples.

FeO^+ = total iron (Fe_2O_3 x 0.8998 + FeO).

$*K_2O$ and Na_2O recalculated at SiO_2 = 65wt. %.
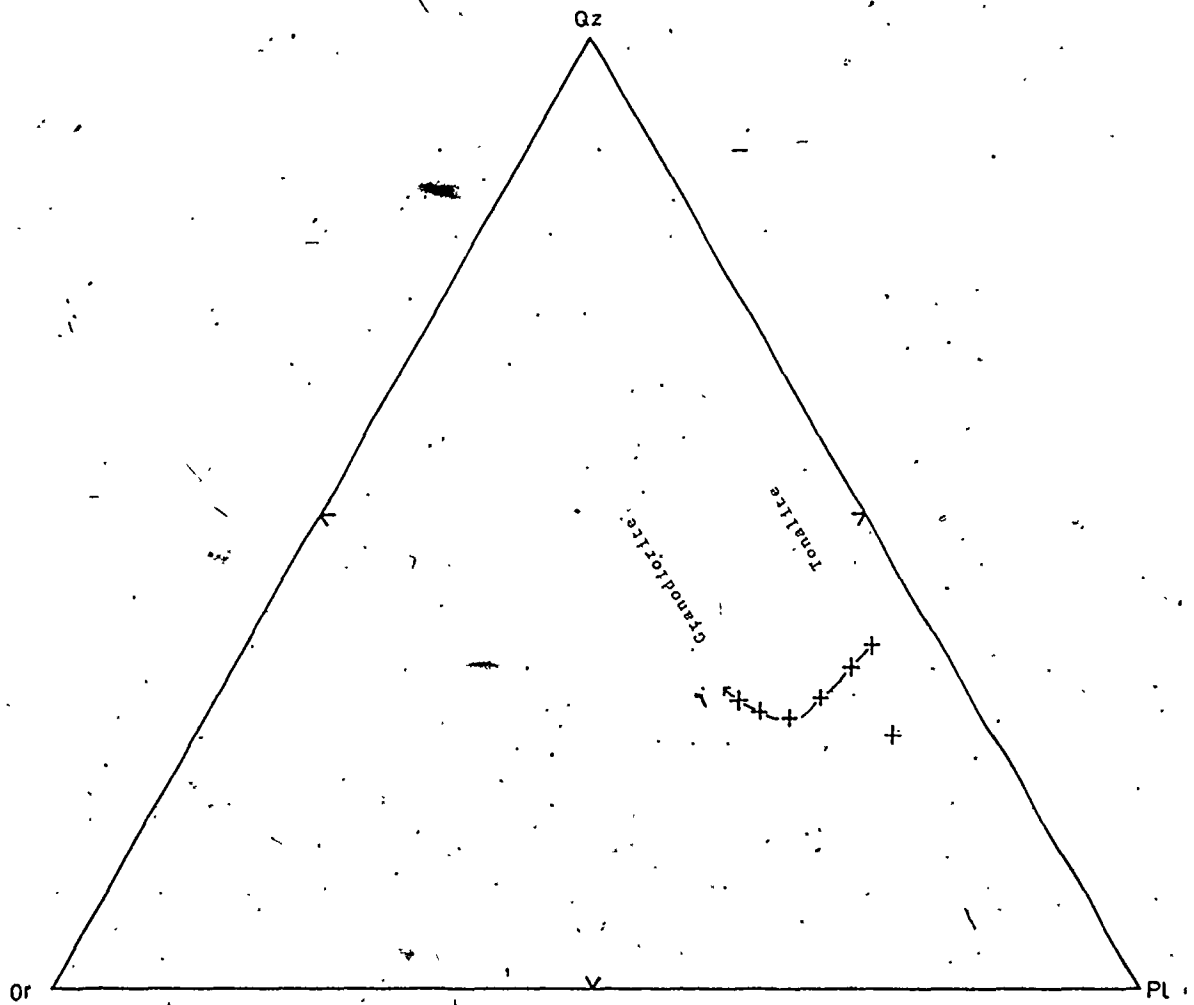
Fig. 28. Or-Qz-Pl diagram of the gneissic granodiorite.
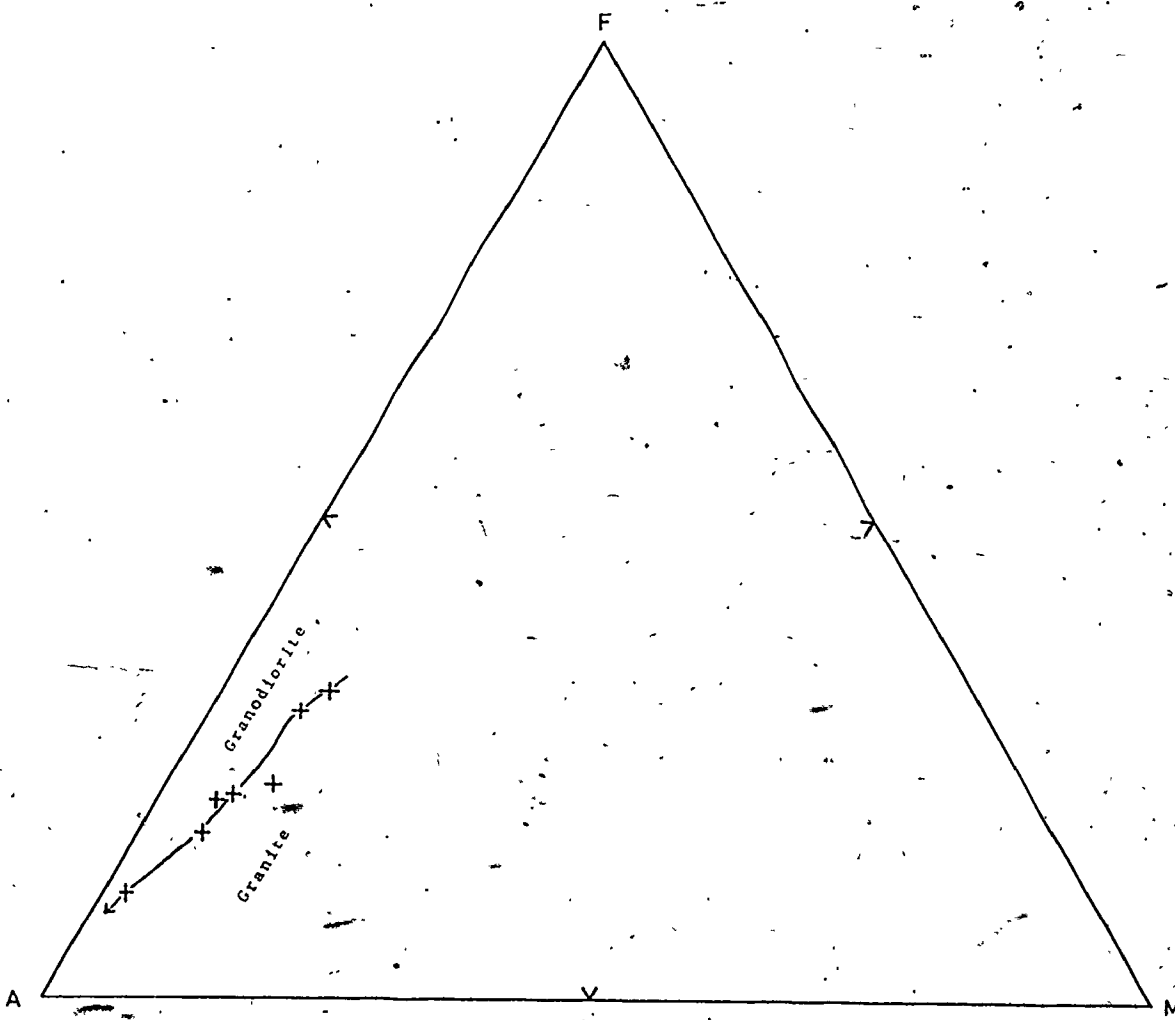
Fig. 29.   A-F-M diagram of the gneissic granodiorite.
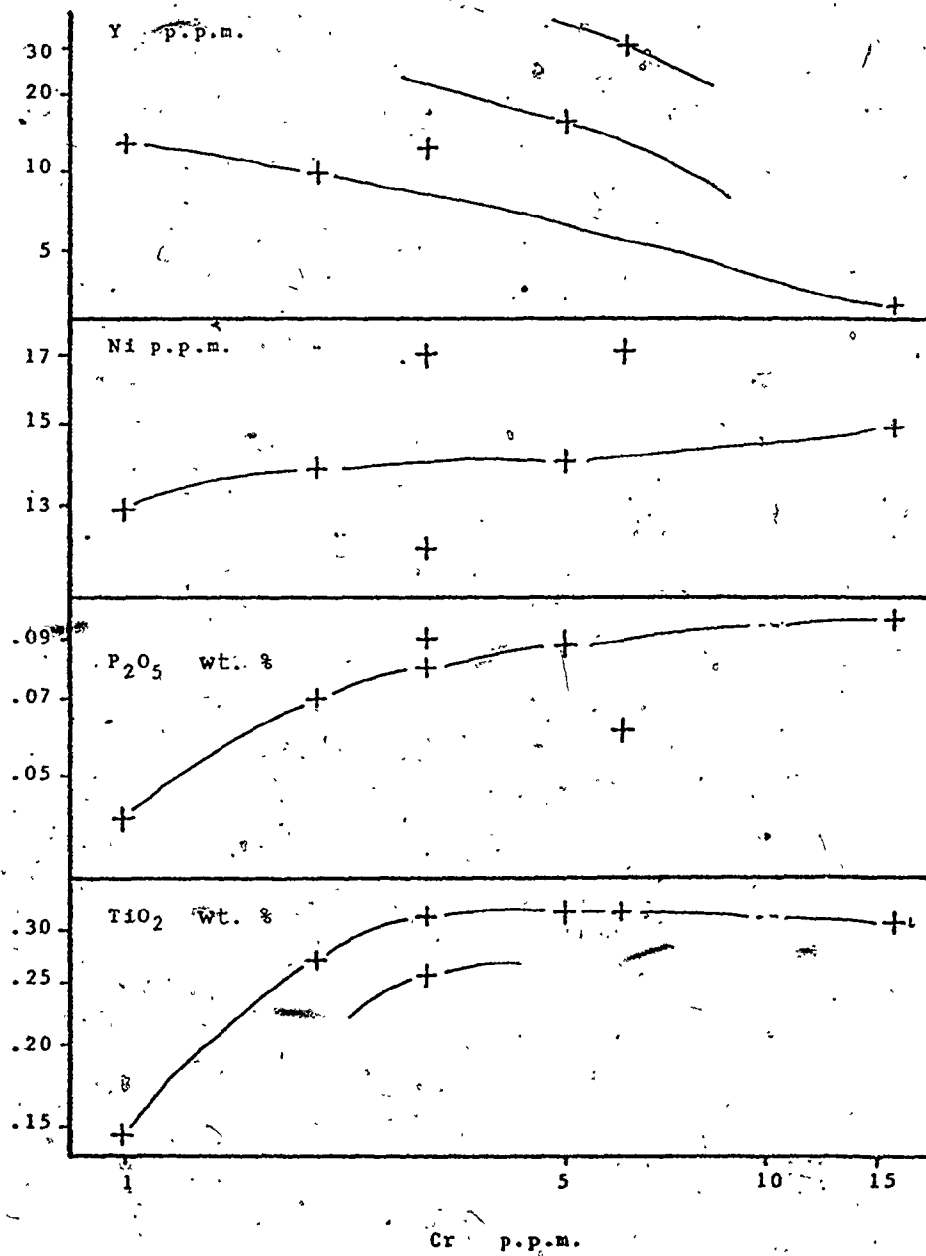
Fig. 30. Plot of Cr against TiO_2, P_2O_5, Ni, and Y of the gneissic granodiorite.
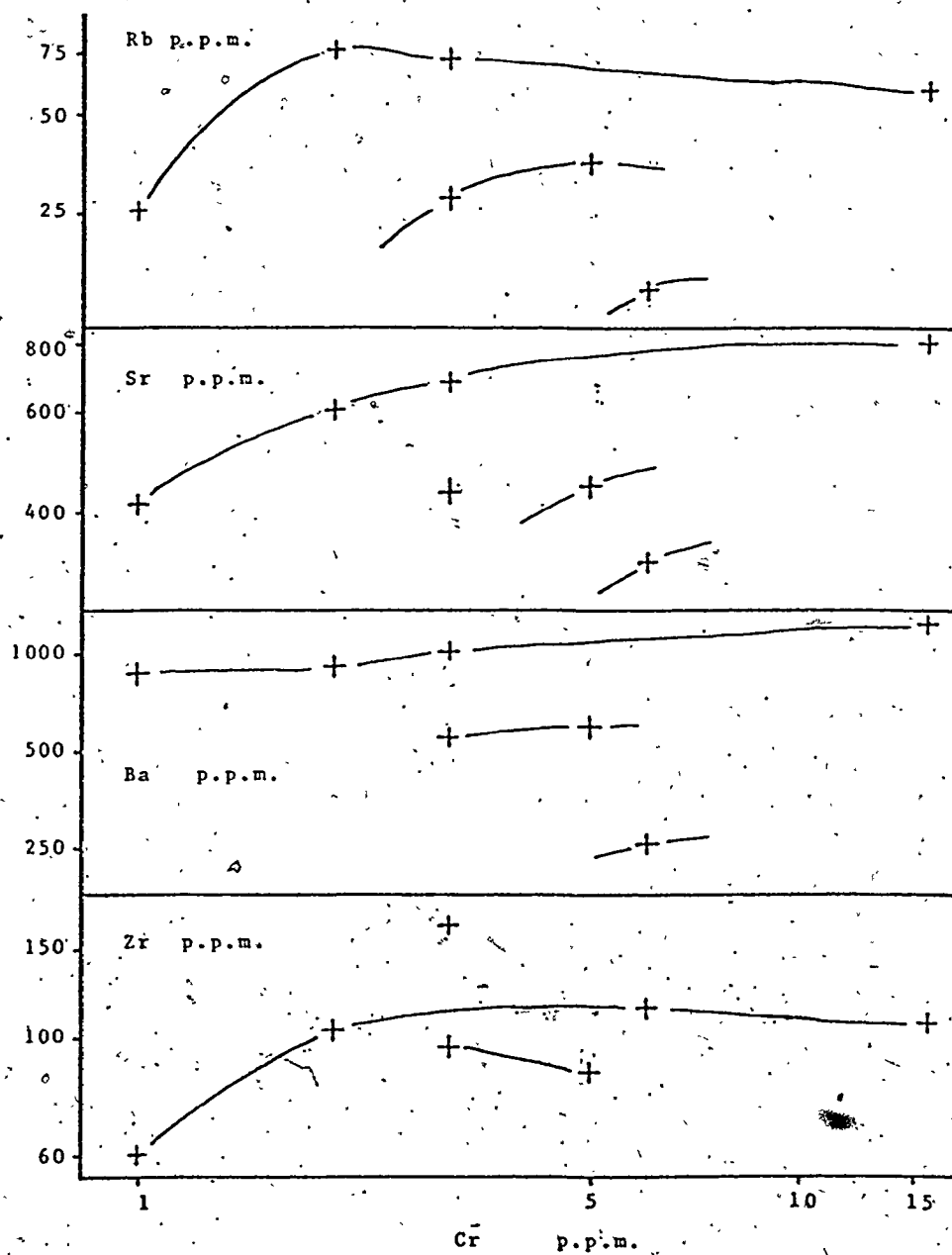
Fig. 31. Plot of Cr against Zr, Ba, Sr, and Rb
of the gneissic granodiorite.

rubidium exhibit no regular variation relative to chromium.

Figure 32 is a plot of the major oxides against phosphorous. Total iron and calcium tend to increase as phosphorous content increases, whereas silica decreases. Total alkalies indicate little change.

Plots of major oxides against silica content (Fig. 33) show that calcium and alumina tend to decrease slightly with increasing silica. Total iron and total alkalies give no regular patterns.

Plots of calcium, barium, and rubidium in the gneissic granodiorite against potassium content (Fig. 34) reveal that calcium decreases as potassium increases, indicating that plagioclase decreases as potassic-feldspar and biotite increase. Barium and rubidium tend to increase with potassium. Barium and rubidium tend to substitute for potassium in potassic-feldspar and biotite.

3.6.3. Gabbro-diorite intrusives

Gabbros are common intrusive rocks in the southern part of the thesis area where they form large circular to elliptical bodies (Plate 8-D). They intrude the gneissic granodiorites of the basement complex and Meherga formation but they do not intrude the Al Amar formation. The gabbros are coarse-grained rock, black to greenish gray in colour. Some of the gabbros exhibit layering and are clearly cumulates (Plate 8-E). The layers are made up of gabbro and norite in the lower parts of the intrusions,
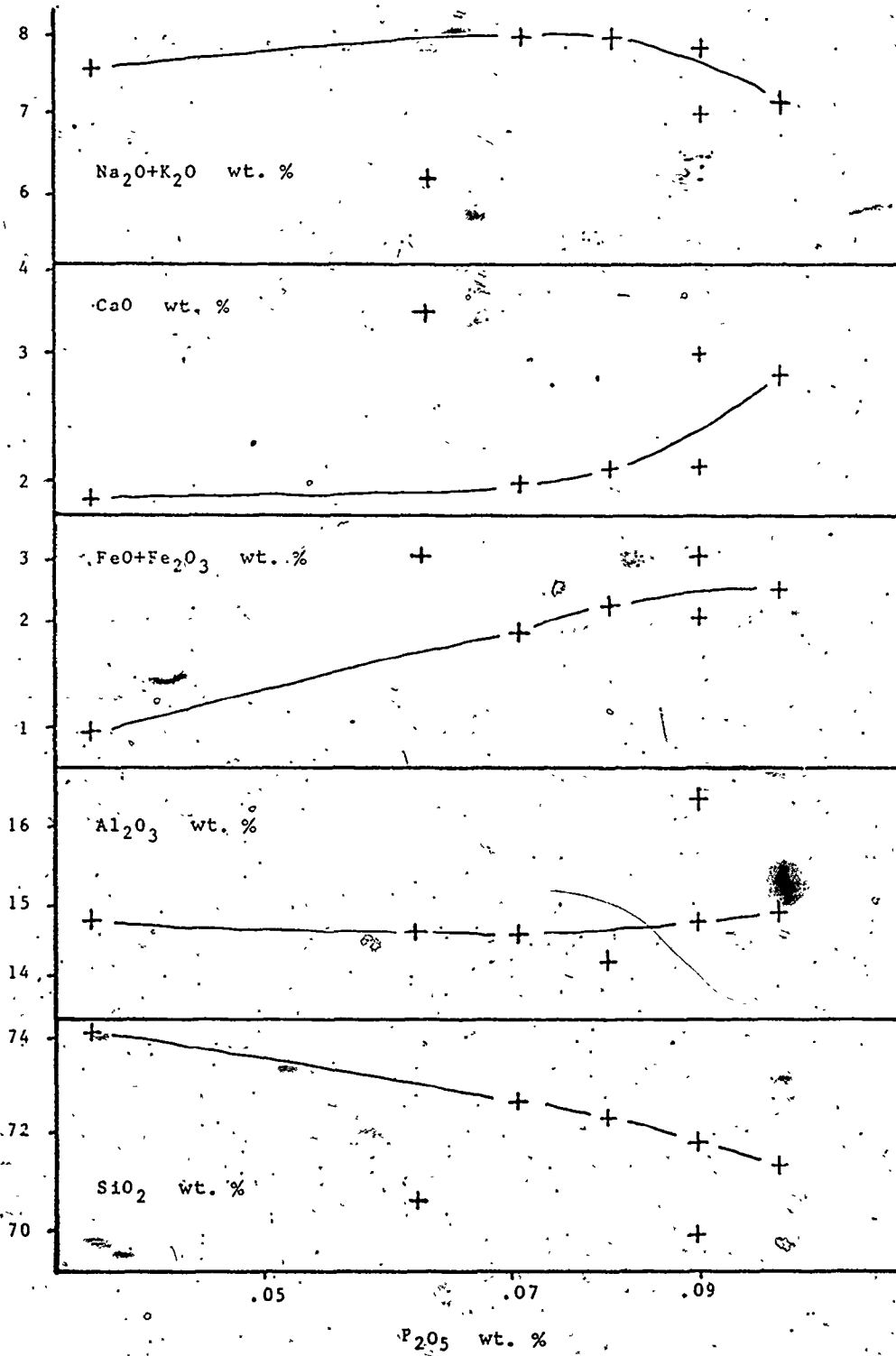
Fig. 32. Plot of P_2O_5 against SiO_2, Al_2O_3, FeO+ Fe_2O_3, CaO, and Na_2O+K_2O of the gneissic granodiorite.
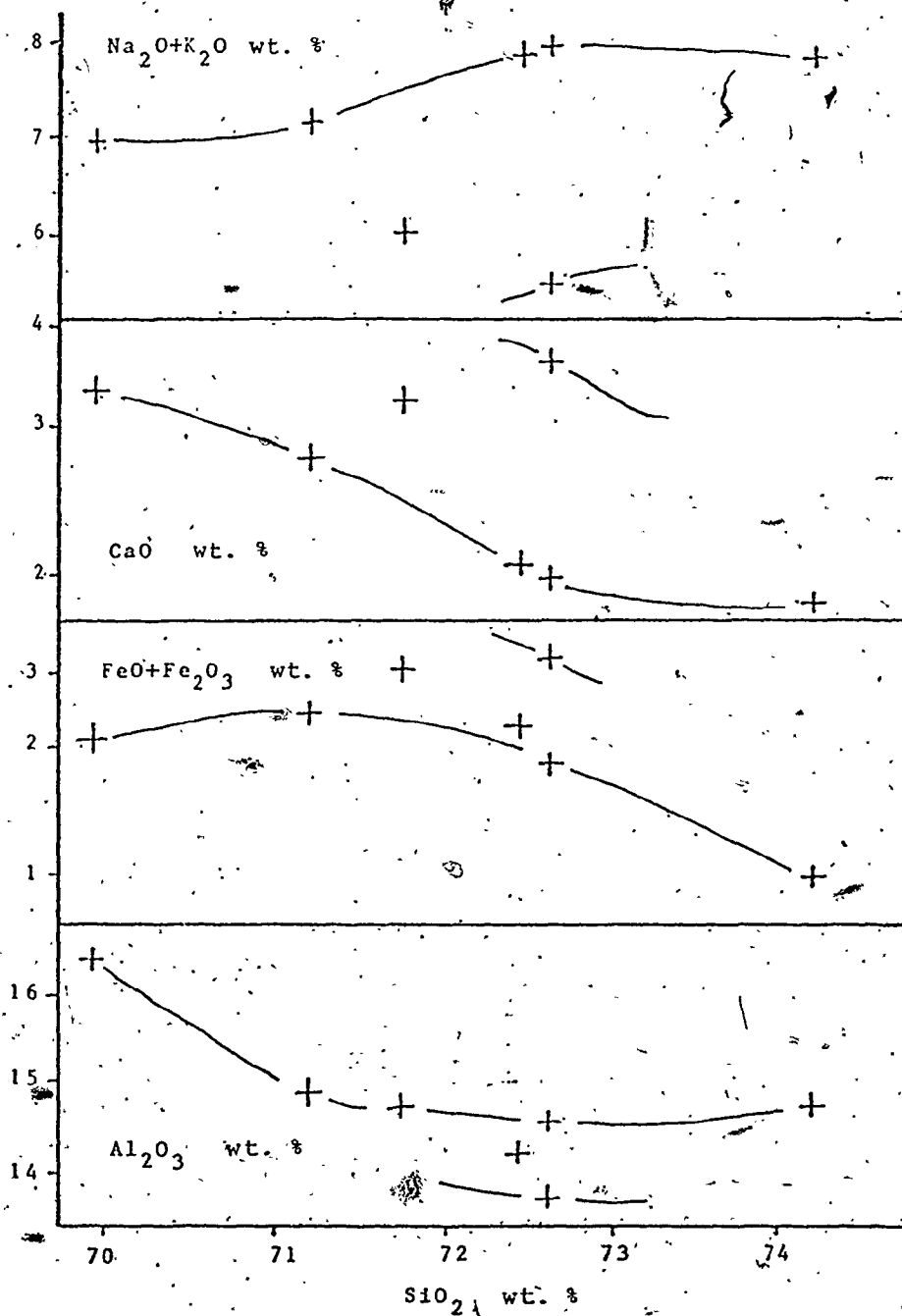
Fig. 33. Plot of SiO_2 against Al_2O_3, $FeO+Fe_2O_3$, CaO, and Na_2O+K_2O of the gneissic granodiorite.
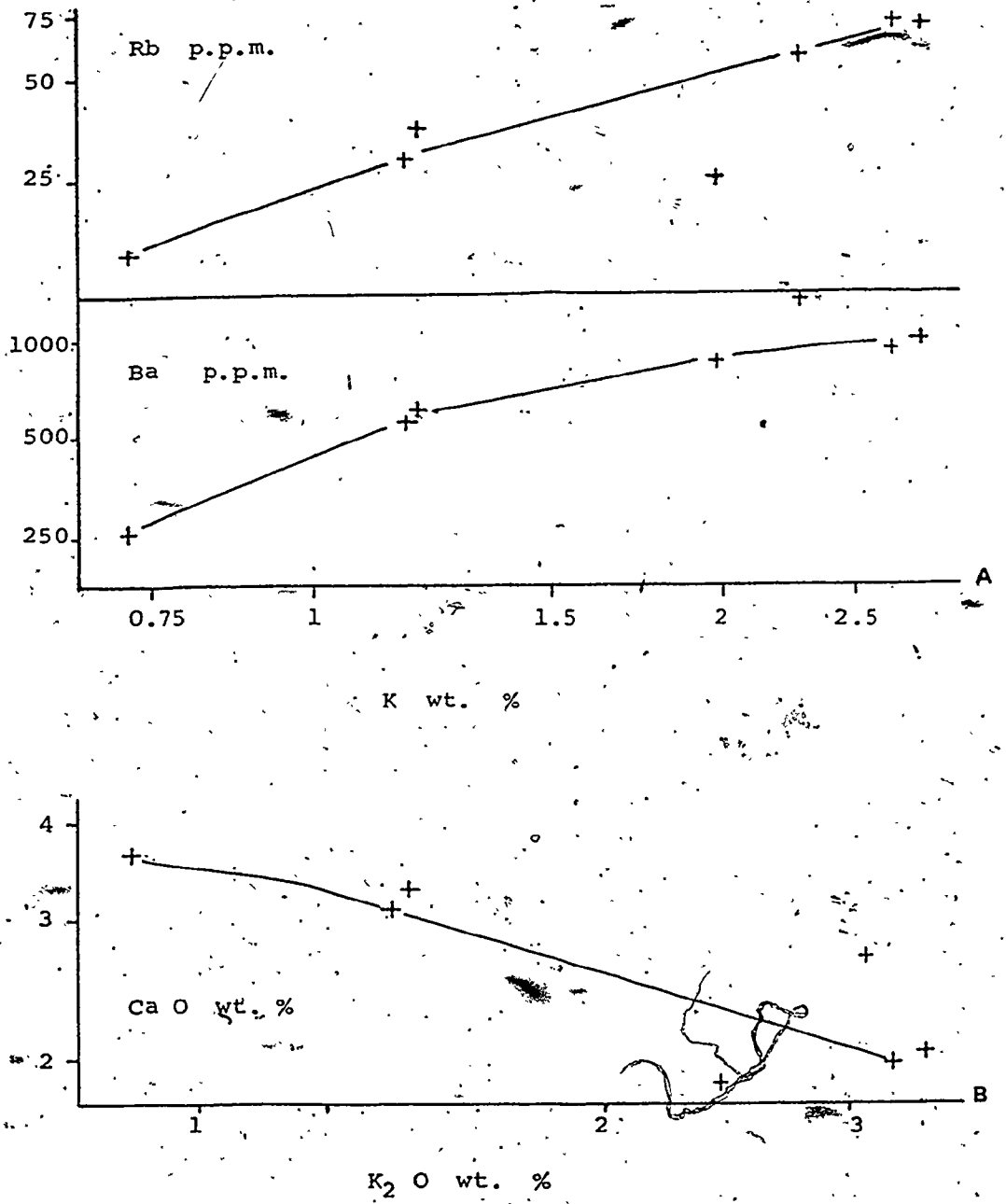
Fig. 34. (A) Plot of K against Ba and Rb, and (B) K$_2$O versus CaO of the gneissic granodiorite.

whereas layers in the upper parts are composed of olivine gabbro and peridotite (Zubeir, 1976).

The gabbros are composed of plagioclase, olivine, pyroxene, hornblende and opaque minerals.

Plagioclase occurs as tabular, euhedral crystals and make up more than 60% of the rock. Plagioclase separated from the cumulate rocks, range in composition from An_{93} at the base to An_{78} at the top (Zubeir, 1976).

Olivine is the second most important cumulate mineral (25%). It occurs as medium to large euhedral crystals of forsterite (Zubeir, 1976). Incipient serpentinization of olivine along cracks and around its margins is widespread (Plate 8-F).

Pyroxene, orthopyroxene (hypersthene) and clinopyroxene (diopside and augite) are present only as minor constituent of the cumulate rocks. They are more abundant in the normal gabbros.

Hornblende is brown in colour and occurs usually as an interstatial mineral or sometimes as a replacement of pyroxene.

Opaque minerals usually interstitial, include magnetite, ilmenite, and secondary hematite.

Diorites are more abundant in the central and northern parts of the thesis area and form either large elongate bodies trending northwest-southeast parallel to the Al Amar-Idsas fault (Plate 9-A) or semicircular bodies

PLATE 8

A - Gneissic granodiorite, weathered, altered, and locally foliated.

B - Zenolith of the old metasediments in the gneissic granodiorite.

C - Thin section of the gneissic granodiorite consist of quartz (Q), albite, (P), biotite (B), and muscovite (M).

D - Eliptical to circular bodies of gabbros in the Al Amar-Idsas region.

E - Cumulate gabbro exhibit layering. The layers are made up of plagioclase, olivine and/or pyroxene.

F - Thin section of serpentinized olivine of the layered gabbro.

PLATE 8

A

B

C .8 mm

D Gabbro

E

F .6 mm
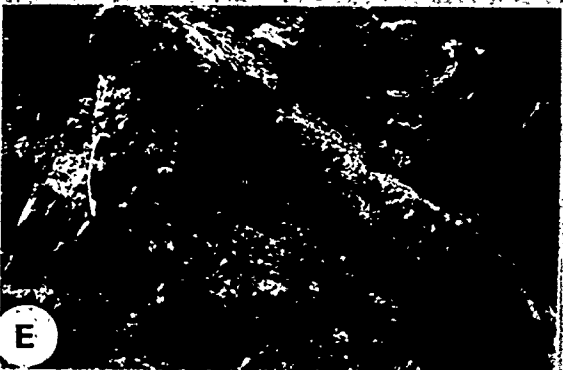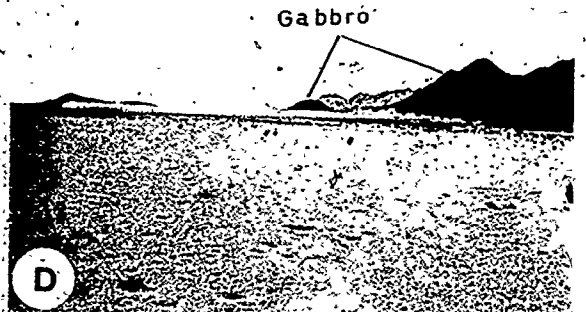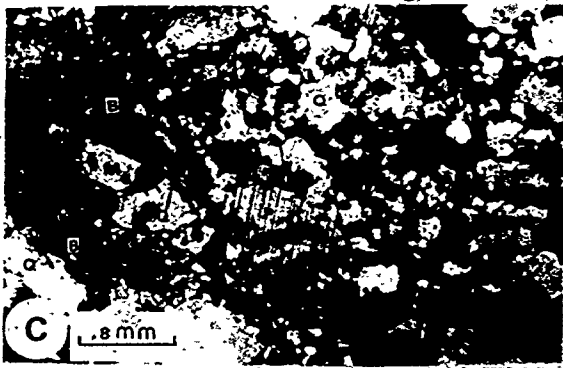
associated with the gabbros. The diorites are coarse to medium-grained rocks, grayish green in colour. They are foliated along their borders but have massive cores. The diorites are composed of plagioclase, hornblende, biotite, quartz and secondary minerals chlorite, sericite and epidote (Fig. 9-B). Opaque minerals include ilmenite and hematite.

The gabbros and diorites contain xenoliths of the gneissic granodiorites of the basement complex, and rocks of the Meherga formation. Rocks of the Al Amar formation have not, however, been observed as xenoliths in the gabbro-diorite rocks.

The average chemical composition of the gabbros and diorites is given in Table 8, and analyses of individual samples are presented in Appendix 8.

3.6.4. Syntectonic granodiorite

Plutons of syntectonic granodiorite are found scattered throughout the area east of the Al Amar-Idsas fault (Fig. 5). These plutons, although similar to the gneissic granodiorite mineralogically and chemically, are not gneissic. The syntectonic granodiorites are gray in colour, massive, coarse-grained in the center, but medium-grained, lineated and schistose at their margins (Plate 9-C). The border zones are also richer in mafic minerals. Along their contacts, the syntectonic granodiorite plutons

TABLE 8 - Average and range of chemical composition and CIPW norm values for the gabbros and diorites of AlAmar-Idsas region.

	Gabbro		Diorite	
	Ave. I	Range	Ave. II	Range
SiO_2	48.67	45.04 - 52.95	59.20	51.18 - 64.52
TiO_2	0.61	0.17 - 1.16	0.76	0.51 - 1.00
Al_2O_3	18.98	15.09 - 25.64	16.56	14.90 - 18.02
Fe_2O_3	2.37	1.69 - 2.90	2.08	1.85 - 2.34
FeO	7.62	1.63 - 11.30	5.76	3.14 - 9.30
MnO	0.17	0.07 - 0.26	0.13	0.08 - 0.17
MgO	6.31	4.11 - 10.80	3.35	2.44 - 5.01
CaO	12.04	8.84 - 16.15	7.05	4.85 - 10.16
Na_2O	2.28	1.12 - 4.33	3.50	2.30 - 4.43
K_2O	0.27	0.08 - 0.56	1.11	0.54 - 2.14
P_2O_5	0.34	0.01 - 0.63	0.44	0.11 - 0.76
Total	99.64		99.94	
$\frac{FeO^+}{MgO}$	1.55		2.28	
Trace elements (P.P.M.)				
Cr	152	25 - 315	41	8 - 160
Ba	168	68 - 436	439	180 - 1270
Ni	38	0 - 114	17	0 - 49
Nb	3	0 - 8	4	0 - 9
Zr	13	0 - 47	89	26 - 185
Y	8	1 - 17	19	11 - 25
Sr	511	163 - 1026	389	248 - 639
Rb	7	2 - 14	27	7 - 71

Norm (CIPW)

	Gabbro		Diorite	
	Ave.	Range	Ave.	Range
Q	0.25	0.17 - 1.80	13.49	1.97 - 21.72
or	1.59	0.45 - 3.31	6.54	1.96 - 12.53
ab	19.11	9.47 - 36.76	29.61	19.56 - 37.27
an	41.03	31.79 - 62.41	26.22	18.86 - 36.20
di	13.53	6.95 - 17.69	4.91	0.31 - 10.28
hy	15.07	4.58 - 27.18	13.75	8.89 - 15.33
ol	3.97	.0 - 16.68	-	
mt	3.45	2.45 - 4.20	3.02	2.68 - 3.38
il	1.31	0.32 - 3.15	1.44	0.98 - 1.87
ap	0.87	0.02 - 1.59	1.03	0.26 - 1.81
$*\frac{K_2O}{K_2O+Na_2O}$	.11		.24	

I = 10 samples; II = 10 samples.

FeO^+ = total iron (Fe_2O_3 x 0.8998 + FeO).

$*K_2O$ and Na_2O recalculated at SiO_2 = 65 wt. %.

tend to exhibit flow banding and develop narrow metamorphic contact aureoles in the Halaban metavolcanics and metasediments.

Inclusions of gneissic granodiorite, Halaban metavolcanic and metasedimentary units occur in parallel alignment and have trends parallel to that of the country rocks (Plate 9-D). In the southern part of the thesis area large inclusions of gabbro and diorite are present in the granodiorites.

Fleck quoted in Greenwood et al. (1975) reported that syntectonic granodiorites in the southern Hijaz quadrangle range in age from 650 to 600 my. Also, Brown quoted in Overstreet et al. (1972) stated that the quartz diorite of the component plutons east of the Al Amar-Idsas fault has a K-Ar age of 604 ± 12 my.

The syntectonic granodiorite is hypidomorphic in texture and generally composed of 30% plagioclase, 30% quartz, 20% orthoclase, 13% biotite, 5% hornblende, and less than 1% zircon and apatite (Plate 9-E;-9-F).

Chemically, the syntectonic granodiorites are similar to the gneissic granodiorite of the basement except that the syntectonic granodiorites are richer in total iron reflecting their greater concentration of biotite. The syntectonic granodiorites are also higher in chromium, nickel, zircon, yttrium and rubidium than the gneissic granodiorite but lower in barium and strontium.

PLATE 9

A - Large elongated bodies of diorite trending NW-SE
    parallel to the Al Amar-Idsas fault.

B - Thin section of the diorite consist of oligoclase-
    andesine (PL), biotite (B), hornblende (AM), and
    quartz (QZ).

C - General view of the syntectonic granodiorite.

D - Syntectonic granodiorite containing inclusions of
    diorite and gabbro.

E - Thin section of the syntectonic granodiorite consist
    of plagioclase (PL), quartz, hornblende, biotite, and
    ilmenite.

F - Handspecimen of the syntectonic granodiorite composed
    of plagioclase, quartz, amphibole and opaque minerals.

PLATE 9

A

B .6mm

C

D

E .8mm

F 0 5Cm
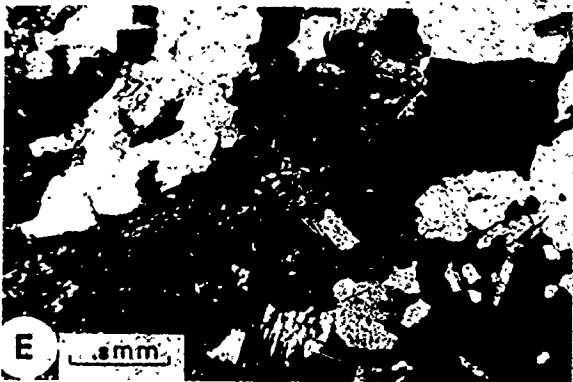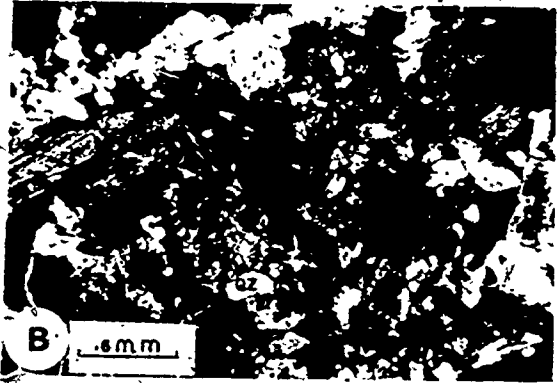
The average chemical composition of the syntectonic granodiorites is given in Table 9, and individual analyses are presented in Appendix 9.

3.6.5. Post-tectonic granite

Late to post-tectonic granites underlie a large part of the western sector of the thesis area but are present only as small scattered circular to oval plugs in the eastern part (Fig. 5). They are medium to fine-grained, pink to red in colour, massive, and unaltered. The post-tectonic granite have a well developed metamorphic contact aureoles where they intrude metasedimentary rocks, and often contain inclusions of diorite, meta-andesite and sericite chlorite schist. The granites are cut by two sets of fractures, N 10° E/80° E and N 80° E/70° W, the first set of which provided channel-ways for solutions rich in iron, as indicated by the deep colour of the fracture surfaces (Plate 10-A).

The post-tectonic granites are equigranular and consist of 50% orthoclase and/or perthite, 20% quartz, 15% plagioclase, 10% biotite, 3% amphibole and less than 2% apatite and/or sphene. Some of the post-tectonic granites contain phenocrysts of white feldspar up to 1 cm long (Plate 10-B) whereas others are poor in quartz and are syenitic.

The post-tectonic granites have strong scintillo-

metric anomalies indicating that they are enriched in radioactive elements. Even where granites are covered up by sand or gravel, a scintillometric anomaly may still be detected. The most radioactive granites are also the most deeply coloured red. Lacombe and Latalenet (1970) reported that the radioactivity ranged from 100 to 450 c/s.

The average chemical composition of the post-tectonic granites is presented in Table 9. The post-tectonic granites are enriched in silica and potassium and impoverished in titanium, aluminium and calcium compared with the gneissic granodiorites and syntectonic granodiorites. Average chromium, nickel, zirconium, and yttrium content of the granites is much higher than that of the syntectonic granodiorites which however have higher barium and strontium values. The scintillometer anomalies may reflect enrichment in zirconium and yttrium of the post-tectonic granites.

Chemical analyses of post-tectonic granite samples are given in Appendix 9.

On a calcium-total alkalies versus silica diagram, the Al Amar-Idsas region plutonic rocks form two groups:

a) a calcic to calc-alkalic group which includes the gabbros and diorites (Fig. 35) in addition to the gneissic granodiorites of the basement and the syntectonic granodiorites (Fig. 36) intrusive into the Meherga formation;

B) a calc-alkalic to alkalic group consisting of the

Table 9 - Average and range of chemical composition and CIPW norm values of the syntectonic granodiorites and post-tectonic granites.

	Syntectonic granodiorite		Post-tectonic granite	
	Ave. I	Range	Ave. II	Range
SiO_2	71.57	70.10 - 73.46	73.34	66.41 - 77.75
TiO_2	0.32	0.24 - 0.49	0.23	0.07 - 0.67
Al_2O_3	14.22	12.66 - 15.62	13.30	11.97 - 13.91
Fe_2O_3	1.36	0.28 - 1.68	1.02	0.50 - 1.98
FeO	1.17	0.44 - 2.40	1.46	0.53 - 4.36
MnO	0.05	0.03 - 0.08	0.05	0.02 - 0.13
MgO	0.78	0.16 - 1.69	0.24	0.00 - 0.67
CaO	2.54	1.98 - 3.46	1.13	0.54 - 2.02
Na_2O	4.23	3.24 - 5.64	4.06	3.74 - 5.05
K_2O	2.15	1.53 - 3.33	4.33	3.02 - 5.40
P_2O_5	0.29	0.03 - 0.63	0.09	0.04 - 0.24
Total	98.68		99.25	
$\frac{*K_2O}{K_2O+Na_2O}$	.34		.52	

Norms (CIPW)

Q	32.81	25.13 - 41.03	30.21	21.12 - 35.67
or	12.68	8.50 - 19.92	25.76	17.87 - 32.19
ab	36.34	27.75 - 47.86	34.57	31.92 - 42.78
an	9.81	8.68 - 10.49	4.68	1.08 - 8.39
cor	0.64	0.00 - 1.58	0.25	.0 - 0.87
di	0.33	0.00 - 1.48	0.33	.0 - 1.06
hy	2.97	1.31 - 6.63	2.10	0.47 - 7.19
ol	-		-	
mt	1.80	1.44 - 2.47	1.34	0.73 - 2.91
il	0.62	0.45 - 0.94	0.44	0.13 - 1.29
ap	0.66	0.07 - 1.51	0.38	0.10 - 0.90
hm	-		0.12	.0 - 0.58

Trace elements (P.P.M.)

Cr	116	2 - 510	257	0 - 670
Ba	602	86 - 1066	388	83 - 788
Ni	48	7 - 194	115	11 - 266
Nb	12	10 - 14	18	15 - 24
Zr	157	109 - 238	268	129 - 355
Y	28	8 - 44	135	62 - 329
Sr	378	56 - 709	83	21 - 188
Rb	55	47 - 59	156	21 - 233

*K_2O and Na_2O recalculated at SiO_2 = 65 wt. %.

I = 5 samples   II = 5 samples
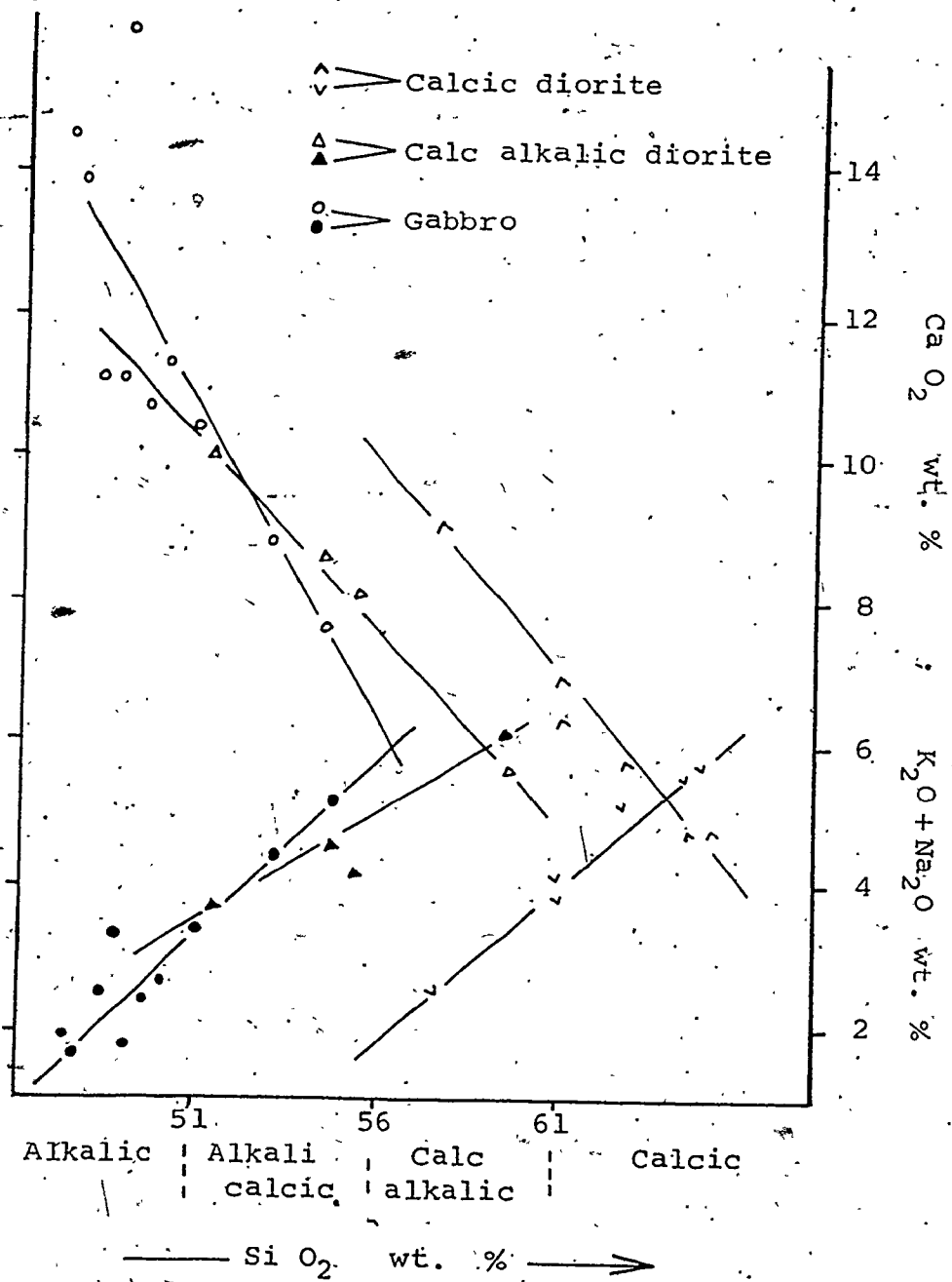
Fig. 35. Peacock's diagram applied to the gabbro and diorite of the Al Amar-Idsas region.

post-tectonic granites (Fig. 36).

The gneissic granodiorites of the basement possibly represent different granites as follows:

a) samples 154, 159, and 225 are calc-alkalic $[K_2O/(K_2O+Na_2O) = 0.25$ to $0.41]$ and have chemically high values of rubidium, potassium, barium and low values of yttrium, calcium, and total iron;

b) sample 147 in contrast is calcic $[K_2O/(K_2O+Na_2O) = 0.16]$ and has high values of yttrium, total iron, and calcium and low values of rubidium, potassium, strontium, barium, and aluminium;

c) samples 204, and 325 with intermediate characteristics lie between group a and group b.

The syntectonic granodiorites are very similar to the gneissic granodiorites of the basement and can also be divided into two groups:

a) samples 152, and 161 are high in aluminium, total alkalies, strontium. barium, and normative or, ab, and an;

b) samples 172, 175, and 275 are characterized by low aluminium, total alkalies, strontium, barium and normative or, ab, and an.

The post-tectonic granite sample 188, collected from east of the Al Amar-Idsas fault, is significantly lower in K_2O and higher in Na_2O when compared with the post-tectonic granites which intrude the Abt schist west of the Al Amar-Idsas fault.

The differentiation index (DI) of the Al Amar-Idsas
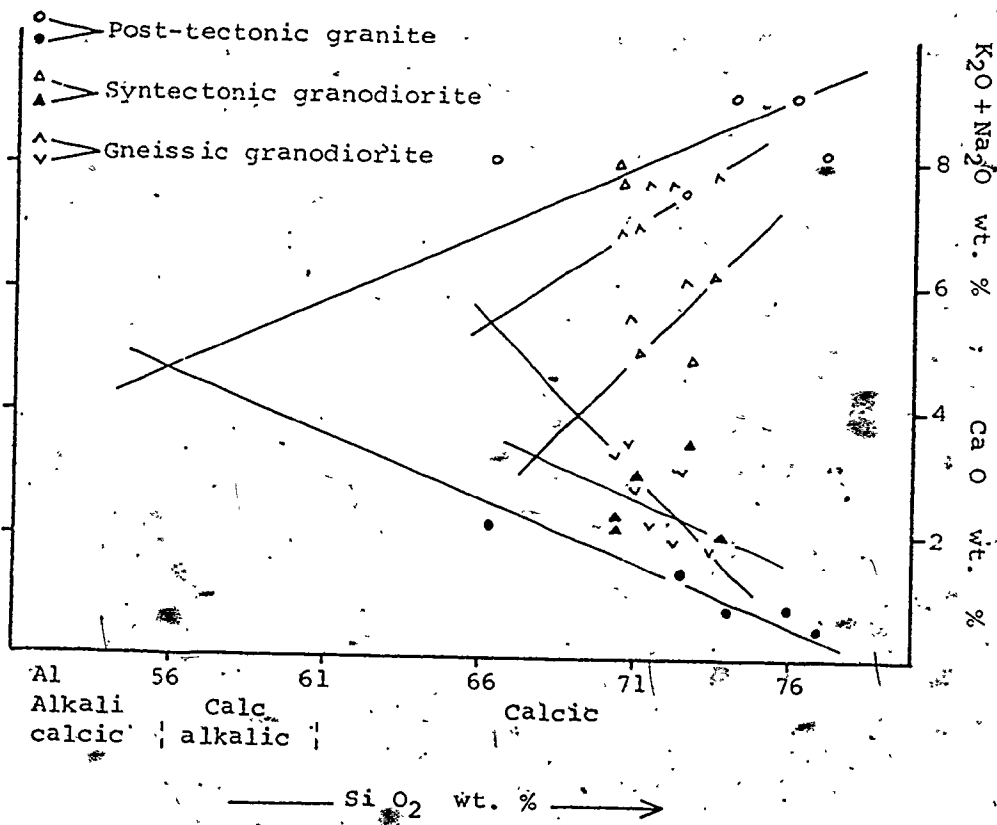
Fig. 36. Peacock's diagram applied to the gneissic granodiorite, syntectonic granodiorite, and post-tectonic granite of the Al Amar-Idsas region.

plutonic rocks increases generally with increasing silica
(Fig. 37). However, there are two breaks associated by
slight shifting in the plutonic rocks trend, the first at
about DI 40 and the second at DI 65. This may indicate
that the plutonic bodies were emplaced by several pulses.

On a plot of MgO versus TiO_2 in the plutonic rocks
(Fig. 38), it is evident that the diorites form two groups:

a) a high K_2O (Ave. = 1.27 wt %) high silica diorite
group characterized by MgO values less than 4%;

b) a low K_2O (Ave. = 0.72 wt %) low silica diorite
group characterized by MgO values more than 4%.

The low K_2O diorites have similar $MgO-TiO_2$ character-
istics to some of the gabbros and may be gentically re-
lated to them. The high K_2O diorites may be gentically
related to the syntectonic granodiorites. The gneissic
granodiorite and syntectonic granodiorite geochemical
trends are similar, whereas geochemical trends in the
post-tectonic granites are quite different.

3.7. Khuff Formation

The crystalline and metamorphic rocks are uncon-
formably overlain at the eastern borders by the Permian
Khuff Formation (Fig. 5). The contact between the Khuff
Formation and Precambrian rocks is marked by a cliff the
height of which does not exceed 50 m (Plate 10-C). The
lowest unit of the Permian strata, which dips gently 5°
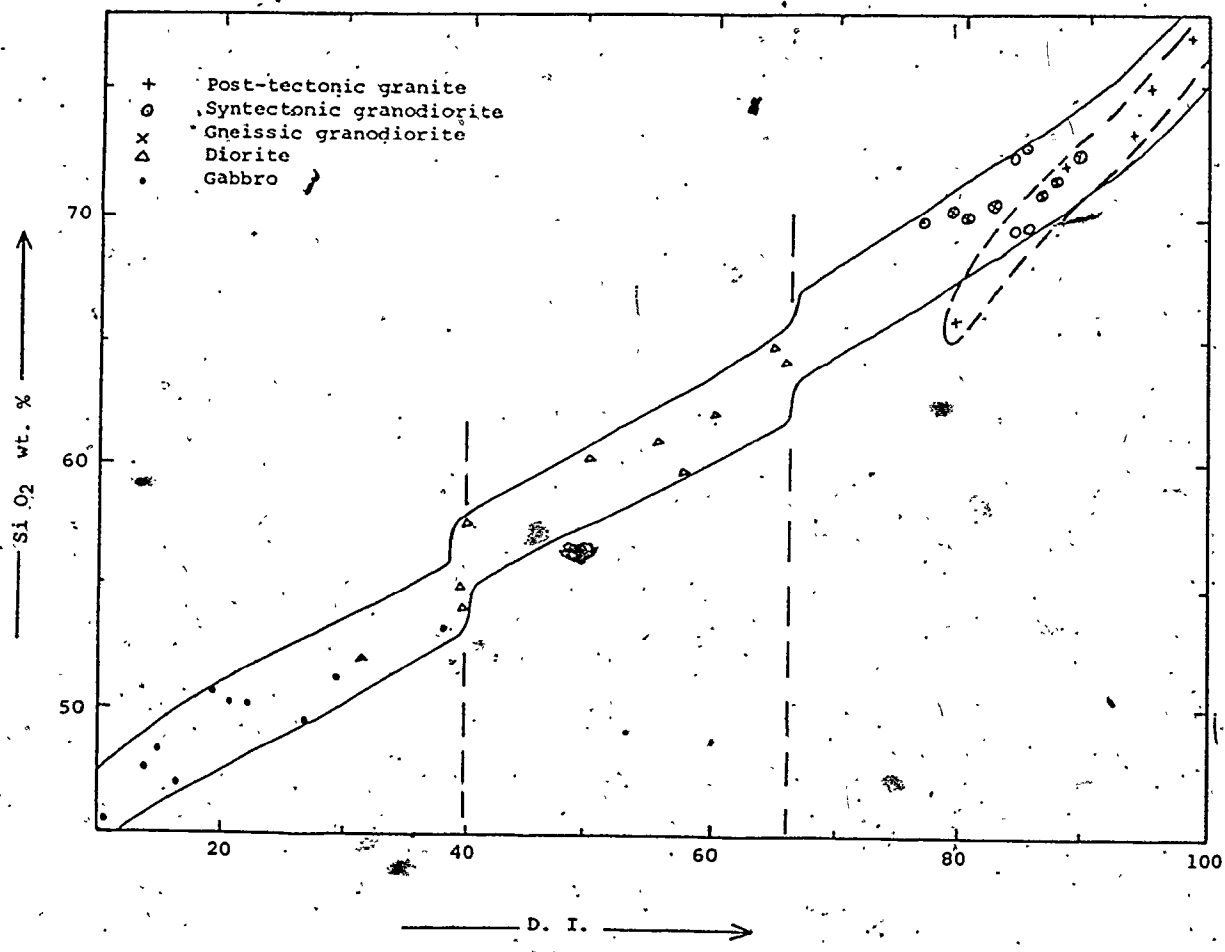
Fig. 37. Differentiation index plotted versus silica content of the plutonic rocks of the Al Amar-Idsas region.

124
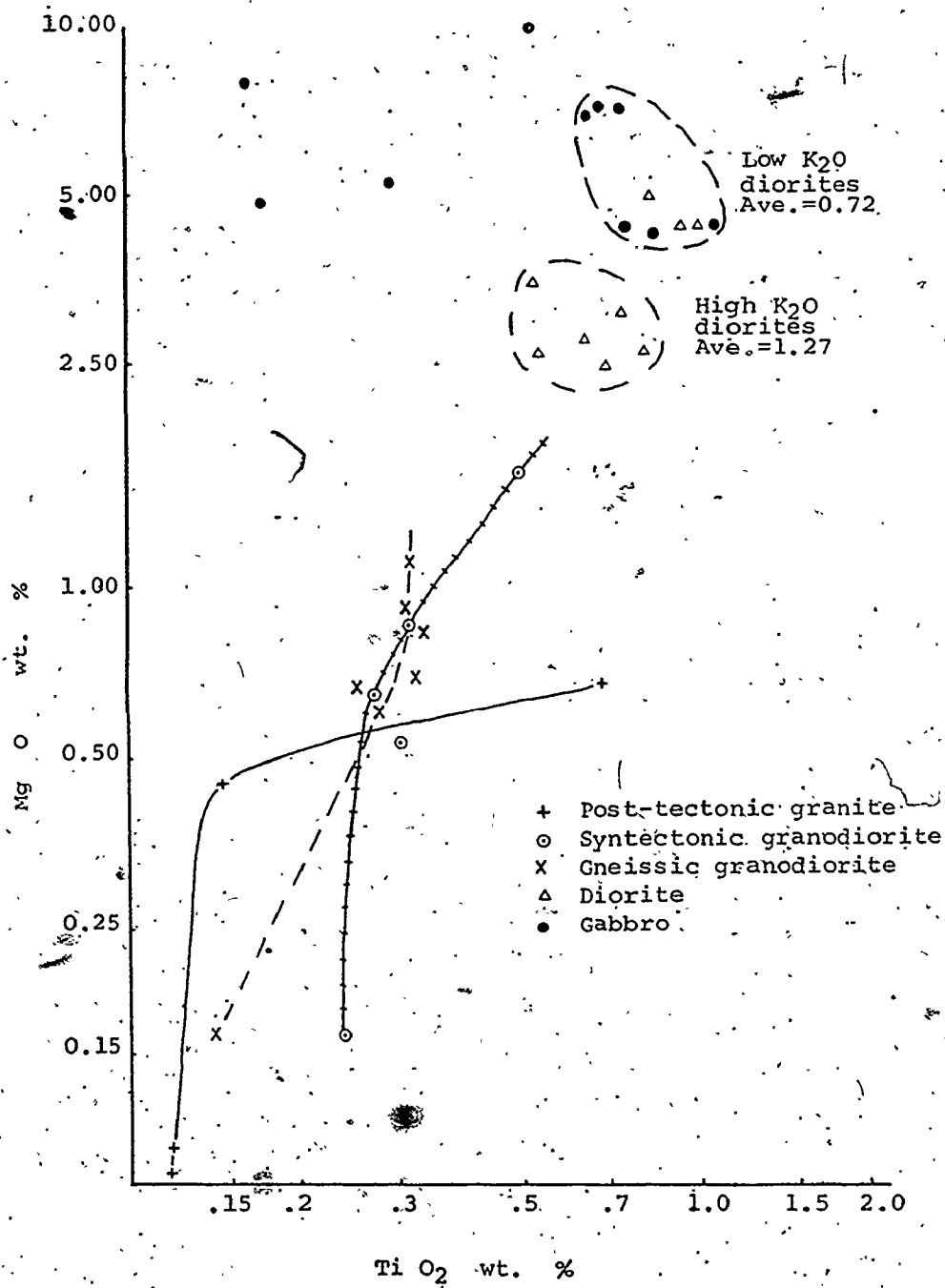
Fig. 38. Plot of MgO against TiO_2 of the plutonic rocks of the Al Amar-Idsas region.

due east, is composed of coarse-grained and heterogeneous cross bedded sandstone (Plate 10-D). The upper units are mainly formed of impure limestone (Plate 10-E) and/or dolomite containing some gypsiferous horizons.

Chemical analysis of the Khuff Formation impure limestone are given in Appendix 9.

PLATE 10

A - Major fracture surface in the post-tectonic granite
    serves as channel-way for solutions rich in iron.

B - Thin section of the post-tectonic granite consists of
    perthite, orthoclase (OR), quartz (QZ), and plagio-
    clase (PL).

C - General view of the contact relationship between the
    Precambrian rocks (g) and the Paleozoic cover (LS).

D - Cross bedding in the sandstone of the Paleozoic cover
    north of the Al Amar-Idsas region.

E - Handspecimen of the impure limestone of the Paleozoic
    cover east of the Al Amar-Idsas region.

PLATE 10
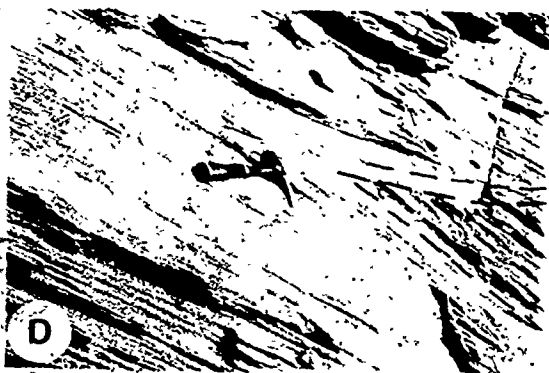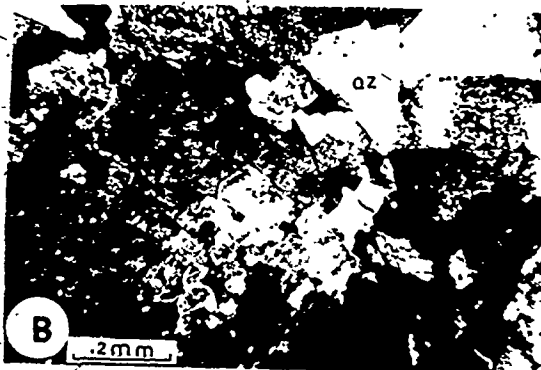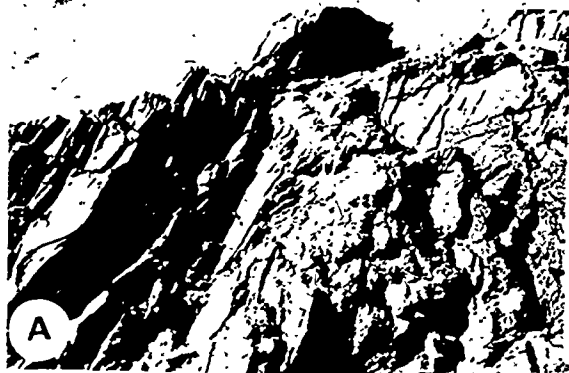
CHAPTER 4

COMPARATIVE PETROCHEMISTRY

One of the main problems encountered in this study of the volcanic rocks of the Al Amar-Idsas region concerns the effect of chemical mobility during weathering, alteration and metamorphism in modifying the original composition of the rocks. The results of an experimental investigation concerning the reaction between seawater and basalts indicated that silica, iron, magnesium, calcium, sodium, and potassium are invariably mobile elements (Bischoff et al., 1975; Seyfried et al., 1977).

Since the Al Amar-Idsas volcanic rocks are altered and contain volatiles up to 7.7 wt % (e.g. sample no. 193), clearly the possibility arises that their bulk chemistry may have undergone modification as a result of secondary alteration processes. For this reason, in the following discussion of the origin of the Halaban rocks in terms of their tectonic environment, reliance is mainly placed on the comparison of relative variation in content of supposedly immobile elements.

In terms of silica content and using the silica classification of basaltic rocks of Bryan et al. (1972), the volcanic rocks of the Halaban Group include:

basalt   samples 84, 104, 164, 165, 180, 257D;

basaltic andesite   samples 181, 182, 193, 205;

andesite   samples 49B, 206A, 207, 308;

dacite   samples 19, 110C, 183, 254A, 254B, 255, 304;

and rhyolite   samples 109, 139, 253.

The group A Halaban volcanic rocks all have silica contents less than 53 wt % and are therefore basalts. Other than sample 84 in which TiO_2 = 1.95 wt %, the basalts tend to have low TiO_2, Cr_2O_3, and NiO content and exhibit a relatively low rate of increase in TiO_2 relative to FeO^t/MgO during fractionation. The Halaban basalts (group A) are comparable in these respects to basalts from Eua island of Tonga (Bryan et al., 1972; Ewart et al., 1972) but are lower in SiO_2. Total alkali content is highly variable and is therefore not considered to be of any use for comparative purposes.

Groups B, C, and D are low titanium high silica calc-alkaline rocks. Groups C and D have higher silica contents relative to FeO^t/MgO and Cr_2O_3 than group A rocks, whereas group B rocks are possibly even more siliceous and similar to the low TiO_2 and FeO^t/MgO and high Cr_2O_3 andesitic rocks of Andes zone A of Lefevre (1973).

Group E rocks are rhyolites with silica contents ranging from 70.25 wt % to 78.17 wt %.

The metavolcanic rocks of the Abt schists include both high and low titanium types.

The high TiO_2 basalts (group A) are relatively fractionated tholeiitic rocks which are similar in TiO_2, FeO^t/MgO and alkali characteristics to the fractionated Galapagose basalts (Byerly and Melson, 1976); the later however are significantly richer in silica. They also, other than having 1 wt % less SiO_2 and a lower TiO_2 content relative to FeO^t/MgO, closely resemble the mid-Atlantic Ridge tholeiite (e.g. sample A 150) described by Shido et al. (1971). The high TiO_2 basalts resemble some basalts of the late stage Korambasanga volcanics of the Lau Island of the Eua-Tonga-Feji arc system (Gill, 1976).

In the low TiO_2 basalts (group B), the more fractionated basalt (sample 278A) is comparable to the oceanic island arc tholeiites of Eua (Bryan et al., 1972), whereas the less fractionated again resemble the late stage basalts of the Korambasonga volcanic group of the Lau Island (Gill, 1976).

The chemistry of the Abt sediments seems to be dominantly of calc-alkalic type. However, relative to chromium and titanium they seem to be enriched in silica and zirconium. The high zirconium content reflects the presence of well developed crystals of zircon, and it is conceiv-

able that the Abt schist contains zirconium and quartz of
continental derivation.

The ultramafic rocks are relatively enriched in iron
(Table 6), and appear to be cumulates rather than mantle
rocks. While they could represent the cumulate part of a
disrupted ophiolite, such a conclusion is far from certain.
Similarly the gabbros are cumulates, relatively iron en-
riched (Table 8), and could have been derived from thole-
iitic or calc-alkalic source rocks. The Al/Ti ratios of
clinopyroxene of the gabbros also indicate a tholeiitic
or calc-alkaline source for these rocks.

On a Qz-Or-Pl plot of various plutonic rocks of the
western United States, Alaska, and western Saudi Arabia
(Fig. 39), the plutonic rocks of the Al Amar-Idsas region
are almost identical to those of northwest Oregon and the
southern California batholiths. They character-
istically exhibit low TiO_2 relative to FeO^t/MgO and low
Nb indicating that they are of calc-alkaline or "orogenic"
character.
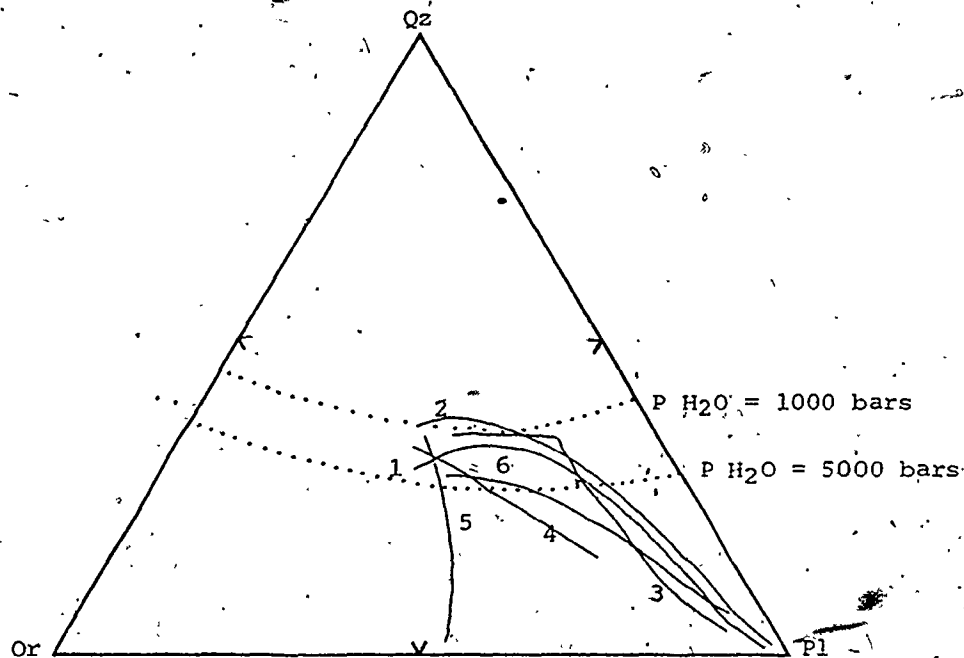
(1) Al Amar-Idsas plutonic rocks;Saudi Arabia,1978.
(2) Plutonic rocks of NW Oregon;U.S.A.(Bateman,1963)
(3) Southern California batholith;U.S.A.(Bateman,1963)
(4) Sierra Nevada batholith;U.S.A.(Bateman,1963)
(5) Plutonic rocks from Alaska;U.S.A.(Bateman,1963)
(6) Al Hadah granitic rocks;Saudi Arabia(Marzouki,1977).

Fig. 39. Comparison between the Al Amar-Idsas
         plutonic rocks and other plutonic
         rocks from Saudi Arabia and U.S.A.
         on the Or-Qz-Pl diagram.

CHAPTER 5

HISTORY OF IDEAS CONCERNING THE EVOLUTION
OF THE ARABIAN SHIELD

To understand the Precambrian tectonic history of the
Arabian Shield we should look to the tectonic history of
Africa in general and to the Pan African event in particu-
lar because until recently (30 my ago; Coleman et al.,
1972) Arabia was part of Africa.

Greenwood et al. (1975) have suggested that the
Arabian Shield formed during two stages of cratonization
of an intra-oceanic island arc in southwestern Saudi
Arabia. The first stage began with deposition of calcic
to calc-alkalic basaltic and dacitic volcanics and im-
mature sediments that were deformed, metamorphosed and
intruded by dioritic batholiths; the second stage of
cratonization, initiated about 595 my ago, also involved
volcanism, deformation, low grade metamorphism, and
intrusion of granitic batholiths. Greenwood et al. (1975)
proposed a northwest trend for the island arc and north-
east dip to the associated Benioff zone on the basis of
the polarity of potassium variation trends identified by

Greenwood and Brown (1973).

Garson and Shalaby (1976) also used a plate tectonic model to describe the evolution of the Red Sea region from Archean to lower Cambrian times. They suggested that the development of the Arabian Shield involved subduction and successive opening and closing of a series of intra-continental marginal basins developed in response to oceanward migration of the primary arc system. Garson and Shalaby (1976) claimed that this process explains the existence of five ophiolite zones in Egypt and Saudi Arabia as well as the Najd fault system. Shackleton (1976) however concluded that throughout Africa the geologic history of cratonic regions and their circumferential tectonic belts is very similar, and that there is no evidence either for cratonization processes involving oceanic island arcs or for large scale plate motions.

According to Brown and Coleman (1972) and Akaad and Noweir (1972) the ultramafic rocks of Saudi Arabia and the Eastern Desert of Egypt trend NNW-SSE. Akaad and Noweir (1972) suggested that the ultramafic bodies were formed as peridotitic crystal mushes composed mainly of olivine and pyroxene lubricated by water vapour extracted either from geosynclinal sediments or nearby granites. In Saudi Arabia, ultramafic rocks identified by several workers (Bakor, 1973; Larry, 1974; and Neary, 1974) occur in linear zones, a feature which led Burke et al. (1977)

to suggest that plate tectonic processes have been opera-
tive throughout the last 2500 my. Kröner (1976, 1977)
concluded that plate tectonic models fail to explain the
evolution of the Precambrian linear fold-belts of South
and East Africa.

Neary et al. (1976) postulated that the granitic
rocks of the Northeast Sudan and of the Arabian Shield
were formed in an island arc environment above an oceanic
subduction zone, and interpreted the five ultramafic zones
of the Eastern Desert of Egypt and the two ultramafic
zones in the Arabian Shield as relicts of oceanic crust
between island arcs. However, Neary et al. (1976) sug-
gested that since paleomagnetic data indicated Africa has
been a unified continental mass for the last 1500 my
(Piper et al., 1973) the oceans between the arcs must have
been closely spaced.

A different plate tectonic model was suggested by
Al Shanti and Mitchell (1976) for the eastern edge of the
Arabian Shield. They proposed that the Al Amar-Idsas
fault marked the site of an eastward dipping subduction
zone, separating a volcanic arc system represented by the
Halaban volcanics on the east, from ocean floor sediments
represented by the Abt schist to the west.

The plutonic rocks of the Al Hadah area in the west
of the Arabian Shield were interpreted by Marzouki (1977)
as having formed in a continental margin subduction zone

environment. The ultramafic zones in the Arabian Shield
were considered by Marzouki and Fyfe (1977) to represent
sutures marking the sites of small, closely spaced basins,
whose closure involved continent-continent collision.

Nasseef and Gass (1977) and Gass (1977) report that
all of the Arabian Shield granites "belong to a low Rb,
Nb, Y provence when compared to the African granites else-
where." On the basis of the suggestion by Pearce and Gale
(1977) that all granitic rocks formed above active Benioff
zones have Nb contents below 15 p.p.m., Gass (1977) con-
cluded that all calc alkalic granites of the Arabian Shield
formed above a Proterozoic Benioff zone. Based on the
evolution of $K_2O/(K_2O+Na_2O)$ variation in supposedly 1000
my old granitic rocks sampled on an east-west traverse
across the Arabian Shield, Gass and Nasseef (in press)
further concluded that the early granites of the Arabian
Shield evolved above four independent arc systems.

Frisch et al. (1977) identified what could be the
largest ophiolite belt in the central part of the Arabian
Shield (the Hulayfah-Hamdah ophiolite belt) and concluded
that the Arabian Shield is built up of several closely
spaced volcanic arcs of late Proterozoic age. According
to these authors the trench sediments between these vol-
canic arcs have been squeezed out as a result of collision.

CHAPTER 6

CONCLUSIONS

The Al Amar-Idsas region is characterized by the presence of:

1 - gneissic granodiorite basement east and west of the Al Amar-Idsas fault as old as 1010 my (Rb/sr).

2 - volcanic rocks ranging in composition from basalt to rhyolite, and which are calc-alkaline.

3 - schists (Abt Formation), a mixture of tholeiitic and calc-alkali volcanic rocks derived from a volcanic arc to the east and calc-alkali sediments perhaps in part derived from a continental source.

4 - a major tectonic discontinuity, the Al Amar-Idsas fault, a distinctive linear feature separating Halaban volcanic rocks from Abt Formation metasediments. The fault is a westward directed thrust fault along which later movements were of strike-slip nature.

5 - ultramafic rocks (serpentine, pyroxenite, peridotite) and carbonate (Shigran) occuring mainly along the Al Amar-Idsas fault or nearby, but in places within the Abt metasediments or Halaban volcanic rocks.

6 - granitic rock of which the $K_2O/(K_2O+Na_2O)$ values increase from east to west.

The geology of the Al Amar-Idsas region can be interpreted in terms of the existence of a westerly dipping subduction zone east of the Al Amar-Idsas region (Fig. 40) responsible for the development of the older (Meherga) formation of calc-alkali volcanic arc rocks and a marginal basin in which the Abt metasediments were deposited as mixtures of tholeiitic to calc-alkali volcanic rocks and immature sediments derived in part from a continental source. Closure of the small ocean basin along an easterly inclined subduction possibly resulted in the formation of the Al Amar formation. Even later, transcurrent fault movements took place along the Al Amar-Idsas fault.

Finally, I would like to emphasize that both the geologic work and the proposed tectonic model in this thesis are the results of a regional study of the Al Amar-Idsas region. For a better understanding of this part of the Arabian Shield I would like to suggest the following:

A, A detailed stratigraphic study of the most southern part of the thesis area to find the relationships between the metavolcanics and metasediments.

B, Completion of a collection from both the Meherga and Al Amar formations for pegrographic and chemical analysis to further understanding of the volcanicity of the area.

C, Age determination of zircons in the metasediments of the Abt Schist.
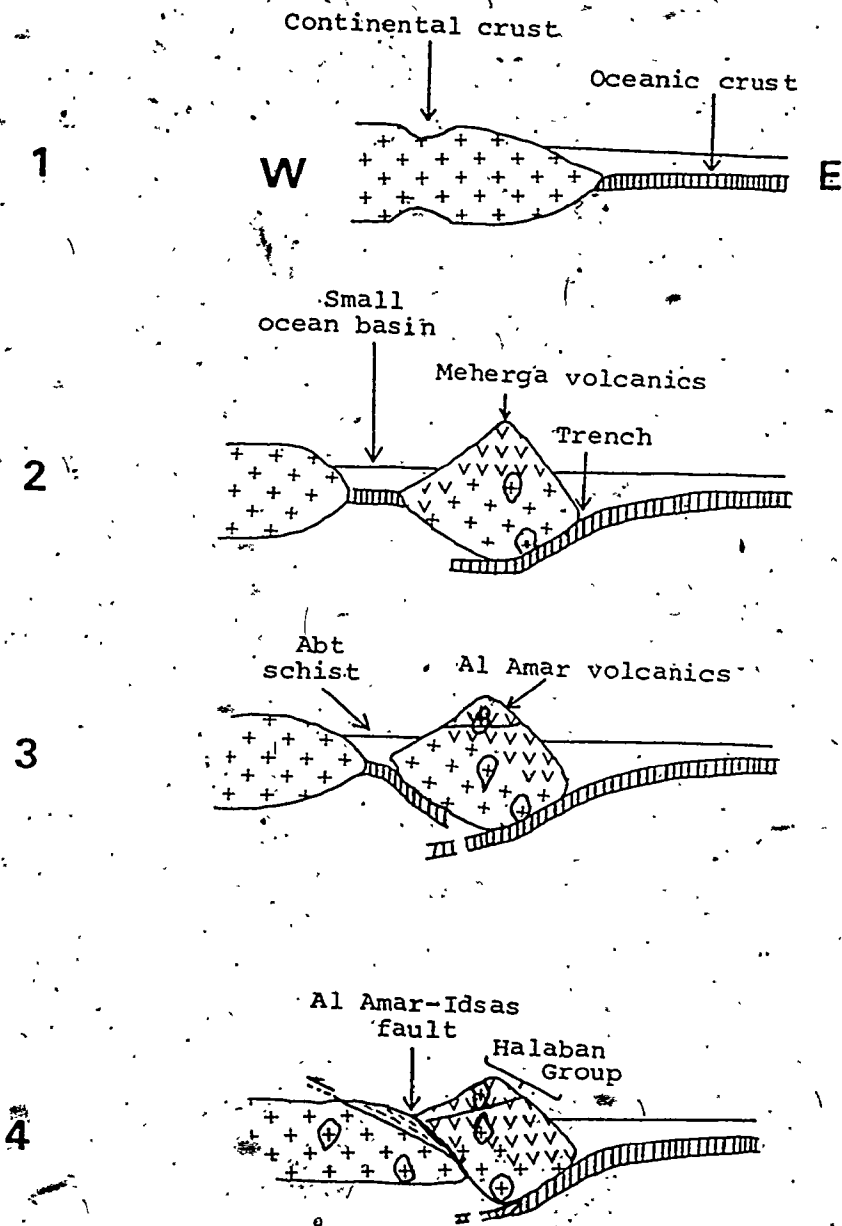
Fig. 40. Plate tectonic model for a possible evolution of the Al Amar-Idsas region of the Arabian Shield.

APPENDICES

Appendix 1   ANALYTICAL PROCEDURES

METHOD

Chemical analyses were determined using the Philips PW 1450 AHP fully automated x-ray fluorescence spectrometer, at the University of Western Ontario. Samples (about 500 gr.) to be analysed were crushed to a fine powder (less than 200 mesh) in a Bleuler Mill. Powder pellets and fused discs were made from the powder of each sample according to the method of Norrish and Chappell (1967) and Norrish and Hutton (1969), respectively. Pellets and discs were then loaded into a sample holder and automatically fed to the machine. Counts were determined for both the unknown samples and the U.S.G.S. standards. The standards used were: FS72 (for all major elements except Na), GA (for Na), AGV-1 (for Ba, Sr and Zr), GSP (for Rb), VSN (for Y), and DTS (for Cr and Ni). The data were printed on a teletype and punched on a paper tape which was then used to generate computer cards. A computer program, obtained from Dr. H. Hunter of the University of Western Ontario, applied the necessary correction factors to the raw data. The calculated chemical composition (in wt %) of the sample analyzed was punched on cards and these were run through a second program which calculated the CIPW molecular norm.

The analyses are accurate to within 1% of the amount present for major elements except Na and to within 10% of

the amount present for trace elements and Na. In general, there is close agreement between the analytical (XRF) and U.S.G.S. standard acceptable values for TiO_2, MnO, MgO, CaO, Na_2O, K_2O and P_2O_5. Values determined for SiO_2 are slightly greater, and Al_2O_3 and total Fe as Fe_2O_3 are slightly less than the U.S.G.S. standard values. The small standard deviations calculated from multiple analyses of the standard samples indicate a high degree of precision for the analytical method used.

DETERMINATION OF VOLATILES

The total volatiles for all the chemically analysed samples were determined using the method of loss on ignition (LOI). About 2 g of sample was weighed, ignited at about 1100°C in a porcaline crucible, cooled in a desicator and reweighed. The weight loss was assumed to be due to volatile loss (= LOI).

Appendix 2 - Total rock analyses and normative values of the Halaban rocks.

	A1	A2	A3	A4	A5	A6
	164	104	165	193	257D	84
SiO_2	46.05	50.59	49.77	48.38	47.60	46.14
TiO_2	0.58	0.68	0.78	1.06	1.10	1.83
Al_2O_3	15.16	17.28	19.80	16.44	17.40	13.05
Fe_2O_3	2.40	2.39	2.22	2.37	2.63	2.75
FeO	8.10	7.90	7.50	7.76	10.09	11.05
MnO	0.26	0.20	0.19	0.24	0.19	0.30
MgO	9.52	7.29	3.93	4.21	4.22	4.03
CaO	14.20	10.59	9.28	6.47	6.10	12.48
Na_2O	0.90	3.00	2.98	3.29	2.28	1.31
K_2O	1.06	0.06	2.01	1.68	1.09	0.15
P_2O_5	0.65	-	0.63	0.25	0.60	0.53
L.O.I.	1.10	-	0.79	7.70	6.65	6.35
Total	99.98	99.98	99.93	99.85	99.95	99.97
$\frac{FeO^t}{MgO}$	1.08	1.37	2.42	2.35	2.95	3.36
$\frac{K}{Rb}$	489	249	556	697	431	415
$\frac{Ba}{Rb}$	23	80	14	35	26	7

Norms (CIPW)

Q	-	-	-	-	6.01	6.30
or	6.33	0.35	11.97	10.77	6.90	0.91
ab	7.69	25.13	25.42	30.20	20.60	11.83
an	34.55	33.72	34.99	27.26	28.34	31.27
cor	-	-	-	-	3.48	-
di	26.30	15.47	5.82	4.82	-	26.24
hy	6.19	16.58	7.98	18.94	27.22	14.27
ol	12.75	4.04	7.46	1.45	-	-
mt	3.52	3.43	3.24	3.73	4.09	4.26
il	1.11	1.28	1.49	2.18	2.24	3.72
ap	1.56	-	1.62	0.64	1.62	1.33

Trace elements (P.P.M.)

Cr	307	125	51	17	39	14
Ba	410	160	428	697	543	21
Ni	82	32	16	7	-	5
Nb	5	4	7	-	-	-
Zr	20	3	35	94	94	61
Y	10	6	18	27	17	28
Sr	197	356	300	591	320	253
Rb	18	2	30	20	21	3

$FeO^t = Fe_2O_3 \times 0.8998 + FeO$

Appendix 2 - Contin.

	B1	B2	B3	B4	B5	C1	C2	C3	C4
	206A	205	19	207	110C	49B	304	254A	255
SiO_2	61.29	54.42	64.67	57.95	64.21	55.18	62.79	63.17	67.49
TiO_2	0.67	0.83	0.53	0.63	0.63	0.54	.40	0.37	0.30
Al_2O_3	14.48	14.57	15.05	14.69	15.09	15.88	8.58	15.58	14.11
Fe_2O_3	2.40	2.49	1.57	1.80	1.86	2.34	1.68	2.10	1.89
FeO	8.09	8.82	0.60	3.03	3.24	6.93	1.60	5.20	3.49
MnO	0.16	0.20	0.02	0.16	0.08	0.17	0.17	0.13	0.10
MgO	3.40	5.71	1.96	2.57	1.96	5.65	2.15	3.22	1.80
CaO	2.28	8.30	5.93	7.87	3.23	9.01	12.27	5.95	6.10
Na_2O	4.68	2.96	5.78	3.56	5.38	3.14	2.10	2.48	2.79
K_2O	0.07	6.69	0.52	1.36	0.39	0.49	0.15	0.98	0.64
P_2O_5	0.17	0.08	0.14	0.47	0.14	0.66	0.35	0.61	0.06
L.O.I.	2.27	0.91	3.05	5.90	3.73	-	7.56	0.25	1.25
Total	99.96	99.98	99.82	100.01	99.99	99.99	100.01	100.04	100.02
$\frac{FeO^t}{MgO}$	3.01	1.93	1.03	1.81	2.51	1.60	1.45	2.20	2.88
$\frac{K}{Rb}$	194	441	480	235	324	1017	249	407	443
$\frac{Ba}{Rb}$	60	18	8	10	13	54	11	19	25

Norms (CIPW)

Q	19.27	6.06	17.61	15.50	21.17	7.31	33.16	25.80	32.80
or	0.42	4.11	3.18	8.53	2.40	2.89	0.96	5.80	3.83
ab	40.53	25.27	50.94	31.95	47.31	26.50	19.29	21.02	23.90
an	10.45	24.95	14.04	21.37	15.71	27.82	14.70	25.62	24.38
cor	3.03	-	-	-	0.29	-	-	1.07	-
di	-	13.55	10.88	13.78	-	10.34	15.65	-	4.86
hy	21.01	3.24	-	3.63	8.73	19.18	-	15.49	6.73
ol	-	-	-	-	-	-	-	-	-
mt	3.56	3.64	0.48	2.78	2.80	3.38	2.64	3.05	2.77
il	1.30	1.59	1.04	1.27	1.24	1.02	0.43	0.70	0.58
ap	0.41	0.19	0.34	1.18	0.30	1.56	0.90	1.4	0.14

Trace elements (P.P.M.)

Cr	624	273	221	86	77	117	56	25	6
Ba	179	231	73	456	126	215	54	371	298
Ni	192	78	79	36	34	31	17	4	8
Nb	7	8	9	6	12	7	4	7	3
Zr	96	84	164	123	194	44	42	46	63
Y	29	31	68	25	29	14	16	18	16
Sr	185	207	206	437	226	253	177	233	240
Rb	3	13	9	48	10	4	5	20	12

$FeO^t = Fe_2O_3 \times 0.8998 + FeO$

Appendix 2 - Contin.

	D1	D2	D3	D4	E1	E2	E3	X	Y
	180	181	182	183	109	139	253	308	254B
SiO_2	49.95	54.12	52.78	65.99	69.55	76.17	78.17	54.87	63.53
TiO_2	0.83	0.70	0.87	0.57	0.30	0.21	0.43	1.68	0.43
Al_2O_3	15.53	16.28	18.10	14.24	14.71	11.86	8.32	15.74	14.62
Fe_2O_3	2.19	2.21	2.31	1.79	1.83	1.67	1.80	2.51	2.15
FeO	6.22	6.34	7.29	2.55	2.99	1.54	2.94	8.16	6.33
MnO	0.20	0.25	0.14	0.08	0.14	0.14	0.20	0.33	0.22
MgO	8.56	5.55	5.39	1.43	0.73	0.55	1.91	4.55	1.66
CaO	11.47	8.92	3.64	3.46	1.48	0.62	5.08	4.01	6.43
Na_2O	2.61	5.16	3.46	3.95	6.60	6.48	0.01	5.19	1.51
K_2O	0.65	0.45	3.13	2.49	0.64	0.07	0.51	0.16	0.40
P_2O_5	0.33	-	0.22	0.15	0.04	0.01	0.65	0.99	0.65
L.O.I.	1.38	-	2.64	3.29	0.90	0.61	0.10	1.72	1.99
Total	99.92	99.98	99.97	99.98	99.91	99.92	100.02	99.91	99.97
$\frac{FeO^t}{MgO}$	0.96	1.50	1.74	2.91	6.35	5.53	2.39	2.29	4.93
$\frac{K}{Rb}$	599	415	541	470	759	291	302	268	369
$\frac{Ba}{Rb}$	20	21	18	18	41	32	17	48	21

Norms (CIPW)

Q	-	-	.82	24.59	23.08	35.71	62.57	6.68	35.17
or	3.89	2.65	19.01	15.22	3.82	0.42	3.01	0.96	2.41
ab	22.40	43.33	30.04	34.56	56.40	55.21	0.08	44.70	13.03
an	29.09	19.87	17.08	14.24	7.15	3.03	20.98	13.73	28.25
cor	-	-	3.02	-	0.57	0.02	0.06	2.12	1.58
di	21.28	19.83	-	2.05	-	-	-	-	-
hy	11.25	-	24.36	5.17	5.62	2.75	8.32	22.47	13.96
ol	6.39	9.55	-	-	-	-	-	-	-
mt	3.23	3.19	3.44	2.68	2.68	2.44	2.61	3.70	3.18
il	1.61	1.40	1.69	1.12	0.58	0.40	0.82	3.25	0.83
ap	0.80	-	0.55	0.37	0.10	0.02	1.54	2.39	1.57

Trace elements (P.P.M.)

Cr	436	183	115	21	1	-	1	-	-
Ba	180	190	861	785	285	63	234	239	193
Ni	121	42	31	9	4	10	-	-	-
Nb	6	7	6	6	11	12	7	5	6
Zr	29	42	77	213	318	317	103	148	18
Y	26	26	19	24	88	79	27	35	14
Sr	377	266	333	437	86	82	277	181	240
Rb	9	9	48	44	7	2	14	5	9

$FeO^t = Fe_2O_3 \times 0.8998 + FeO$

X and Y were omitted from variation diagrams because they do not contain Cr or Ni.

Appendix 3 - Total rock analyses of the marbles.

	198	265A	265C	268	281B
SiO_2	2.30	13.39	17.05	3.88	30.43
TiO_2	.07	.09	.07	.09	.02
Al_2O_3	.22	.55	.17	1.06	.06
Fe_2O_3	.10	1.60	.13	.12	1.64
FeO	.15	.82	.19	.17	.30
MnO	.02	.23	.04	.02	.02
MgO	22.41	14.36	19.28	.59	14.50
CaO	32.69	33.46	27.73	54.22	22.97
Na_2O	–	–	–		–
K_2O	.04	–	.04	.10	–
P_2O_5	.05	–	.01	.06	–
L.O.I.	42.44	36.92	36.30	40.45	30.62
Total	100.49	101.43	101.01	100.72	100.43

Trace elements (P.P.M.)

Cr	–	5	–	1	6
Ba	30	81	2	21	11
Ni	–	–	–	58	1
Nb	2	–	2	5	–
Zr	5	5	3	17	–
Y	5	3	4	–	3
Sr	114	165	53	1808	99
Rb	4	4	6	6	1

Appendix 4 – Total rock analyses and normative values of the Abt Formation.

	A_1	A_2	B_1	B_2	B_3
	269A	276	278A	288	249
SiO_2	47.33	45.75	49.63	46.79	40.24
TiO_2	1.92	2.08	1.09	0.78	0.62
Al_2O_3	14.19	14.73	19.46	17.71	11.87
Fe_2O_3	2.87	2.89	2.34	2.54	2.16
FeO	12.25	12.50	7.58	9.38	6.62
MnO	0.24	0.24	0.17	0.22	0.20
MgO	6.47	7.39	3.67	6.75	5.68
CaO	10.53	11.24	10.04	10.22	16.34
Na_2O	2.58	1.52	2.48	2.39	0.82
K_2O	0.33	0.17	1.10	1.01	0.93
P_2O_5	0.19	0.20	0.34	0.28	0.32
L.O.I.	0.91	1.19	1.96	1.83	13.73
Total	99.81	99.90	99.95	99.90	99.53
$\frac{FeO^t}{MgO}$	2.29	2.04	2.64	1.73	1.51
$\frac{K}{Rb}$	391	282	761	524	270
$\frac{Ba}{Rb}$	19	13	4	6	5

Norms (CIPW)

	A_1	A_2	B_1	B_2	B_3
Q	–	–	1.84	–	–
or	1.97	1.02	7.17	6.08	6.16
ab	22.06	13.02	21.41	20.61	0.70
an	26.44	33.28	39.22	35.28	30.25
di	20.89	18.12	7.79	12.00	50.58
hy	11.27	21.27	16.17	4.48	–
ol	9.00	4.58	–	15.61	2.27
mt	4.20	4.24	3.46	3.75	3.65
il	3.68	4.00	2.11	1.51	1.37
ap	0.45	0.48	0.82	0.68	0.89
ne	–	–	–	–	3.90

Trace elements (P.P.M.)

	A_1	A_2	B_1	B_2	B_3
Cr	94	64	42	98	128
Ba	136	90	267	180	161
Ni	40	47	15	12	25
Nb	3	4	2	1	–
Zr	90	98	84	36	29
Y	19	19	18	13	13
Sr	174	469	545	590	245
Rb	7	5	12	16	26

$FeO^t = Fe_2O_3 \times 0.8998 + FeO$

Appendix 4 - Contin.

	C1	C2	C3	C4	C5	C6	C7	C8
	12	13	59	69	110A	113C	130	132
SiO_2	67.36	67.37	65.33	64.79	67.61	63.28	64.72	62.55
TiO_2	0.44	0.64	0.67	0.64	0.60	0.72	0.61	0.63
Al_2O_3	14.49	13.89	14.06	14.74	13.48	15.17	15.15	14.30
Fe_2O_3	1.77	1.49	1.93	1.90	1.86	2.02	1.89	1.88
FeO	2.41	3.40	3.84	3.64	3.10	5.20	3.63	3.38
MnO	0.60	0.08	0.09	0.09	0.03	0.12	0.08	0.14
MgO	1.81	2.83	2.72	2.30	0.64	3.55	2.72	2.13
CaO	2.67	2.66	4.12	3.56	2.55	3.16	2.86	5.72
Na_2O	3.14	3.35	3.31	3.57	4.15	3.01	3.00	4.14
K_2O	2.41	1.01	0.98	1.78	0.89	1.00	2.20	0.81
P_2O_5	0.14	0.69	0.18	0.16	0.14	0.76	0.21	0.20
L.O.I.	3.19	2.15	2.74	2.69	4.79	2.03	2.92	4.16
Total	99.89	100.01	99.97	99.86	99.84	100.02	99.99	100.04
$\frac{FeO^t}{MgO}$		1.82	2.05	2.33	7.46	1.98	1.96	2.38
$\frac{*K_2O}{K_2O+Na_2O}$	.43	.22	.22	.33	.17	.24	.42	.16

Norms (CIPW)

	C1	C2	C3	C4	C5	C6	C7	C8
Q	31.82	35.06	28.68	25.39	34.26	29.43	28.14	21.56
or	14.73	6.10	5.96	10.82	5.53	6.03	13.39	4.99
ab	27.47	28.95	28.80	31.08	36.94	25.98	26.15	36.53
an	12.76	8.92	19.82	17.11	12.36	10.98	13.22	18.81
cor	2.27	4.17	0.50	0.87	1.46	5.30	3.23	-
di	-	-	-	-	-	-	-	7.74
hy	7.09	11.01	11.61	10.24	5.06	16.07	11.35	5.79
mt	2.65	2.87	2.88	2.83	2.84	2.99	2.82	2.84
il	0.86	1.24	1.31	1.25	1.20	1.39	1.19	1.25
ap	0.34	1.67	0.44	0.39	0.35	1.84	0.51	0.49

Trace elements (P.P.M.)

	C1	C2	C3	C4	C5	C6	C7	C8
Cr	130	93	178	112	85	120	147	108
Ba	258	112	251	515	158	327	581	239
Ni	24	50	35	38	1	30	35	31
Nb	11	13	5	7	13	9	11	6
Zr	178	191	183	185	182	168	160	170
Y	27	28	25	28	38	23	32	27
Sr	139	244	401	382	177	248	422	520
Rb	30	8	29	49	19	25	65	23

$FeO^t = Fe_2O_3 \times 0.8998 + FeO.$

$*K_2O$ and Na_2O recalculated at $SiO_2 = 65$ wt %.

Appendix 4 - Contin.

	C9	C10	C11	C12	C13	C14	C15	C16
	137	166	208	210	219	220	231	236
SiO_2	66.64	62.28	65.50	63.23	61.43	58.50	64.65	65.08
TiO_2	0.60	0.75	0.70	0.72	0.70	0.72	0.57	0.62
Al_2O_3	13.16	15.46	15.53	15.24	15.12	16.03	15.09	14.83
Fe_2O_3	1.89	1.96	2.00	1.99	2.08	2.17	1.91	1.88
FeO	3.10	4.18	3.86	4.18	5.25	5.78	3.10	3.63
MnO	0.09	0.10	0.10	0.11	0.10	0.14	0.10	0.09
MgO	2.36	3.19	2.98	2.89	3.83	4.16	2.35	2.38
CaO	4.05	3.19	2.69	2.74	3.30	3.00	4.15	3.20
Na_2O	3.76	3.23	3.38	4.24	2.94	2.16	3.28	3.55
K_2O	1.07	1.71	1.87	1.18	3.37	1.78	1.93	2.14
P_2O_5	0.12	0.21	0.72	0.20	0.24	0.48	0.17	0.18
L.O.I.	3.17	3.79	0.58	3.18	1.68	5.01	2.65	2.41
Total	100.01	100.05	99.91	99.91	100.04	99.93	99.95	99.99

$\frac{FeO^t}{MgO}$	2.03	1.86	1.90	2.07	1.86	1.86	2.05	2.34
$\frac{*K_2O}{K_2O+Na_2O}$	.22	.35	.36	.22	.53	.45	.37	.38

Norms (CIPW)

Q	28.96	24.58	28.63	22.82	16.42	25.54	25.42	25.00
or	6.53	10.50	11.12	7.21	20.24	11.08	11.72	12.96
ab	32.85	28.39	28.78	37.17	25.29	19.26	28.52	30.78
an	16.39	15.03	8.74	12.71	15.06	12.53	20.03	15.07
Cor	-	3.11	4.79	2.55	1.23	6.54	0.48	1.31
di	2.89	-	-	-	-	-	-	-
hy	8.08	13.45	11.96	12.66	16.76	19.19	9.47	10.43
mt	2.83	2.95	2.92	2.98	3.07	3.32	2.85	2.79
il	1.18	1.48	1.34	1.41	1.35	1.44	1.11	1.21
ap	0.29	0.52	1.72	0.49	0.58	1.18	0.41	0.44

Trace elements (P.P.M.)

Cr	141	175	145	120	287	95	84	101
Ba	274	625	481	307	765	424	491	677
Ni	34	44	46	47	89	62	41	31
Nb	7	9	8	7	12	6	6	7
Zr	152	207	195	182	164	155	137	166
Y	23	30	29	29	32	28	26	28
Sr	323	301	284	268	243	225	318	521
Rb	31	46	39	32	75	51	53	55

$FeO^t = Fe_2O_3 \times 0.8998 + FeO.$

$*K_2O+Na_2O$ recalculated at $SiO_2 = 65$ wt. %.

Appendix 4 - Contin.

	C17	C18	C19	C20	C21	C22	C23
	238A	242	243	246	247	273	282A
SiO_2	65.40	62.84	65.70	60.10	65.97	63.13	64.81
TiO_2	0.57	0.75	0.68	0.79	0.55	0.63	0.81
Al_2O_3	13.99	15.58	14.65	15.38	12.22	13.60	10.61
Fe_2O_3	1.86	1.96	1.96	2.09	1.92	1.98	2.50
FeO	3.25	4.16	4.00	5.23	3.11	4.01	8.99
MnO	0.09	0.09	0.09	0.56	0.13	0.09	0.35
MgO	2.32	3.05	2.78	3.16	2.30	3.01	3.49
CaO	3.59	1.99	2.15	3.23	4.65	5.36	6.99
Na_2O	3.32	3.22	4.20	0.98	1.97	2.95	1.08
K_2O	1.86	5.56	1.43	2.92	1.98	0.91	0.42
P_2O_5	0.14	0.19	0.18	0.47	0.45	0.14	0.29
L.O.I.	3.69	0.68	2.31	4.97	4.69	5.08	–
Total	100.08	100.07	100.13	99.88	99.94	100.89	100.34
$\frac{FeO^t}{MgO}$	2.12	1.94	2.07	2.25	2.10	1.92	3.22
$\frac{*K_2O}{K_2O+Na_2O}$	.36	.63	.25	.75	.50	.24	.28

Norms (CIPW)

Q	27.53	12.37	25.94	31.09	35.27	26.79	33.30
or	11.40	33.06	8.64	18.15	12.25	5.61	2.47
ab	29.14	27.41	36.33	8.69	17.42	26.05	9.10
an	17.54	8.70	9.71	13.64	19.56	22.10	22.77
cor	0.33	1.10	2.77	6.20	–	–	–
di	–	–	–	–	2.59	3.84	8.35
hy	9.79	12.62	11.95	16.29	9.00	11.02	18.17
mt	2.80	2.86	2.90	3.19	2.93	3.00	3.61
il	1.12	1.53	1.32	1.58	1.10	1.25	1.63
ap	0.34	0.45	0.44	1.18	1.12	0.35	0.68

Trace elements (P.P.M.)

Cr	130	129	147	95	78	92	52
Ba	520	707	502	733	475	258	44
Ni	40	41	45	45	27	23	7
Nb	10	8	6	10	8	7	–
Zr	176	193	171	166	136	151	83
Y	31	29	27	34	25	26	40
Sr	366	319	372	147	287	315	133
Rb	51	69	46	89	54	24	5

$FeO^t = Fe_2O_3 \times 0.8998 + FeO$.

$*K_2O+Na_2O$ recalculated at $SiO_2 = 65$ wt. %.

Appendix 4 - Contin.

	C24	C25	C26	C27	C28	C29
	<u>15</u>	<u>57</u>	<u>74</u>	<u>199</u>	<u>215</u>	<u>233</u>
SiO_2	71.03	68.77	66.50	73.01	68.53	70.28
TiO_2	0.70	0.56	0.48	0.32	0.50	0.21
Al_2O_3	13.61	14.35	13.51	13.10	12.57	15.05
Fe_2O_3	1.77	1.70	1.80	1.52	1.75	0.60
FeO	2.90	2.87	2.80	1.21	2.80	0.88
MnO	0.07	0.07	0.09	0.05	0.09	0.04
MgO	1.67	2.36	1.99	1.19	1.79	0.54
CaO	2.31	3.37	3.00	2.80	4.84	2.57
Na_2O	5.72	4.08	3.64	6.28	4.30	6.89
K_2O	0.38	1.25	1.56	0.57	0.46	1.04
P_2O_5	0.66	0.69	0.16	0.61	0.17	0.08
L.O.I.	-	-	4.31	-	1.21	1.90
Total	100.82	100.07	99.84	100.72	99.01	100.08

$\dfrac{*K_2O}{K_2O+Na_2O}$	.06	.23	.30	.08	.10	.13

Norms (CIPW)

Q	29.16	30.01	30.38	29.20	30.47	21.25
or	2.23	7.38	9.65	3.28	2.78	6.26
ab	47.99	34.48	32.24	51.71	37.19	59.37
an	7.13	12.24	14.49	7.04	13.94	7.20
cor	1.14	1.79	0.79	-	-	-
di	-	-	-	2.32	7.76	4.30
hy	6.94	8.94	8.36	2.31	3.87	0.14
mt	2.54	2.46	2.73	2.14	2.59	0.89
il	1.32	1.06	0.95	0.59	0.97	0.41
ap	1.55	1.63	0.40	1.41	0.41	0.19

Trace elements (P.P.M.)

Cr	93	91	47	-	66	4
Ba	112	364	442	183	145	420
Ni	8	45	15	-	22	14
Nb	13	13	3	8	5	11
Zr	191	140	108	140	97	72
Y	28	26	21	24	20	1
Sr	244	295	280	142	522	693
Rb	8	33	46	9	14	35

$*K_2O$ and Na_2O recalculated at SiO_2 = 65 wt. %.

Appendix 5 - Total rock analyses and normative values of the Shigran carbonates and the magnesite and barite veins of the Al Amar-Idsas region.

				Shigran Carbonate				
	113B	121B	208E	309	312	313B	315	316A
SiO_2	38.38	31.30	32.23	24.25	33.14	25.42	41.48	37.09
TiO_2	.13	.03	.04	.06	.05	.02	.07	.03
Al_2O_3	1.69	.54	.44	.43	.44	.23	1.93	1.41
Fe_2O_3	1.93	1.89	1.89	1.96	1.91	1.88	2.15	2.05
FeO	3.86	3.49	3.53	4.14	3.60	3.41	5.80	4.94
MnO	.19	.17	.17	.10	.09	.18	.19	.18
MgO	6.64	26.37	24.74	19.61	28.15	35.19	12.56	20.70
CaO	24.07	5.41	6.98	18.32	2.47	.58	14.70	11.77
Na_2O	-	-	-	-	-	-	-	-
K_2O	.22	-	-	.04	.08	-	-	-
P_2O_5	.01	-	-	-	-	-	-	-
L.O.I.	22.99	31.27	30.27	31.44	31.04	33.53	21.81	22.25
Total	100.11	100.30	100.29	100.34	100.97	100.26	100.51	100.25
$\frac{FeO^+}{MgO}$	.84	.20	.21	.30	.19	.14	.62	.33

Norms (CIPW)

Q	-	-	-		-		2.391	-
Or	-	-	-		.68		-	-
ab	-	-	-				-	-
an	5.26	2.13	1.72		1.38		6.69	4.93
di	61.47	28.83	37.57		12.67		68.67	55.23
hy	-	8.38	6.53		32.15		18.12	2.93
ol	2.43	56.60	50.15		49.03		-	33.02
mt	3.71	3.97	3.92		3.96		3.96	3.81
il	.33	.08	.11		.14		.17	.07
ap	.03	-	-		-		-	-

Trace element (P.P.M.)

Cr	1598	2269	1967	2321	2079	3886	1836	2229
Ba	54	-	20	1552	7	90	130	30
Ni	737	1666	1592	1649	1683	2466	1098	1529
Nb	9	9	4	11	21	5	-	-
Zr	9	-	-	3	2	-	-	-
Y	2	-	1	-	3	2	-	-
Sr	362	263	481	533	288	38	375	263
Rb	9	5	5	4	2	3	2	1

FeO^+ = total iron ($Fe_2O_3 \times 0.8998 + FeO$)

Appendix 5 -Contin.

	Altered Shigran Carbonates				Magnesite	Barite
	110B	113A	222	272A	322	114
SiO$_2$	53.42	65.78	47.65	33.68	3.44	.81
TiO$_2$	1.89	.38	.07	.08	.06	.41
Al$_2$O$_3$	15.44	11.03	.59	.81	.06	4.78
Fe$_2$O$_3$	2.30	2.07	1.58	2.42	1.67	.04
FeO	7.20	5.06	.75	8.19	1.52	.11
MnO	.12	.25	.07	.18	.04	.11
MgO	1.98	.28	11.02	7.64	22.78	.76
CaO	5.61	4.79	16.49	23.21	30.77	.90
Na$_2$O	4.52	4.10		-	-	-
K$_2$O	.30	.06	.14	.09	.12	.07
P$_2$O$_5$	.85	.12	-	-	.02	.89
L.O.I.	6.14	6.12	21.92	24.21	39.85	
Total	99.77	100.02	100.29	100.50	100.32	8.88
$\frac{FeO^+}{MgO}$	4.68	23.73	.20	1.36	.13	.19

Norms (CIPW)

Q	10.51	32.40	16.24	-		
Or	1.89	.38	1.06	-		
ab	40.82	36.91	-	-		
an	22.37	12.25	1.53	2.89		
di	1.24	10.79	75.75	65.89		
hy	13.63	3.00	-	-		
ol	-	-	-	25.16		
mt	3.56	3.19	2.92	5.22		
il	3.83	.77	.17	.23		
ap	2.15	.30	-	-		

Trace elements (P.P.M.)

Cr	-	15	438	821	87	-
Ba	180	5166	21	243	31	(51.8%)
Ni	102	113	377	381	151	-
Nb	32	12	13	6	9	8
Zr	259	63	16	5	-	69
Y	17	14	-	-	68	-
Sr	364	235	2165	706	892	2703
Rb	7	2	8	5	3	13

FeO$^+$ = total iron (Fe$_2$O$_3$ x 0.8998 + FeO)

Appendix 6 – Total rock analyses and normative values of the ultramafic rocks.

	Ultramafic						
	190	195	.260	280B	287	224A	224B	224C
SiO_2	41.22	41.69	41.35	37.95	29.53	15.18	20.12	41.48
TiO_2	.07	.06	.15	.09	.05	.21	.15	.15
Al_2O_3	1.33	1.05	5.89	1.00	.60	2.42	4.78	10.81
Fe_2O_3	2.00	2.24	2.45	2.76	1.95	2.75	2.05	2.52
FeO	6.06	6.66	8.09	11.29	4.01	11.18	4.91	9.16
MnO	.13	.14	.17	.22	.17	.08	.11	.18
MgO	38.73	39.22	29.52	37.13	33.73	5.49	8.70	18.62
CaO	.13	.02	6.12	1.38	1.29	35.57	33.01	9.94
Na_2O	.05	–	.18	–	–	–	–	–
K_2O	.04	.01	.11	.03	.06	–	.05	–
P_2O_5	.50	–	–	.01	–	–	–	–
L.O.I.	10.66	10.71	6.37	8.83	29.30	27.56	27.08	7.41
Total	100.92	101.80	99.33	100.68	100.70	100.38	100.88	100.09
$\dfrac{FeO^+}{MgO}$	.20	.22	.35	.37	.17	2.49	.78	.61

Norms (CIPW)

Or		.06	.69	.19	.50			–
ab		–	1.62	–	–			
an		.11	15.89	2.87	2.05			31.82
cor		1.10	–	–	–			–
di		–	13.00	3.62	5.43			17.13
hy		37.50	12.89	12.92	2.72			19.66
ol		57.54	51.84	75.83	85.22			27.14
mt		3.57	3.78	4.36	3.96			3.94
il		.13	.30	.19	.13			.31
ap		–	–	.03	–			

Trace elements (P.P.M.)

	190	195	.260	280B	287	224A	224B	224C
Cr	2603	3019	2007	2827	2482	714	409	887
Ba	296	10	13	14	26	210	100	10
Ni	2729	2537	971	977	1950	317	205	359
Nb	2	14	–	9	22	1	–	–
Zr	–	2	3	–	2	3	7	–
Y	–	73	6	2	3	4	–	2
Sr	10	3	54	24	39	114	361	404
Rb	1	1	5	2	–	1	4	3

FeO^+ = total iron ($Fe_2O_3 \times 0.8998 + FeO$).

Appendix 7 - Total rock analyses and normative values of the gneissic granodiorites.

	Gneissic Granodiorite (Basement)						
	98	147	154	159	204	225	325
SiO_2	71.37	70.82	71.91	71.02	71.90	73.32	70.47
TiO_2	0.32	0.31	0.27	0.31	0.32	0.14	0.25
Al_2O_3	14.03	13.29	14.45	14.89	14.78	14.58	16.85
Fe_2O_3	1.57	1.67	1.53	1.59	1.66	0.20	1.56
FeO	0.59	1.50	0.30	0.85	1.45	0.57	0.56
MnO	0.05	0.05	0.05	0.05	0.07	0.06	0.04
MgO	0.69	0.91	0.61	1.10	0.83	0.16	0.63
CaO	2.02	3.48	1.94	2.76	3.02	1.82	3.35
Na_2O	4.43	4.55	4.63	4.26	4.58	5.34	5.51
K_2O	3.34	0.87	3.26	2.82	1.50	2.38	1.44
P_2O_5	0.08	0.06	0.07	0.10	0.09	0.04	0.09
Total	98.49	97.57	99.02	99.75	100.20	98.61	100.75
$\dfrac{*K_2O}{K_2O+Na_2O}$	.43	.16	.41	.40	.25	.31	.21

Norms (CIPW)							
Q	28.32	33.55	27.99	26.37	31.70	28.97	24.85
or	20.04	5.27	19.46	16.65	8.77	14.24	8.45
ab	38.06	39.48	39.48	39.05	38.61	45.74	46.27
an	8.66	13.61	9.15	11.55	14.35	8.88	15.92
cor	-	-	-	-	0.42	0.01	0.35
di	0.77	2.98	0.09	1.15	-	-	-
hy	1.39	1.87	1.49	2.20	2.95	1.51	1.56
mt	1.15	2.48	0.35	2.00	2.38	0.29	1.20
il	0.62	0.60	0.52	0.59	0.60	0.27	0.47
ap	0.19	0.15	0.17	0.24	0.21	0.10	0.21
he	0.80	-	1.30	0.21	-	-	0.72

Trace elements (P.P.M.)							
Cr	3	6	2	16	5	1	3
Ba	985	254	927	1408	585	858	541
Ni	17	17	14	15	14	13	12
Nb	8	7	13	7	9	8	8
Zr	167	114	104	107	87	60	98
Y	12	31	10	3	15	13	-
Sr	438	320	605	811	435	419	668
Rb	73	14	74	58	34	25	28

*K_2O and Na_2O recalculated at SiO_2 = 65 wt. %.

Appendix 8 - Total rock analyses and normative values of the
gabbros and diorites.

	Gabbro									
	23	26	40	44	45	64	94A	97	184	289B
SiO$_2$	50.80	48.93	47.48	49.12	48.23	45.04	46.62	48.00	52.95	49.49
TiO$_2$	1.16	0.86	0.29	0.65	0.74	0.52	0.29	0.17	0.73	0.67
Al$_2$O$_3$	17.95	17.97	19.64	16.88	15.66	15.09	21.84	25.64	19.75	16.33
Fe$_2$O$_3$	2.54	2.80	2.03	2.39	2.88	2.90	1.88	1.69	2.15	2.44
FeO	9.29	10.01	4.74	9.06	10.96	11.30	3.42	1.63	5.79	9.95
MnO	0.15	0.16	0.16	0.22	0.26	0.23	0.08	0.07	0.13	0.23
MgO	4.32	4.11	7.97	7.07	7.02	10.80	5.39	4.90	4.36	7.16
CaO	10.30	11.19	13.86	11.35	11.15	12.23	14.50	16.15	8.84	10.78
Na$_2$O	2.75	2.85	1.23	2.51	2.38	1.12	1.66	1.57	4.33	2.15
K$_2$O	0.56	0.47	0.38	0.14	0.08	0.12	0.26	0.17	0.31	0.21
P$_2$O$_5$	0.17	0.65	0.04	0.49	0.63	0.60	0.03	0.01	0.29	0.47
L.O.I.	–	–	2.11	–	–	–	0.99	–	0.40	–
Total	99.99	100.00	99.93	99.88	99.99	99.95	99.96	100.00	99.63	99.88
$\frac{FeO^+}{MgO}$	2.68	3.05	.82	1.59	1.93	1.29	.95	.64	1.77	1.70
$\frac{*K_2O}{K_2O+Na_2O}$	.17	.14	.24	.05	.03	.10	.14	.10	.07	.19

Norms (CIPW)

	23	26	40	44	45	64	94A	97	184	289B
Q	1.80	–	–	–	–	–	–	–	0.17	0.28
or	3.31	2.80	2.30	0.89	0.45	0.71	1.55	1.00	1.84	1.27
ab	23.26	24.09	10.64	21.09	20.15	9.47	14.19	13.28	36.76	18.16
an	34.99	34.80	47.98	34.50	31.79	35.78	60.17	62.41	33.65	34.27
di	12.52	13.83	17.69	14.68	16.05	17.18	9.87	13.92	6.95	12.65
hy	17.84	14.40	14.95	18.71	18.72	13.56	4.58	5.35	15.41	27.18
ol	–	2.85	2.77	4.16	5.75	16.68	6.25	1.24	–	–
mt	3.68	4.06	3.01	3.46	4.18	4.20	2.75	2.45	3.13	3.54
il	2.20	3.15	0.56	1.24	1.40	0.99	0.56	0.32	1.39	1.24
ap	0.40	1.59	0.10	1.48	1.50	1.42	0.07	0.02	0.69	1.41

Trace elements (P.P.M.)

	23	26	40	44	45	64	94A	97	184	289B
Cr	25	160	154	164	89	164	80	267	315	104
Ba	142	436	76	88	79	68	119	146	392	131
Ni	16	27	63	8	–	–	47	74	114	31
Nb	–	–	–	5	5	5	–	1	8	6
Zr	33	47	10	1	–	2	12	–	21	3
Y	17	17	5	8	8	3	1	2	10	5
Sr	297	550	370	253	198	163	946	1026	981	325
Rb	14	14	3	2	4	4	11	3	5	5

FeO$^+$ = total iron (Fe$_2$O$_3$ x 0.8998 + FeO).

*K$_2$O and Na$_2$O recalculated at SiO$_2$ = 65 wt. %.

Appendix 8 - Contin.

	Diorite									
	20	24	25	33	88	149	150	186	301	306
SiO_2	51.18	55.24	64.48	54.58	64.52	60.99	60.97	59.68	57.68	62.71
TiO_2	0.95	1.00	0.69	0.83	0.63	0.51	0.79	0.73	0.93	0.52
Al_2O_3	17.73	15.72	14.90	18.02	15.93	15.62	15.57	17.65	17.34	17.07
Fe_2O_3	2.34	2.22	2.01	2.17	1.85	2.15	2.06	1.90	2.23	1.87
FeO	9.30	8.71	4.10	5.84	3.14	5.65	6.32	4.70	6.54	3.30
MnO	0.16	0.17	0.09	0.14	0.08	0.14	0.15	0.12	0.15	0.10
MgO	4.43	4.45	2.44	5.01	2.77	3.40	2.61	3.14	2.69	2.56
CaO	10.16	8.29	4.85	8.69	4.85	6.94	6.17	5.73	9.06	5.76
Na_2O	2.98	3.19	3.53	3.84	4.18	3.16	3.47	4.43	2.30	3.89
K_2O	0.54	0.94	2.14	0.69	1.77	0.77	0.78	1.70	0.33	1.41
P_2O_5	0.70	0.74	0.68	0.15	0.17	0.11	0.76	0.75	0.20	0.15
Total	100.49	100.67	99.91	99.96	99.89	99.44	99.65	100.53	99.45	99.34
$\frac{FeO^+}{MgO}$	2.57	2.41	2.42	1.56	1.73	2.23	3.13	2.04	3.18	1.95
$\frac{*K_2O}{K_2O+Na_2O}$	.15	.23	.38	.15	.30	.20	.18	.28	.13	.27

Norms (CIPW)

	20	24	25	33	88	149	150	186	301	306
Q	1.97	7.35	21.72	2.75	18.63	17.99	19.06	9.77	17.86	17.78
or	3.14	5.46	12.53	4.12	10.47	4.62	4.62	9.99	1.96	8.47
ab	24.83	26.53	29.59	32.82	35.40	27.16	29.45	37.27	19.56	33.47
an	33.43	25.89	18.86	29.65	19.50	26.02	24.68	23.12	36.20	24.82
di	10.28	8.52	0.79	10.22	2.83	6.48	0.92	0.31	6.43	2.32
hy	19.57	19.48	10.72	15.33	8.89	13.35	14.97	13.67	12.48	9.04
mt	3.38	3.18	2.90	3.15	2.68	3.14	3.00	2.74	3.25	2.74
il	1.78	1.87	1.30	1.59	1.20	0.98	1.50	1.38	1.78	1.00
ap	1.61	1.72	1.60	0.30	0.40	0.26	1.81	1.74	0.48	0.36

Trace elements (P.P.M.)

	20	24	25	33	88	149	150	186	301	306
Cr	37	42	26	160	62	23	13	8	21	13
Ba	180	229	464	436	419	243	1270	537	233	382
Ni	17	11	9	27	49	13	-1	18	10	14
Nb	5	5	6	-	5	1	6	9	-	4
Zr	26	96	140	47	185	49	54	131	58	106
Y	11	18	23	17	25	21	21	15	23	15
Sr	310	257	277	550	470	248	311	639	278	552
Rb	8	23	71	14	47	14	12	33	7	43

FeO^+ = total iron (Fe_2O_3 x 0.8998 + FeO).

$*K_2O$ and Na_2O recalculated at SiO_2 = 65 wt. %.

Appendix 9 - Total rock analyses and normative values of the syntectonic granodiorite, post-tectonic granites, and Khuff Formation.

	Syntectonic granodiorites				
	152	161	172	175	275
SiO_2	70.18	70.10	72.97	73.46	71.16
TiO_2	0.31	0.31	0.24	0.27	0.49
Al_2O_3	15.07	15.62	14.06	13.70	12.66
Fe_2O_3	1.58	1.64	0.28	1.62	1.68
FeO	0.68	1.24	0.44	1.11	2.40
MnO	0.04	0.08	0.03	0.05	0.07
MgO	0.55	0.84	0.16	0.65	1.69
CaO	2.24	2.10	3.46	1.98	2.91
Na_2O	4.70	5.64	3.38	4.21	3.24
K_2O	3.33	2.06	1.5	1.99	1.82
P_2O_5	0.11	0.09	0.60	0.03	0.63
$L.O.I.$	1.19	0.24	2.81	0.90	1.21
Total	99.98	99.96	99.96	99.97	99.96
$\frac{*K_2O}{K_2O+Na_2O}$	.41	.27	.31	.32	.36
			Norms (CIPW)		
Q	25.13	23.72	41.03	36.41	37.74
or	19.92	12.21	8.50	11.87	10.89
ab	40.25	47.86	29.90	35.96	27.75
an	10.31	9.86	8.68	9.72	10.49
Cor	-	0.51	-	1.10	1.58
di	0.17	-	1.48	-	-
hy	1.31	2.66	2.28	1.98	6.63
mt	1.44	2.38	0.36	2.37	2.47
il	0.60	0.59	0.45	0.52	0.94
ap	0.26	0.21	1.25	0.07	1.51
			Trace elements (P.P.M.)		
Cr	510	10	8	2	51
Ba	1066	655	86	386	816
Ni	194	18	9	7	11
Nb	14	11	14	11	10
Zr	238	109	135	156	145
Y	29	8	34	44	23
Sr	709	543	56	196	388
Rb	59	55	56	58	47

*K_2O and Na_2O recalculated at SiO_2 = 65 wt. %

Appendix 9 - Contin.

	Post-tectonic granite						Khuff
	10	55	123	188	244		100D
SiO_2	72.46	66.41	76.03	77.75	74.05		2.23
TiO_2	0.15	0.67	0.12	0.13	0.07		0.09
Al_2O_3	13.69	13.91	13.24	11.97	13.70		0.97
Fe_2O_3	1.56	1.98	0.55	0.50	0.53		0.21
FeO	0.53	4.36	0.82	0.76	0.81		0.31
MnO	0.04	0.13	0.03	0.03	0.02		0.17
MgO	0.45	0.67	0.01	0.06	–		16.27
CaO	1.46	2.02	0.84	0.54	0.77		38.67
Na_2O	3.92	3.76	3.81	5.05	3.74		
K_2O	3.60	4.34	5.28	3.02	5.40		0.18
P_2O_5	0.07	0.24	0.04	0.06	0.04		–
Total	97.93	98.49	100.77	100.68	99.13		59.10
$\frac{*K_2O}{K_2O+Na_2O}$	.48	.54	.58	.37	.59		

Norms (CIPW)							
Q	32.95	21.12	31.40	35.67	29.91		
or	21.72	26.04	30.96	17.87	32.19		
ab	33.87	32.30	31.99	42.78	31.92		
an	6.93	8.39	3.41	1.08	3.59		
cor	0.87		–	–	0.40		
di	–	6.18	0.42	1.06	–		
hy	1.14	7.19	0.70	0.47	0.98		
mt	1.47	2.91	0.79	0.73	0.78		
il	0.29	1.29	0.23	0.25	0.13		
ap	0.17	0.58	0.90	0.14	0.10		
hm	0.58						

Trace elements (P.P.M.)							
Cr	670	–	1	–	613		3
Ba	460	505	83	788	104		24
Ni	266	11	17	16	264		
Nb	15	17	24	18	15		82
Zr	208	472	129	178	355		10
Y	108	62	80	86	329		74
Sr	188	145	21	21	39		107
Rb	217	126	183	21	233		6

*K_2O and Na_2O recalculated at SiO_2 = 65 wt. %
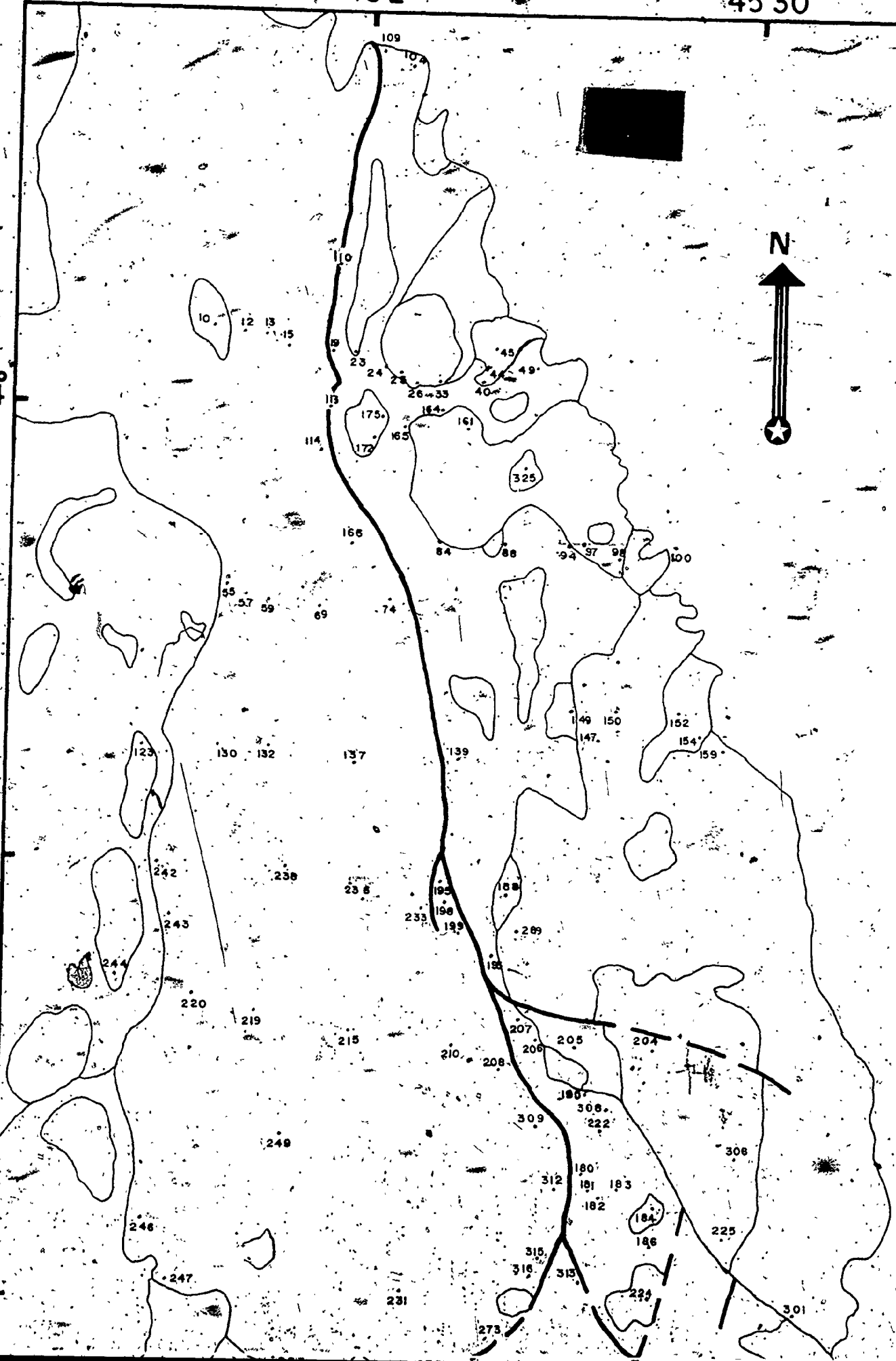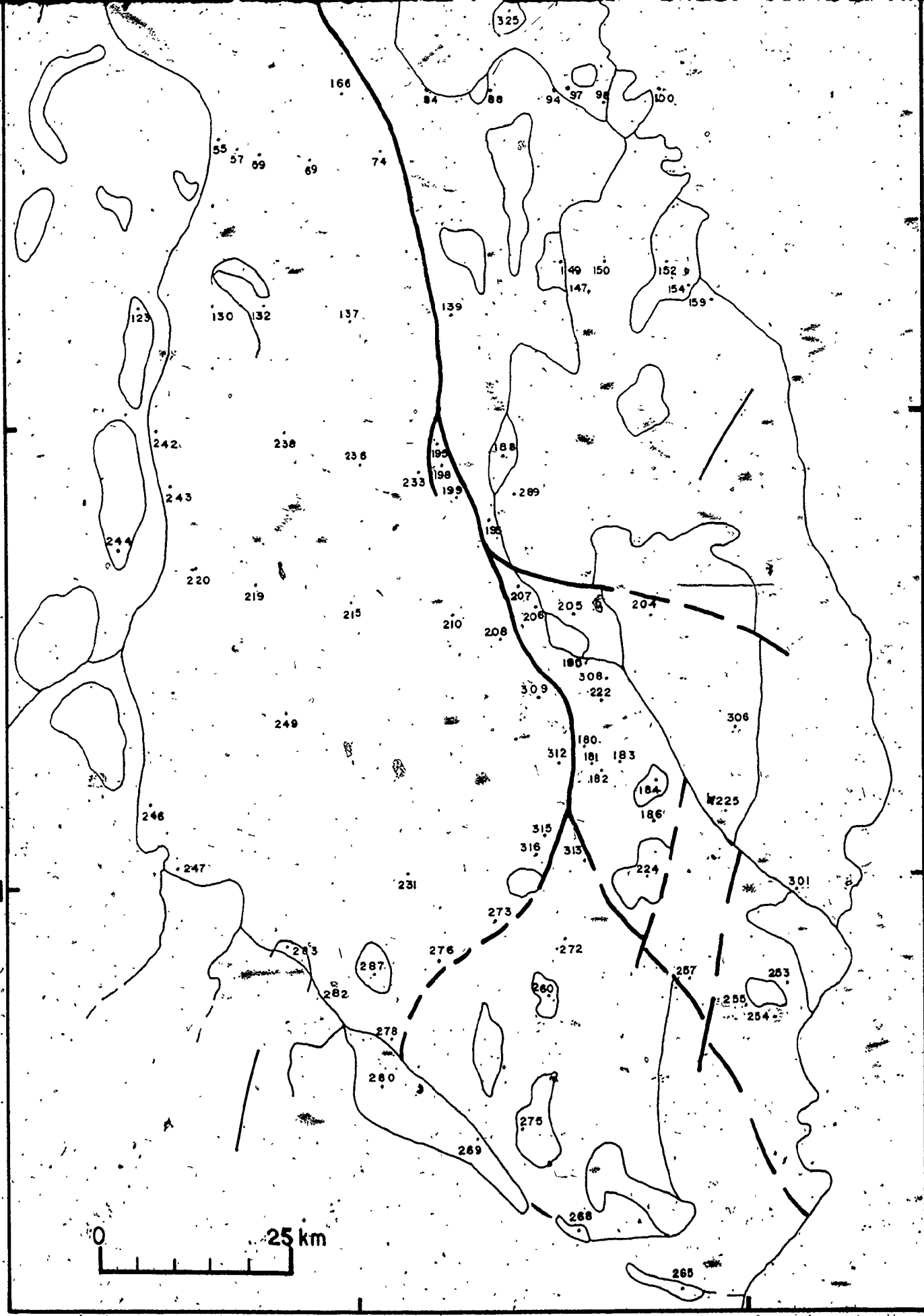
Geochemical sample location map

REFERENCES

Abdulaziz, M. I., 1974: Geological, mineralogical, and
geochemical studies on Jabal Idsas iron ore and its
origin. Unpublished M.Sc. thesis, Center for
Applied Geology, Jeddah, Saudi Arabia.

Aerocarto, 1964: Colour aerial photographs of ancient
mining sites at Idsas, Fawara, and Selib. Saudi
Arabia Directorate General of Mineral Resources
Open-file-Mining-site low-altitude aerial photo-
graphs, Scale 1:12,500.

Akaad, M. K and Noweir, A. M., 1972: Some aspects of the
serpentinites and their associated derivatives along
Qift-Quseir road. Annals of the Geological Servey
of Egypt, Cairo, vol. II. pp. 251-270.

Al Shanti, A.M.S., 1973: The geology and mineralization of
the Ad Dawadimi district of Saudi Arabia. Unpub-
lished Ph.D. thesis, the University of London,
323 pp.

_____ and A.H.G. Mitchell, 1976: Late Precambrian
subduction and collision in the Al Amar-Idsas
region, Arabian Shield, Kingdom of Saudi Arabia.
Tectonophysics 30; pp. 41-43.

Bakor, A. R., 1973: Jabal Al Wask: a Precambrian basic and
ultrabasic igneous complex in the northern Hijaz of
Saudi Arabia. Unpublished Ph.D. thesis, University
of Leeds.

162

————————, I. G. Gass and C. R. Neary, 1976: Jabal
Al Wask, northeast Saudi Arabia: an Eocambrian back
arc ophiolite. Earth and Planetary Science Letters
30; pp. 1-9.

Bateman, P. C., L. D. Clarck, N. K. Huber, J. C. Moore and
C. D. Rinehart, 1963: The Sierra Nevada Batholith.
U.S.G.S. Prof. Paper 414-D.

Bischoff, J. and F. Dickson, 1975: Seawater-basalt inter-
action at 200°C and 500 bars: implications for
origin of seawater heavy metal deposits and regula-
tion of seawater chemistry. Earth and Planetary
Science Letters, 25, pp. 385-397.

Bois, J. and M. Shanti, 1970: Mineral resources and geology
of the As Sakhen quadrangle, Kingdom of Saudi Arabia.
B.R.G.M. Unpublished Report 70JED6. pp. 45.

Bouladan, J., 1968: Current problems in mineral prospect-
ing in zones I, II, and III - Geologic and metallo-
genetic aspects, Saudi Arabia. B.R.G.M. Unpublished
Report 41.

Bramkamp, R., R. Gierhart, G. Brown and R. Jackson, 1956:
Geology of the southern Tuwayg quadrangle, Kingdom
of Saudi Arabia. U.S.G.S. Misc. Geol. Inv. Map I-
212A.

————————— and L. Ramirez, 1958: Geology of the north-
ern Tuwayg quadrangle, Kingdom of Saudi Arabia.
U.S.G.S. Misc. Geol. Inv. Map I-207A.

_____, L. Ramirez, G. Brown and A. Pocoock, 1963: Geologic map of the Wadi Ar Rimah quadrangle, Kingdom of Saudi Arabia. U.S.G.S. Misc. Geol. Inv. Map I-206A.

Brown, G. F., 1970: Eastern margin of the Red Sea and the coastal structures in Saudi Arabia. Phil. Trans. Roy. Soc. London. A. 267, pp. 75-87.

_____, 1972: Tectonic map of the Arabian Peninsula. Map AP-2, Directorate General of Mineral Resources, Jeddah, Kingdom of Saudi Arabia.

_____ and R. O. Jackson, 1960: The Arabian Shield. Proc. International Geologic Congress, 21 St., Copenhagen, Rept. pt. 9, pp. 69-77.

_____ and R. G. Coleman, 1972: The tectonic framework of the Arabian Peninsula. 24th International Geol. Congress, Montreal, Sect. 3, Tectonics, pp. 300-305.

Bryan, W. B., G. D. Stice and A. Ewart, 1972: Geology, petrography, and geochemistry of the volcanic islands of Tonga. Journal of Geophysical Researce, vol. 77, no. 8, pp. 1566-1585.

Burke, K., J. F. Dewey and W.S.F. Kidd, 1977: World distribution of sutures - the sites of former oceans. Tectonophysics 40, pp. 69-99.

Byerly, G. R., W. G. Melson and P. R. Vogt, 1976: Rhyodacites, andesites, ferro-basalts, and ocean tholeiites from the Galapagos spreading center. Earth

and Planetary Science Letters 30, pp. 215-220.

Cann, J. R., 1969: Spilites from the Carlsperg Ridge; Indian Ocean. Journal of Petrology 10, pp. 1-19.

——————————, 1970: Rb, Sr, Y, Zr, and Nb in some ocean floor basaltic rocks. Earth and Planetary Science Letters 10, pp. 7-11.

Coish, R. A., 1977: Ocean floor metamorphism in the Betts Cove ophiolite, Newfoundland. Contributions to Mineralogy and Petrology, vol. 60, pp. 255-270.

Coleman, R. G., R. J. Fleck, C. E. Hedge and E. D. Ghent, 1975: The volcanic rocks of southwest Saudi Arabia and the opening of the Red Sea. Kingdom of Saudi Arabia. U.S.G.S. Unpublished Report SA(IR)-194, 60 pp.

Delfour, J., 1966: The mineral resources and geology of the Hulayfah-Musaynaah region; Kingdom of Saudi Arabia. B.R.G.M. Report SG.JED.66A8, 143 pp.

Directorate General of Mineral Resources; 1959: Geology, ancient mines, and mineral resources of the Duwadamy, Quay-Lyah, Haliban area, Saudi Arabia. Directorate General of Mineral Resources open-file Report.

——————————, 1965: Mineral resources of Saudi Arabia: a guide for investment and development, Saudi Arabia. Directorate General of Mineral Resources Bull. 1, pp. 73.

Eijkelboom, G., 1966: The mineral resources and geology of the Jabal Dhuhaylan-Jabal Al Urd region; Kingdom of Saudi Arabia. B.R.G.M. Unpublished Report 66A12.

—————————, 1966: The mineral resources and geology of Jabal Damkh-Arwah region, Saudi Arabia. B.R.G.M. Unpublished Report 66 A13, 21 pp.

—————————, 1966: The mineral resources and geology of the Al Amar-Ar Rayn region, Saudi Arabia. B.R.G.M. Unpublished Report 66 A14, 17 pp.

—————————, 1966: The mineral resources and geology of the Idsas-Wadi Jifr region; Kingdom of Saudi Arabia. B.R.G.M. Unpublished Report 66 A15, pp. 38.

—————————, M. Gendi, B. Henry, X. Leca, M. Shanti, P. Delange and J. Pflam, 1970: Geology and mineral resources of the Al Amar-Ar Rayn quadrangle, Kingdom of Saudi Arabia. Directorate General of Mineral Resources Map MI-18.

Ewart, A. and W. B. Bryan, 1972: Petrography and geochemistry of the igneous rock from Eua, Tonga Islands. Geological Society of American Bulletin, v. 83, pp. 3281-3298.

Fleck, R. J., R. G. Coleman, H. R. Cornwall, W. R. Greenwood, D. G. Hadley, D. L. Schmidt, W. C. Prinz and J. C. Ratte, 1976: Geochronology of the Arabian Shield, Western Saudi Arabia: K-Ar results. Geological Society of America Bull., v. 87, pp. 9-21.

Frisch, W. and A. Al Shanti, 1977: Ophiolite belts and the
    collision of island arcs in the Arabian Shield.
    Tectonophysics 43, pp. 293-306.

Garson, M. S. and I. M. Shalaby, 1976: Precambrian-Lower
    Paleozoic plate-tectonics and metalogenesis in the
    Red Sea region. Geological Association of Canada,
    Special Paper no. 14, pp. 573-596.

Gass, I. G. and I. L. Gibson, 1969: Structural evolution
    of the rift zones in the Middle East. Nature,
    London, 221, pp. 926-930.

Gass, I., 1977: The evolution of the Pan African crystal-
    line basement in NE Africa and Arabia. Journal of
    Geological Society - London. Vol. 134; pp.
    ———————— and A. O. Nasseef (In press): Arabian Shield
    granite traverse, Saudi Arabia. Institute of
    Applied Geology, Bull. Contribution no. ; pp.

Gill, J. B., 1976: Composition and age of Lau basin and
    ridge volcanic rocks: Implications for evolution of
    an interarc basin and remnant arc. Geological
    Society of American Bulletin, v. 87, pp. 1384-1395.

Greenwood, W. R. and G. F. Brown, 1973: Petrology and
    chemical analysis of selected plutonic rocks from
    the Arabian Shield, Kingdom of Saudi Arabia.
    Directorate General of Mineral Resources Bull. 9,
    9 pp.

——————————, D. G. Hadley, R. E. Anderson, R. J. Fleck and D. L. Schmidt, 1975: Late Proterozoic cratonization in southwestern Saudi Arabia. U.S.G.S.; Saudi Arabian Project Report 196, 22 pp.

Hart, R. A., 1973: A model for the chemical exchange in the basalt-seawater system of oceanic layer 2. Canadian journal of Earth Science 10, pp. 799-815.

Herness, S. K. and V. P. Kahr, 1963: Report on field trip to Jabal Idsas, Saudi Arabia. Directorate General of Mineral Resources open-file Report 3-212-1568.

Hobbs, B. E., D. M. Winthrop and P. F. Williams, 1976: An outline of structural geology. John Wiley and Sons, Inc., New York. London. Sydney. Toronto. pp. 571.

Hunting Survey Corporation Limited, 1962: Airborne magneto-meter-scintillation counter survey Jabal Idsas, Saudi Arabia. Directorate General of Mineral Resources open-file Maps, Scale 1:50,000.

Hutchison, C. S., 1974: Laboratory handbook of petrographic techniques. John Wiley and Sons, Inc., New York. London. Sydney. Toronto.

Jackson, R.; R. Bogue, G. Brown and R. Gierhart, 1963: Geology of the southern Najd quadrangle, Kingdom of Saudi Arabia. U.S.G.S. Misc. Geol. Inv. Map I-211A.

Kahr, V. P., 1962: Jabal Idsas area, geology and minerali-zation, Saudi Arabia. Directorate General of Mineral Resources open-file Report 3-212-6013, pp. 26.

Kahr, V., W. Overstreet, J. Whitlow and A. Ankary, 1972: Reconnaissance geology of the Jabal Bitran quadrangle, Kingdom of Saudi Arabia. U.S.G.S. Unpublished Report SA(IR)-124, 70 pp.

Khukandy, M. E., 1975: Geology of the mafic, ultramafic and related rocks of Jabal Batran Area; Unpublished M.Sc. thesis, Center for Applied Geology, Jeddah, Saudi Arabia.

Kroner, A., 1976: Proterozoic crustal evolution in parts of southern Africa and evidence for extensive sialic crust since the end of the Archean. Phil. Trans. Roy. Soc. London, Ser. A280, pp. 541-553.

——————, 1977: Precambrian mobile belts of southern and eastern Africa - ancient sutures or sites of ensialic mobility? a case for crustal evolution towards plate tectonics. Tectonophysics 40, pp. 101-135.

Kuno, H., 1966: Lateral variation of basalt magma across continental margins and island arcs. Canadian Geol. Surv. Paper 66-15, pp. 317-336.

Lacombe, P. and J. Letalenet, 1970: Mineral resources and geology of the Jabal Al Hawshah quadrangle, Kingdom of Saudi Arabia. B.R.G.M. Unpublished Report 70 JED 26, 32 pp.

Lambolez, B., 1968: Airborne magnetic-scintillometric sheet 118 interpretation, Kingdom of Saudi Arabia. B.R.G.M. Unpublished Report 68 JED 52, pp. 6.

Larry, A. M., 1974: Geology of the basic and ultrabasic
        rocks west of Jabal Al Wask, Saudi Arabia. Un-
        published M.Phil. thesis, University of Leeds.

Lefèvre, C., 1973: Les caractères magmatiques du volcanisme
        plio-Quaternaire des Andes dans le Sud. du Pérou.
        Contr. Mineral. and Petrol., vol. 41, pp. 259-272.

MacLean, W. H., 1958a: Report on Fawara hills district,
        Saudi Arabia. Directorate General of Mineral Re-
        sources open-file Report.

——————————, 1958b: Report on Idsas, Saudi Arabia.
        Directorate General of Mineral Resources open-file
        Report.

Marzouki, F.M.H., 1977: Petrogenesis of Al Hadah plutonic
        rocks, Kingdom of Saudi Arabia. Unpublished Ph.D.
        thesis, University of Western Ontario, Canada, 267 pp.

——————————— and W. S. Fyfe, 1977: Pan-African plates:
        additional evidence from igneous events in Saudi
        Arabia. Contributions to Mineralogy and Petrology,
        v. 60, pp. 219-224.

Moore, J. M., 1976: A major lineament in the Arabian Shield
        and its relationship to mineralization. Mineralium
        Deposita 11, no. 3, pp. 323-328.

Mytton, J., 1966: Geologic map of the Al Urd quadrangle,
        Kingdom of Saudi Arabia. Directorate General of
        Mineral Resources, Mineral Inv. Map MI-4.

Nasseef, A. O. and I. G. Gass, 1977: Granitic and meta-
morphic rocks of the Taif area, western Saudi Arabia.
Geological Society of America Bull., v. 88, pp.
1721-1730.

Neary, C. R., 1974: Chromitiferous ultrabasic rocks in the
northern Hijaz of Saudi Arabia. Unpublished Ph.D.
thesis, University of Leeds.

_____, I. G. Gass and B. J. Cavanagh, 1976: The
granitic association of northeastern Sudan. Geo-
logical Society of America Bull., v. 87, pp. 1501-
1512.

Nebert, K., 1970: Geology of western Al Quwayiyah region,
Saudi Arabia. Neues Jahrbuch für Geologie und
Paläontologie Abhandlungen Band 135, no. 2, pp. 150-
170.

Nicholls, G. D. and M. R. Islam, 1971: Geochemical investi-
gations of basalts and associated rocks from the
ocean floor and their implications. Phil. Trans.
Royal Society of London 268, pp. 469-486.

Overstreet, W. C., J. W. Whitlow, V. P. Kahr and A. O.
Ankary, 1972: Reconnaissance geology of the Bir Al
Badriyah quadrangle, Kingdom of Saudi Arabia.
U.S.G.S. Unpublished Report SA(IR)-126, 47 pp.

Pearce, J. A., 1975: Basalt geochemistry used to investi-
gate past environments on Cyprus. Tectonophysics
25, pp. 41-67.
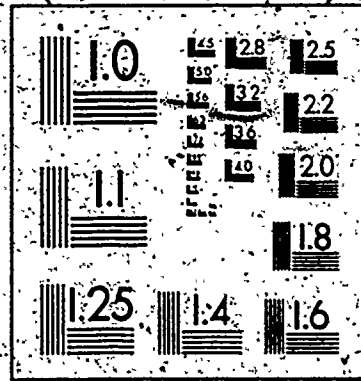
———————— and J. R. Gale, 1977: Identification of ore-deposition environment from trace-element geochemistry. In Volcanic Processes in ore genesis. Spec. Publ. Inst. Min. and Metallurgy/Geol. Soc. London. vol. 134, pp.

Piper, J. D., J. C. Briden and K. Lomax, 1973: Precambrian Africa and South America as a single continent. Nature, London 245, pp. 244-248.

Schaffner, D. F., 1955: Report on Fawara hills district, Saudi Arabia. Directorate General of Mineral Resources open-file Report 3-212-4039.

———————————, 1956b: Report on Idsas, Saudi Arabia. Directorate General of Mineral Resources open-file Report 3-212-2005.

Seyfried, W. and J. Bischoff, 1977: Hydrothermal transport of heavy metals by seawater: the role of seawater-basalt ratio. Earth and Planetary Science Letters, 34, pp. 71-77.

Shackleton, R. M., 1976: Pan-African structures. Phil. Trans. Royal Society of London, Ser. A 280, pp. 491-497.

Shido, F., A. Miyashiro and M. Ewing, 1971: Crystallization of abyssal tholeiites. Contribution to Mineralogy and Petrology, vol. 31, pp. 251-266.

Streckeisen, A., 1976: To each plutonic rock its proper name. Earth Science Reviews, vol. 12, pp. 1-33.

Thekair, M. E., 1976: Carbonate rocks in Al Amar-Asihailiya district of Saudi Arabia. Unpublished M.Sc. thesis, Center for Applied Geology, Jeddah; 210 pp.

Taylor, S. R., 1966: The application of trace element data to problems in petrology. Physics and Chemistry of the Earth, v. 6, pp. 133-213.

―――――――――, C. C. Annette, A. L. Graham and D. H. Blake, 1969: Trace element abundances in andesites. Contribution to Mineralogy and Petrology, vol. 23, pp. 1-26.

U.S. Geological Survey and Arabian American Oil Co., 1963: Geologic map of the Arabian Peninsula. U.S. Geol. Surv. Misc. Geol. Inv. Map I-270A.

Vincent, C., 1968: Geology and mineral resources of the Halaban-Sabhah region, Kingdom of Saudi Arabia. B.R.G.M. Unpublished Report 68 JED 1, pp. 47.

Williams, H., F. J. Turner and C. M. Gilbert, 1954: Petrography - An introduction to the study of rocks in thin section. San Francisco, W. H. Freeman and Co., 406 pp.

Wood, D. A., I. L. Gibson and R. N. Thompson, 1976: Elemental mobility during zeolite facies metamorphism to the Tertiary basalts of eastern Iceland. Contributions to Mineralog and Petrology, vol. 55, pp. 241-254.

Zubeir, M. O., 1976. Geological, petrological, and geochemical study on the Rugaan mafic - ultramafic layered intrusion. Unpublished M.Sc. thesis, Institute of Applied Geology, Jeddah, Saudi Arabia.